Antenna Diversity for Mobile Terminals

Timothy W. C. Brown

Submitted for the Degree of
Doctor of Philosophy
from the
University of Surrey

Centre for Communication Systems Research
School of Electronics and Physical Sciences
University of Surrey
Guildford, Surrey GU2 7XH, UK

September 2002

Abstract

Antenna diversity has been used at the base station in mobile communications as a way to reduce the impact of multipath fading for many years. At present, network operators in the Far East have also implemented antenna diversity at the mobile and it is likely that with upcoming third generation and fourth generation mobile networks this will become more common. Despite being already used, the mechanisms for successful diversity antennas at the mobile are largely unstudied and how their performance can be optimised is not well understood. Therefore there is a need for a new method from which the designer can evaluate the diversity performance of mobile antennas and use the results to determine how they are performing.

This thesis presents a new diversity modelling technique that can be used to evaluate the main antenna diversity contributions at a mobile terminal namely spatial, polarisation and angular diversity. Many mobile terminals will consist of a combination of all three and so evaluating them will assist the designer to find why there is diversity. Further to this it will present simulations that show how the results should be interpreted correctly for the benefit of the designer. Optimising the efficiency as well as the diversity is an important factor at the mobile, which will also be considered.

Results are also presented for two case study applications of the evaluation method. The first is a typical mobile handset with a diversity antenna and the other examines the diversity potential of an Intelligent Quadrifilar Helix Antenna. Finally the thesis ends with a proposal for a mobile fading environment simulator to verify the diversity performance of mobile handsets with different angle of arrival environments that will be of benefit in the future.

Key words: Antenna diversity, complex correlation, envelope correlation, spatial diversity, angular diversity, polarisation diversity, angle of arrival, cross-polar ratio, mean effective gain, intelligent quadrifilar helix antenna

Email: t.brown@eim.surrey.ac.uk

WWW: http://www.ee.surrey.ac.uk/cgi-bin/showstaff?T.Brown

Acknowledgments

Following completion, there are a number of people to whom thanks is due. I would like to thank my supervisor, Dr Simon Saunders, for his direction and guidance throughout the course of the past three years. Many thanks also goes to contacts at *Nokia Mobile Phones* who are sponsors of this work; such guidance has proved invaluable from the industrial perspective. Thanks is also due to the *Engineering and Physical Sciences Research Council* (EPSRC) who helped to fund this work as well. Internally, the assistance of many colleagues within the *Centre for Communication Systems Research* (CCSR) is much appreciated, especially that of Mr Daniel Chew, Dr Steve Leach and Dr Panomporn Suvannapatanna.

Many thanks also goes to countless people within the University and the Students' Union that have worked with me during the course of my time as a postgraduate in the capacity of president of the Postgraduate Association along with other responsibilities. Such experience has been an invaluable complement to my research studies. Further thanks goes to colleagues in the National Postgraduate Committee (NPC) whom I have worked with and gained further experience on a national level to enhance my future academic career.

I would also like to thank members of my family for their support, especially that of my parents, Prof and Mrs M. W. Brown. Their guidance and upbringing have been instrumental in enabling me to attain such levels of academic achievement.

Last but not least, I give praise to God for his unending faithfulness. Completion of this thesis and sustained effort throughout the past three years testify to the reality of his presence every step of the way.

Contents

List of Figures

List of Tables

Glossary of Terms

AOA	Angle of Arrival
AR	Axial Ratio
BW	Antenna beamwidth, either 3dB beamwidth for gain or 30^{o} beamwidth for phase
DF	Degradation Factor in diversity gain due to non zero correlation
DG	Diversity Gain
E-field	Electric Field
EGC	Equal Gain Combining
IQHA	Intelligent Quadrifilar Helix Antenna
L-antennas	"L shaped" antennas
MEG	Mean Effective Gain
MIMO	Multiple Input Multiple Output
MRC	Maximum Ratio Combining
MUSIC	MUltiple Signal Identification and Classification
NLOS	Non Line of Sight
PDC	Personal Digital Communications
PIFA	Planar Inverted-F Antenna
SG	System Gain
SNR	Signal to Noise Ratio
WLAN	Wireless Local Area Network
XPD	Cross-polar Discrimination
XPR	Cross-polar Ratio
3G	Third Generation Mobile
4G	Fourth Generation Mobile

List of Symbols

A	Weighting constant for Gaussian elevation angle of arrival
AR	Axial Ratio [Linear factor or dB]
a	Coefficient for polarisation diversity evaluation
α	Rotation angle used in polarisation diversity [^{o}]
A_θ	Complex amplitude in the θ range [V]
A_ϕ	Complex amplitude in the ϕ range [V]
b	Coefficient for polarisation diversity evaluation
β	Phase constant [radiansm^{-1} or radians per unit distance]
c	Coefficient for polarisation diversity evaluation
d	Coefficient for polarisation diversity evaluation (for polarisation diversity)
d	Horizontal spacing between two points (for spatial diversity) [m or unit distance]
$\delta\theta$	Offset angle for spatial diversity in the elevation [^{o}]
$\delta\theta_1$	Offset angle in the elevation for analysis of interaction of spatial and angular diversity [^{o}]
$\delta\theta_2$	Offset angle in the elevation for analysis of interaction of spatial and angular diversity [^{o}]
$\delta\phi$	Offset angle for spatial diversity in the azimuth [^{o}]
$\delta\phi_1$	Offset angle in the azimuth for analysis of interaction of spatial and angular diversity [^{o}]
$\delta\phi_2$	Offset angle in the azimuth for analysis of interaction of spatial and angular diversity [^{o}]
DG	Diversity Gain
e	Coefficient for polarisation diversity evaluation
E_x	E-field in the x range [Vm^{-1}]
E_y	E-field in the y range [Vm^{-1}]
E_z	E-field in the z range [Vm^{-1}]
E_θ	E-field in the θ range [Vm^{-1}]
E_ϕ	E-field in the ϕ range [Vm^{-1}]

ε	Polarisation angular spacing for symmetrically polarised antennas [^{o}]
f	Coefficient for polarisation diversity evaluation
f_d	Doppler shift frequency [Hz]
G_θ	Gain in the θ range [Linear or dBi]
G_ϕ	Gain in the ϕ range [Linear or dBi]
h	Vertical spacing between two points [m or unit distance]
ϕ	Angle that is relative to the horizontal x direction [^{o}]
γ_s	Instantaneous signal to noise ratio [Linear or dB]
Γ	Mean signal to noise ratio [Linear or dB]
H_x	H-field in the x range [Hm^{-1}]
H_y	H-field in the y range [Hm^{-1}]
H_z	H-field in the z range [Hm^{-1}]
K	Ricean K factor [Linear or dB]
k	Branch power ratio [Linear or dB]
L	Signal to noise ratio factor compared to a single reference branch for the maximum diversity branch [Linear or dB]
M	Polarisation impurity matrix
m	Polarisation impurity of a single antenna branch
φ	Polarisation angular spacing for symmetrically polarised antennas [^{o}]
P_{fade}	Probability that a signal falls beyond a given threshold
p_θ	Probability density function in the θ range
p_ϕ	Probability density function in the ϕ range
θ	Angle that is relative to the vertical z direction [^{o} or radians]
$\overline{\theta}$	Mean angle of arrival in elevation above the horizontal [^{o} or radians]
Q	Symbol for Q function
r_{11}	Input resistance parameter [Ω]
r_{12}	Mutual resistance [Ω]

ρ_{12}	Complex correlation
$\lvert\rho_{12}\rvert$	Complex correlation magnitude
ρ_e	Envelope correlation
ρ_p	Power correlation
σ_A	Standard deviation on the angle of arrival in elevation [^{o} or radians]
σ_n	Standard deviation of a diversity branch output [V]
$\mathbf{S}$	Scattering parameter matrix
$\mathbf{S}_T$	Transfer matrix for two antennas
s_{11}	Reflection parameter for antenna A in a diversity system
s_{22}	Reflection parameter for antenna B in a diversity system
s_{12}/s_{21}	Transmission parameter between two antennas in a diversity system
SG	System Gain
$\mathbf{V}_A$	Antenna voltage vector [V]
$\mathbf{V}_E$	*E*-field voltage vector [V]
$\mathbf{V}_L$	Load voltage vector [V]
v_1	Voltage of a fading signal branch [V]
v_2	Voltage of a fading signal branch [V]
Ω	Angular spacing used in polarisation diversity [^{o}]
x	Cartesian horizontal coordinate [m or unit distance]
x_{11}	Input reactance [Ω]
x_{12}	Mutual reactance [Ω]
XPD	Cross polar discrimination [Linear or dB]
XPR	Cross polar ratio [Linear or dB]
y	Cartesian horizontal coordinate [m or unit distance]
ψ	Sector opening size for analysis of interaction of spatial and angular diversity [^{o}]
Z_a	Impedance of antenna A in a diversity system [Ω]
Z_b	Impedance of antenna B in a diversity system [Ω]

Z_m	Mutual impedance between two antennas in a diversity system [Ω]
$\mathbf{Z}_\mathrm{A}$	Antenna impedance matrix for a diversity system
$\mathbf{Z}_L$	Load impedance matrix for a diversity system
z	Cartesian vertical coordinate [m or unit distance]
z_{11}	Input impedance for antenna A in a diversity system [Ω]
z_{22}	Input impedance for antenna B in a diversity system [Ω]
z_{12}/z_{21}	Mutual impedance between two antennas in a diversity system [Ω]
ζ	Three dimensional angle used in spatial diversity [$^\mathrm{o}$]

Chapter 1

1 Introduction

In mobile radio propagation, a common problem of multipath fading occurs in urban, suburban and indoor environments. Unlike other factors such as path loss and shadowing, the rapid change in signal level from multipath fading while in motion causes significant degradation of signal to noise ratios (SNRs) such that bit error rates are increased significantly and likewise the quality of service is not acceptable. Antenna diversity has been used for many generations in a number of applications of radio communications including mobile radio to mitigate fading effects. In the general case, diversity antennas work by having two antenna branches that ideally have independent (i.e. uncorrelated) fading signals at their output along with the same mean signal level. Following this the two fading signals can be combined such that the resultant fading signal will have significantly less points where there is an extreme minima since the two fading signals are seldom at such a level at the same time. Consequently the SNR is increased on the resultant signal, therefore providing a diversity gain. More than two antenna branches can be used in order to increase the diversity gain further. There are different ways of allowing the antennas to have low correlation and similar mean power levels. In mobile radio this has conventionally been carried out at the base station by spacing two antennas an appropriate distance apart providing spatial diversity or in more recent days it has been carried out by using two different polarisations to achieve polarisation diversity. This thesis is, however, focused on the relatively unstudied area of antenna diversity at the mobile terminal.

1.1 Motivation

While diversity has conventionally been implemented at the base station for many current mobile networks, the Personal Digital Communications (PDC) network in the Far East also uses diversity at the mobile. With increased demand for data transmission to the mobile in the future, it is possible that there will be requirements for diversity to be implemented at the mobile in 3G and 4G networks. The same conditions of achieving low correlation and equal mean power apply at the mobile as well although they also have the problem of maintaining efficiency being often small, closely spaced antennas, which is not so much the case at the base station. Further to this, the mobile will not normally have straight forward spatial or polarisation diversity antennas like

the base station has. Due to the way the antennas interact with each other, there will be some joint contribution of the main forms of antenna diversity being spatial, angular and polarisation states.

Analysing the spatial, angular and polarisation contributions to diversity at the mobile is vital to determine why there is diversity, if any at all, from two antennas. This has therefore given motivation to analyse diversity at the mobile and devise a method to evaluate it in order to assist the designer in optimising the performance both in terms of diversity and efficiency. Many scenarios are different between the base station and the mobile in addition so they have to be taken into account. These scenarios include a different angle of arrival distribution in the propagation environment and different antenna properties such as mutual coupling, impedance differences and the effect the antennas have on their field patterns when in the presence of each other. Taking these scenarios into account, new models have been developed to evaluate the spatial, angular and polarisation correlation properties of mobile terminal antennas. Using the results generated from these models the designer can predict whether and to what extent two mobile terminal antennas provide diversity. This does depend on correct interpretation of the results, which this thesis will also outline. Optimising the diversity in terms of correlation and equal mean power level between the branches can also come at the expense of reduction in efficiency, which this thesis considers.

1.2 Structure of Thesis

To begin with, chapter 2 covers the background theory to diversity, explaining and defining a number of notations and terminologies that will be used throughout the thesis to avoid confusion. An important element of this chapter discusses the propagation models for angle of arrival and cross-polarisation coupling that have been chosen, with reasoning, for evaluating correlation and Mean Effective Gain (MEG). Other literature studied on existing mobile terminal diversity antennas is summarised giving typical examples of how they are implemented.

Chapter 3 gives detailed theoretical analysis of the new models developed to model the spatial, angular and polarisation diversity at the mobile. The new models consider the impedance, mutual coupling and antenna field pattern effects on diversity. Using these new theoretical models, chapter 4 shows how they are applied to antenna measurements or simulations and how they are adapted to the antenna field pattern results taken. Following this, chapter 4 presents simulations undertaken to show how angular diversity interacts with spatial diversity to affect the overall diversity from which some principles are drawn. Further to this it illustrates how polarisation diversity, if present, is inherent within angular diversity.

Chapter 5 demonstrates the practical application of the diversity analysis methods by taking two real applications as case studies. The first one is based on a handset model of a dual band GSM planar antenna with a meander line antenna at the other end of the handset. Effects of the human head are also looked at briefly. The second application analyses the diversity potential of an Intelligent Quadrifilar Helix Antenna (IQHA).

Finally chapter 6 finishes off with a proposal for a mobile radio fading simulator, with investigations made into its feasibility. The purpose of such a testing rig would allow diversity at the mobile to be analysed under different angle of arrival and cross-polar coupling conditions and hence verify theoretical models used. Conclusions and ideas for future work are given in chapter 7.

1.3 Novel Work Undertaken

The following original contributions to knowledge presented in this thesis are listed below chronologically:

1. Modelling and characterising polarisation diversity of both mobile and static fading environments.
2. Derivation of spatial diversity at the mobile for both horizontally and vertically spaced points at the mobile such that the diagonal spatial correlation can be evaluated.
3. Calculation of spatial diversity produced at the receiver in the presence of mutual coupling and impedance differences in the antennas.
4. Derivation of angular diversity characteristics at the output port of the antennas with impedance effects considered.
5. The method for evaluation of diversity at the mobile from measurements or simulations carried out.
6. Analysis of the contributions of spatial, angular and polarisation diversity and how they interact to affect the overall diversity performance.
7. Evaluation of the diversity characteristics of a typical mobile handset and what the main contributions are.
8. Analysis of the diversity potential of an Intelligent Quadrifilar Helix Antenna (IQHA).

1.4 Publications

The following journal publications have been written awaiting submission:

- T. W. C. Brown, S. R. Saunders, M. Fiacco, "Characterisation of Polarization Diversity at the Mobile"
- T. W. C. Brown, S. R. Saunders, "Analysis of Mobile Terminal Diversity Antennas"

The following conference publications have also been produced:

- T. W. C. Brown, S. R. Saunders, "Spatial Diversity of Two Closely Spaced Dipoles", *EPSRC Postgraduate Research in Electronics, Photonics, Communications and Software (PREP)*, April 2001; awarded best paper in the communications track.
- T. W. C. Brown, S. R. Saunders, "Modelling Polarisation Diversity at the Mobile Terminal", *IEE International Conference on Antennas and Propagation (ICAP)*, April 2001.
- T. W. C. Brown, K. C. D. Chew, S. R. Saunders, "Analysis of the Diversity Potential of an Intelligent Quadrifilar Helix Antenna", *Submitted to the International Conference on Antennas and Propagation (ICAP)*, April 2003.

Chapter 2

2 Background to Diversity

For diversity to be successful in a mobile fading environment, there are specific conditions that have to be met including low branch correlation, equal branch power and minimum efficiency loss, which will be summarised. At the mobile, the situation is more complex with greater restrictions than the base station as far as antenna design is concerned; hence there is greater difficulty in meeting the conditions. It may be the case that the mobile terminal has a limited level of diversity performance due to inherent problems encountered at the mobile. Therefore the implications will be discussed in this chapter.

Before considering the effects of the antennas at the mobile, the propagation environment must be taken into account, which will be different to that of the base station. Major differences will include incoming angle of arrival (AOA) of signals and their polarisation. In depth investigation and experimentation on the angle of arrival is beyond the scope of this thesis although a suitable model is proposed based on literature reviewed.

The final part of this chapter will explore ways in which diversity already has or could be implemented at the mobile. Since more mobile terminal devices will become wireless in the future, possible methods for implementation are considered there as well.

2.1 Diversity Systems and Diversity Gain

A number of resources have used different names and notations related to diversity, which can in many cases cause confusion. It is important therefore that the terms used in this thesis are properly explained, which include the different forms of correlation, cross-polar ratio, diversity gain and how they are related to each other.

2.1.1 Diversity receivers

The basic structure of a diversity receiver is shown in Figure 2-1 where the two receiver antennas, “Antenna 1” and “Antenna 2”, receive different (or uncorrelated) multipath fading signals with some deep nulls as the mobile moves. If the two signals are uncorrelated, it is rarely the case that the two multipath fading signals will be in a deep null at the same time. Therefore with the two

signals combined, there are few deep nulls at the output. Combining the two signals creates a higher mean signal to noise ratio at the output compared to a single branch, resulting in a diversity gain.

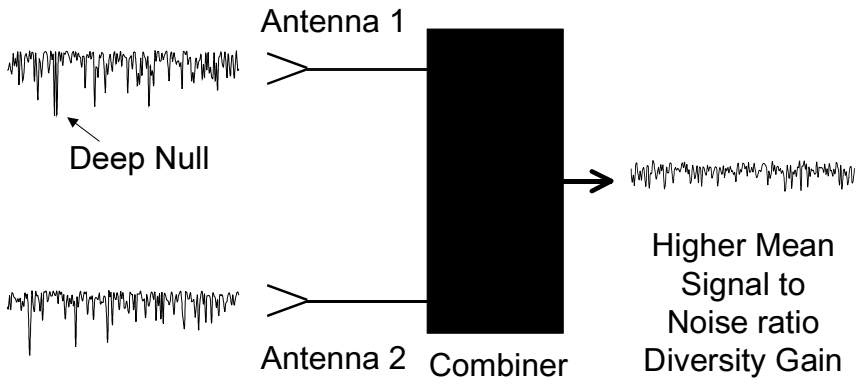

Figure 2-1 Diagram showing a basic diversity receiver structure

The combiner shown in Figure 2-1 is effectively a "black box" since there are different ways in which the signals can be combined. Before reading further, the four types of diversity combiner need to be noted [Saund99], which are selection combining, switched, equal gain combining (EGC) and maximum ratio combining (MRC). Selection combining works by selecting the maximum branch at any instantaneous point. Switched combining works by switching to the other branch when one branch falls below a threshold. EGC works by adding the branches together when they are co-phased. Finally MRC applies phase weights to each branch such that the output will be the sum of their signal to noise ratios.

All the combining methods except the switched combiner require two receivers if there are two diversity branches. At the mobile terminal, implementing two receivers is often uneconomical. In addition to the economic restrictions are limited battery life, size restrictions and complexity. Therefore a switched combiner is implemented in mobile terminals at present. It may, however, be the case that in the future the above problems will be overcome by integrated circuit technology advances so a second receiver could be implemented at the mobile [Knud01]. In any instance, this has little effect on much of the work presented in this thesis.

Modelling a switched combiner is difficult since it relies on the correct threshold being set in order to switch when necessary. The maximum performance that a switched combiner can achieve is the same as that of a selection combiner. Given that a selection combiner is simple to model and that it is the ideal case for a switched combiner, it will be used in this thesis to model the diversity gain unless otherwise stated.

2.1.2 Diversity gain at the mobile

In a Rayleigh Fading environment as encountered in most non line of sight (NLOS) multipath environments, it is well known that the fading signal is a complex Gaussian distributed noise signal multiplied by the carrier signal. Therefore this Gaussian signal has a cumulative distribution function given as [Saund99]:

$$P(\gamma < \gamma_s / \Gamma) = \left(1 - e^{-\frac{\gamma_S}{\Gamma}}\right) \tag{2.1}$$

where Γ is the mean signal to noise ratio, γ is the instantaneous signal to noise ratio, $P(\gamma < \gamma_s/\Gamma)$ is the probability that the signal to noise ratio will fall below the given threshold, γ_s/Γ. For a selection combiner, if the two branches are assumed to have independent signals and equal mean SNRs then the new cumulative distribution becomes:

$$P(\gamma < \gamma_s / \Gamma)_N = \left(1 - e^{-\frac{\gamma_S}{\Gamma}}\right)^N \tag{2.2}$$

where N is the number of branches.

Equations (2.1) and (2.2) are plotted in Figure 2-2 so it can be seen how increasing the number of branches, N, reduces the probability of fades below a given threshold. Also shown here is the Diversity Gain, DG, which is the increase in signal to noise ratio of a combined output compared to a single branch. In this case, the Diversity Gain is evaluated when there is a $P(\gamma < \gamma_s/\Gamma)$ of 1% (i.e. 99% reliability). Analysis of diversity receivers from [Sch66] shows that by approximation, if the ratio of γ_s to Γ is less than –10dB then:

$$P(\gamma < \gamma_s / \Gamma)_N \approx \left(\frac{\gamma_s}{\Gamma}\right)^N \tag{2.3}$$

so that by re-arranging the equation the diversity gain for a 100% efficient two branch selection combiner is 10dB with $P(\gamma < \gamma_s/\Gamma)$ at 1%. Another way of identifying the diversity gain can be found from Figure 2-2 where the increase in signal to noise ratio is shown. Further branches will increase the diversity gain further. Current mobile terminals such as handsets will generally use only two branches. Future technology is looking towards implementing more diversity branches [Nørk01] [Leach00], which will be required when moving towards broadband multimedia communications at the mobile. Examples of this are Multiple Input Multiple Output (MIMO) techniques [Beach01] and space time coding applications [Katz01]. When diversity gain is referred to in this thesis it will be for 99% reliability.

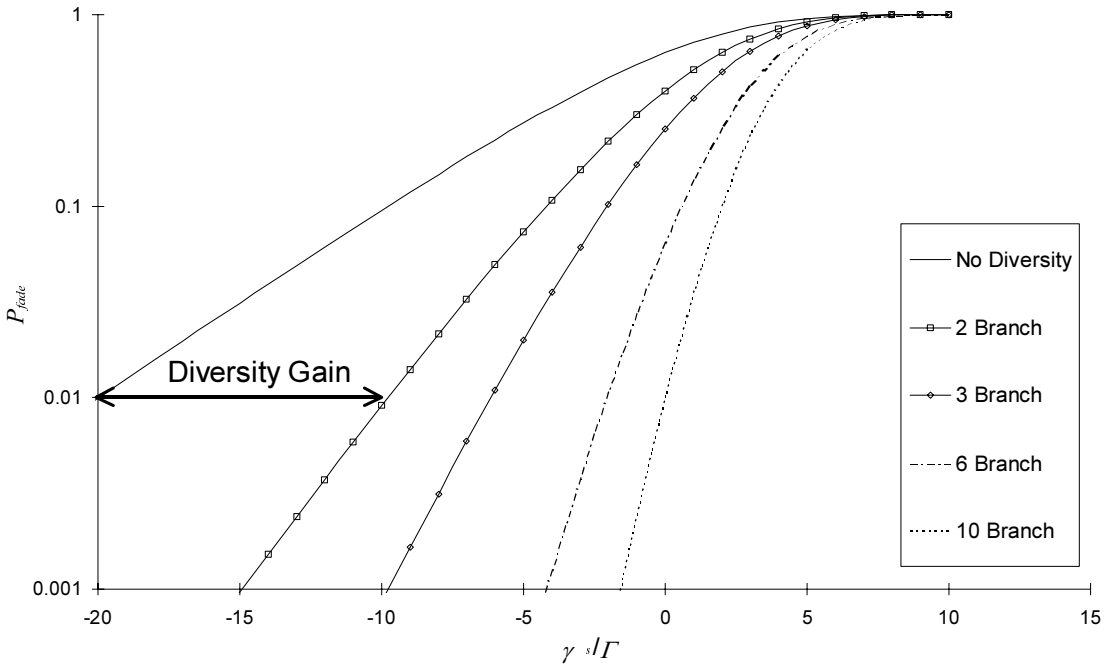

Figure 2-2: Cumulative distribution of Rayleigh fading signals for different numbers of diversity branch

2.1.3 Correlation and its effects on diversity gain

One of the conditions for diversity is that the correlation is low, as defined later, or ideally zero. A number of different names and notations are used for correlation, which can cause confusion. In general there are three types of correlation being complex, envelope and power correlation [Coulb98] all of which are related although these three names are by no means general. To begin with, the complex correlation, ρ_{12}, is described as "the complex correlation between two signal envelopes" [Ada86]. Therefore the magnitude and phase are used to calculate correlation. In the time domain, the complex correlation is defined in closed form as follows:

$$\rho_{12} = \frac{\int_0^T \left(v_1(t) - \overline{v_1}\right)\left(v_2(t) - \overline{v_2}\right)^* dt}{\sqrt{\int_0^T \left|v_1(t) - \overline{v_1}\right|^2 dt \int_0^T \left|v_2(t) - \overline{v_2}\right|^2 dt}} \tag{2.4}$$

Where t is the instantaneous time point and T is the time period over which the fading signals are taken over to correlate. The two fading signals $v_1(t)$ and $v_2(t)$ are voltage functions of time and have mean values $\overline{v_1}$ and $\overline{v_2}$ in volts, V.

For evaluating correlation between two antennas, the complex correlation is evaluated in the angular domain as follows [Ped96]:

$$\rho_{12} = \frac{\int_0^{\pi}\int_0^{2\pi}\left(XPR.E_{\theta 1}(\theta,\phi)E^*_{\theta 2}(\theta,\phi)p_\theta(\theta,\phi) + E_{\phi 1}(\theta,\phi)E^*_{\phi 2}(\theta,\phi)p_\phi(\theta,\phi)\right)\sin\theta d\phi d\theta}{\sqrt{\sigma_1^2\sigma_2^2}} \tag{2.5}$$

where the variance, σ_n^2 is the variance of branch *n* in V^2:

$$\sigma_n^2 = \int_0^{\pi}\int_0^{2\pi}\left(XPR.E_{\theta n}(\theta,\phi)E^*_{\theta n}(\theta,\phi)p_\theta(\theta,\phi) + E_{\phi n}(\theta,\phi)E^*_{\phi n}(\theta,\phi)p_\phi(\theta,\phi)\right)\sin\theta d\phi d\theta \tag{2.6}$$

where *XPR* is the ratio of time averaged vertical power to time averaged horizontal power [Jen94 eq. (8)] in the fading environment in linear form:

$$XPR = \frac{P_V}{P_H} \tag{2.7}$$

where P_V is the average vertical power and P_H is the average horizontal power. It is important to note here that *XPR* is sometimes referred to as cross-polar discrimination (*XPD*). This notation has been avoided in the thesis due to confusion with the axial ratio definition used for polarisation [Alln89] in linear form:

$$XPD = \frac{1+|AR|}{1-|AR|} \tag{2.8}$$

Where *AR* is the axial ratio defined as the ratio to the vertical Cartesian *E*-field, E_z [Vm^{-1}] to the horizontal Cartesian *E*-field, E_y [Vm^{-1}]. Both branches in equation (2.5) have *E*-fields, $E_{\theta n}$ and $E_{\phi n}$, [Vm^{-1}] respectively. As well as the fields at each angle, the angle of arrival density in both the vertical and horizontal planes (i.e. $p_\theta(\theta,\phi)$ and $p_\phi(\theta,\phi)$) affect the correlation. Finally it is not obvious here what the angles θ and ϕ [°] represent so for reference purposes, θ is relative to the vertical axis, *z*, and ϕ is in the horizontal plane as shown in Figure 2-3.

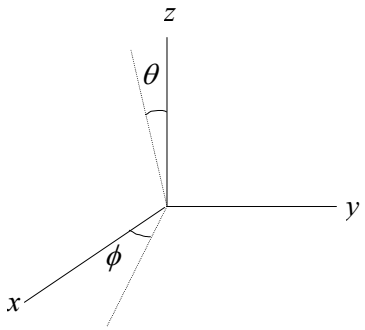

Figure 2-3 Diagram showing the relation of angular coordinates to Cartesian coordinates

If there is an imaginary component present in the complex correlation it indicates that there is a phase shift at the output of one of the branches relative to each other. Such scenarios can occur at the mobile terminal due to the magnitude and phase patterns of the antennas being different, leading to a resultant imaginary component when evaluated.

The next form of correlation is the envelope correlation, ρ_e, which is the correlation between two signal envelopes without considering the phase [Ada86]:

$$\rho_e = \frac{\int_0^T \left(\sqrt{R_1^2(t)} - \overline{\sqrt{R_1^2}} \right) \left(\sqrt{R_2^2(t)} - \overline{\sqrt{R_2^2}} \right) dt}{\sqrt{\int_0^T \left(\sqrt{R_1^2(t)} - \overline{\sqrt{R_1^2}} \right)^2 dt \int_0^T \left(\sqrt{R_2^2(t)} - \overline{\sqrt{R_2^2}} \right)^2 dt}} \tag{2.9}$$

Where $R_1^2(t)$ and $R_2^2(t)$ are the square envelope [V^2] of $v_1(t)$ and $v_2(t)$ respectively, i.e. $|v_1(t)|^2$ and $|v_2(t)|^2$. As phase is not defined with the square envelope, ρ_e is always real. In a Rayleigh fading environment it is assumed that with independent Gaussian sources the envelope correlation is related to the complex correlation by [Clarke66]:

$$\rho_e \approx |\rho_{12}|^2 \tag{2.10}$$

Finally the power correlation, ρ_p, is a correlation of the square envelope [Ada86]:

$$\rho_p = \frac{\int_0^T \left(R_1^2(t) - \overline{R_1^2} \right) \left(R_2^2(t) - \overline{R_2^2} \right) dt}{\sqrt{\int_0^T \left(R_1^2(t) - \overline{R_1^2} \right)^2 dt \int_0^T \left(R_2^2(t) - \overline{R_2^2} \right)^2 dt}} \tag{2.11}$$

which is also real. Analysis has shown [PieSte60] that ρ_p and ρ_e are assumed found to be similar enough to be considered equal, which sometimes helps in computation of ρ_e. Throughout this thesis, the complex correlation will be evaluated with application to equation (2.5). The reason for using complex correlation is that the fading environment is only assumed Rayleigh in this thesis and the theoretical models presented in later chapters could be applied to non Rayleigh environments. In such circumstances, equation (2.10) would not be valid so it could not be applied to calculate envelope correlation; an alternative formula does not exist at present.

Effects of envelope correlation on diversity gain can be found using application of the Q function [Sch66] which will find the probability error on the cumulative distribution function, $P(\gamma < \gamma_s/\Gamma)$. Changing the cumulative distribution function will cause a resultant change in the diversity gain. Analysis [Sch66] shows that in the case where ρ_e is 0.7 or less then the degradation factor (i.e. the factor by which the diversity gain reduces due to non-zero correlation), DF, is related to the envelope correlation by the following equation.

$$\mathrm{DF} = \sqrt{1-\rho_e} \tag{2.12}$$

For values above 0.7, a lookup table needs to be used to find DF and interpolated from if necessary. Figure 2-4 shows a comparison of equation (2.12) with the actual values of DF calculated from using the Q function.

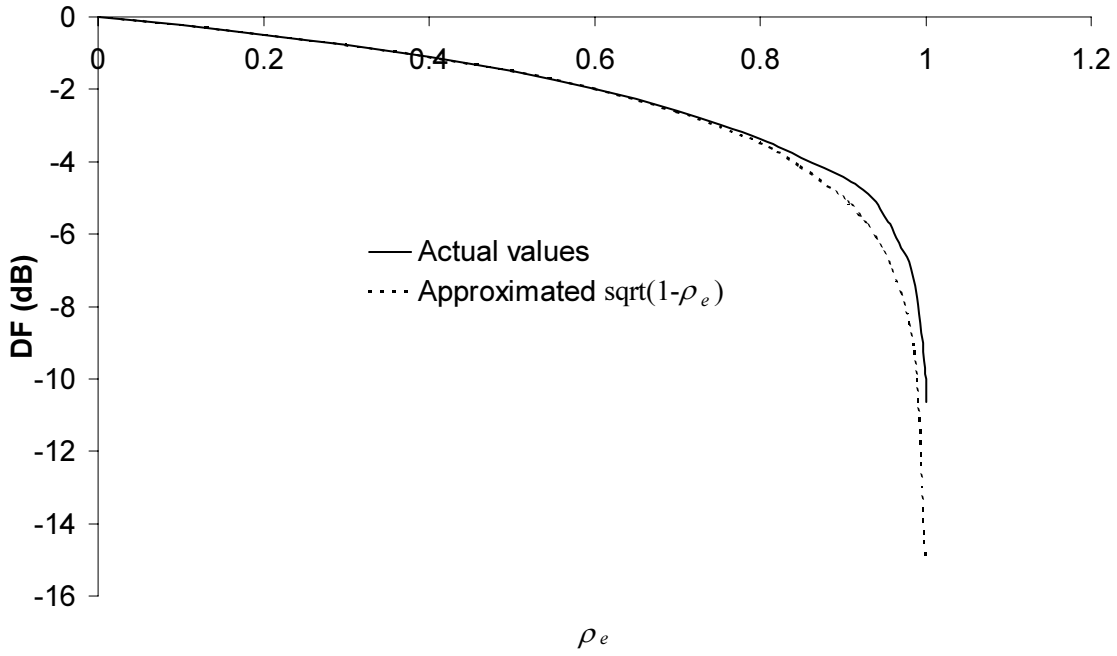

Figure 2-4 Graph showing comparison of approximated degradation factor in diversity gain compared with the real values

2.1.4 Effects of unequal branch power on diversity gain

The other main condition for diversity is that the power levels of the two branches are equal. Like correlation, this condition is not always met so the effects that this has on diversity also need to be evaluated. The best way of showing this is by using the ratio of the two branch power levels, *k*, as follows in linear form:

$$k = \frac{P_{\min}}{P_{\max}} \tag{2.13}$$

Where $P_{\min}$ [W] is the power from the branch with the lower power level and $P_{\max}$ [W] is the power from the branch with the higher level of power. Therefore the condition is met that $0 < k \leq 1$ where unity is the ideal case. Under this condition, *k* can be multiplied by the diversity gain of a two-branch system to find the new diversity gain for a selection combiner [Sch66]. This is due to the fact that equation (2.3), when $N = 2$, becomes:

$$P\left(\gamma < \gamma_s / \Gamma\right)_2 \approx \frac{1}{k}\left(\frac{\gamma_s}{\Gamma}\right)^2 \tag{2.14}$$

To avoid significant loss in diversity gain *k* should be greater than –3dB (assuming the correlation is low). If diversity gain is to be at all possible then *k* will need to be above –10dB or otherwise the system is invalid. Unequal branch power is therefore a disadvantage to selection diversity. However it should be noted that MRC provides optimal combining such that the signal to noise ratios of each branch are added, which reduces the impact of *k* [Jak94].

2.1.5 Efficiency of a diversity system and system gain

While both low correlation and equal mean power in the two branches may allow the selection combiner to work to its optimum performance, this may occur at the expense of losing efficiency at the mobile terminal. Therefore the efficiency could reduce so much compared to the single reference branch that there is possibly no resultant gain. It may be possible that the signal increases with improvement in antenna gain. Hence a signal to noise ratio factor, *L*, has to be brought into the equation such that in linear form:

$$L = \frac{\max\left(P_1, P_2\right)}{P_0} \tag{2.15}$$

where P_1 and P_2 [W] are the power levels in branches 1 and 2 respectively and P_0 is the power from the original single branch.

Having established the diversity gain, DG, from the correlation and branch power ratio, it is proposed here that the system gain should be introduced. The system gain, SG, is defined in linear form as:

$$\mathrm{SG} = \mathrm{DG} \times L \tag{2.16}$$

In some cases, it may be argued that the system gain should still be termed as diversity gain since it is a direct comparison of two systems. In certain cases this creates a problem making this definition of diversity gain intuitive since the following cases might occur:

1. The two branches are correlated or they have low mean branch power ratio. There is still significant gain because of high efficiency but the combiner is dormant.
2. The combiner, on the other hand, may be working effectively due to low correlation and equal branch power. However, the two antennas are inefficient compared to a single one in which case comparing the two systems gives a gain of less than unity, i.e. a loss.

The above two cases cannot be considered as diversity gain, which are both vulnerable to occurring at the mobile. To begin with, no correlated branches provide any diversity gain, nor if their branch power ratio is less than -10dB. Hence the gain is only because the system (or the antennas to be more precise) has a better efficiency. As for the second scenario, diversity gain cannot be defined when it is less than unity.

In conclusion, diversity gain can be considered the same as the system gain when the value for L, is close enough to unity. In some circumstances L is unity although often at the mobile terminal there will be degradation in efficiency so it must not be ignored.

2.2 Types of Antenna Diversity

Using antennas there are four main ways of achieving diversity in order to generate de-correlated signals at the same branch power level. In the general case these are known as spatial, angular, polarisation and field diversity. All are summarised below. It is important that their distinctions are identified since at the mobile, there is often a combination of different types of antenna diversity to give an overall performance, which later chapters will analyse.

2.2.1 Spatial diversity

The simplest and most commonly used form of diversity at the base station is spatial diversity. By having antennas at two separate points in space the phase delay between them can allow the fading signal in the second antenna to be de-correlated from the first antenna. In order to achieve

sufficient de-correlation, the antennas must have a minimum spacing, which is greater than several wavelengths at the base station in an urban area [Jak94]. At the mobile, this is not the case since the angle of arrival is wider. By assuming that there is uniform angle arrival around the azimuth of the mobile and no elevation angle of arrival, the correlation can be derived from the zero order Bessel function, $J_0(x)$ [Saund99]:

$$\rho_{12} = J_0(\beta d) \tag{2.17}$$

where β is the phase constant (i.e. phase in radians per unit distance) and d is the antenna spacing as a unit distance. This equation shows that the minimum distance for negligible correlation between two points in space at the mobile is 0.5 wavelengths. However, this does not consider the mutual coupling between the antennas, which will be shown to change spatial correlation although antennas closer than 0.5 wavelengths such as on a mobile handset can give little scope for spatial diversity. At such distances there is a greater contribution of other forms of antenna diversity, mainly angular diversity, which contribute to lower correlation seen from measurements undertaken with closely spaced dipoles and monopoles [Pars02].

Spatial diversity should not be ruled out at the mobile since larger mobile terminals (e.g. notebook computers and electronic organisers) possibly communicating at higher frequencies in the future could allow the antennas to be spaced far enough apart in terms of wavelengths. This will therefore provide scope for spatial diversity.

2.2.2 Angular diversity

In many cases at the mobile terminal there is an element of angular diversity. In this situation, the antennas will have more significant gain in different directions, which means that they are picking up more signals from different angles. Since the fading signals coming from different directions are independent then angular diversity can be implemented. This has been considered at the base station in some cases and compared with spatial diversity [Vaug98] [Perini98] [Jukka98].

At the mobile terminal angular diversity can occur by two omni-directional antennas interacting with each other while closely spaced. The antennas can act as parasitic elements to each other and change their patterns to allow signals to be picked up at different angles [Leath96]. Further to this some antenna technology has been developed to allow antenna beams to be steered at the mobile by changing the feed point impedance of parasitic elements [Vaug99].

2.2.3 Polarisation diversity

In recent years, research has been carried out to investigate the effectiveness of polarisation diversity at the base station [Turk94] [Cho96]. Further to this it has already been implemented in certain cases [Beck97] and is widely applied in practice for new cellular base station installations. Using spatial diversity at the base station creates large antenna structures, which have great environmental impact. Polarisation diversity is currently being implemented further to alleviate this problem since they are co-located antennas and smaller in size. Theoretical models have been developed in the past [Koz84] [Vaug90] to show that at the base station the largest system gain occurs when the two antennas are polarised at $\pm 45^{o}$ when the vertical is used as a single reference. Also it has been shown how polarisation diversity can be integrated with spatial diversity [Egg93].

At the mobile terminal, polarisation diversity is also an attractive option because of the size limitations involved. However, there is still need for a more appropriate model to use given scenarios such as low isolation between the branches, polarisation impurities, wide angle of arrival distribution and differing antenna field patterns.

2.2.4 Field diversity

The fourth form of antenna diversity that is not used in this thesis but should be mentioned at this point is field diversity. According to Lee [Lee97] an *E*-field, E_z, also generates independent magnetic components H_y and H_x. By using an energy density loop antenna it is possible to extract these three signals to combine them as appropriate. In general, however, mobile terminal antennas are designed as electric field antennas so therefore they cannot contain any field diversity. For this reason, field diversity is not investigated in this thesis due to the difficulties there are in implementing it into current mobile terminals.

2.3 Angle of Arrival Distribution

As shown in equation (2.4) the correlation is dependant on the angle of arrival (AOA) distribution via the probability density functions $p_\theta(\theta,\phi)$ and $p_\phi(\theta,\phi)$. For the correlation to be suitably evaluated in any situation it is necessary to apply a suitable angle of arrival model. A limited number of measurements have been carried out on angle of arrival at the mobile in urban environments and only recently have indoor environments been considered. Further research is still to be carried out in this area therefore and in depth analysis of AOA is beyond the scope of

this thesis. At this point the results found to date are summarised and considered to justify a suitable model to use at the mobile terminal.

2.3.1 Outdoor urban environments

Results have been obtained in the past either by direct measurement campaigns, analysis of time variant data using algorithms such as Multiple Signal Identification and Classification (MUSIC). Further to this there are also proposed models reported in references based on results available at the time. A summary of the results is given in appendix A with the references listed. As well as the results, comments on the methods or equipment used are noted since they will influence the validity of the results. Accuracy and resolution of the AOA measurements will always be limited by the beamwidth of antennas used or by the limits in resolutions of algorithms such as MUSIC.

Despite the constraints, a number of models indicate a uniform angle of arrival distribution in azimuth where there is an NLOS case. This has been reasonable to assume since the base station is not visible from the mobile and there is equal chance of a local (or nearby) scattering object being at any angle around the mobile. It has been reported, however, that in certain cases there is possibly not a uniform angle of arrival either from measurements [Vaug86] or from correlation measurements not giving expected results that would occur if there was a uniform angle of arrival [Diet01]. In recent days, angle of arrival measurements have reported cases of non-uniformity [Kalli01], especially from non-local scatterers [Kuch00]. Recently, it has been suggested that standard urban models have a Laplacian azimuth distribution [SCM02]. Such results still require further investigation into appropriate standard models that can be used for well defined types of urban environment such as street canyons, open squares and heavily cluttered areas. Due to the ambiguity in justifying an appropriate azimuth AOA model, it will be assumed uniform throughout this thesis, which provides ease in diversity evaluation carried out. Variation from this model will have a significant impact on diversity performance, and should therefore be the subject of future investigations.

As for the elevation, the situation becomes complicated since there is always a varying height of scatterers and the base station which does not give consistent AOA statistics from the references in appendix A. Further to this the measurements at different frequencies appear to affect AOA also. Despite the variations, all the results reported appear to indicate that the majority of incoming signals arrive between 0^o and 30^o above the horizontal.

2.3.2 Indoor environments

Since research has only recently been carried out in this area, there are still limited results for indoor AOA distributions which do not give a clear indication of what model can be applied. Results listed in appendix B show that there appears to be a uniform azimuth distribution in the general cases also. Characteristics can change rapidly, however, depending on whether the mobile is in a different room to the transmitter or in the same room possibly with a line of sight. Elevation angle of arrival does not appear to be resolved so it is hard to assume a suitable model here.

2.3.3 Proposed AOA model

As reported by Taga [Taga90] the AOA can be approximated by a Gaussian function based on the results seen. Although the mean is generally constant, the standard deviation of the angle of arrival varies between environments so this should be experimented with to see how diversity is affected. It will be assumed here that the mean or standard deviation can be changed if necessary to give a suitable AOA approximation of any indoor or outdoor AOA model. Therefore the following equation can be used [Taga90]:

$$p(\theta,\phi) = Ae^{-\frac{1}{2}\left(\frac{\theta-\left(\frac{\pi}{2}-\bar{\theta}\right)}{\sigma_A}\right)^2} \tag{2.18}$$

where $\bar{\theta}$ [rad] is the mean elevation angle, σ_A [rad] is the standard deviation and A is a constant. Later on in this thesis will investigate how differing σ_A will affect diversity. It will be assumed now in the general case from measurements taken by Taga that the mean is 20^o and the standard deviation is 20^o for an urban fading environment. For equation (2.18) to be used properly, all angles need to be applied in radians.

2.4 Cross Polar Ratio

Also shown in equation (2.5) is the cross polar ratio of the fading environment, *XPR*, which has a dramatic effect in the case of angular and polarisation diversity. In most cases, a value of around 6dB is reported at frequencies around 900MHz [Lee72] [Koz84] [Vaug90] from the mobile to the base station. Higher *XPR* has been reported at frequencies out of this range, which gives indication that *XPR* might be frequency variant [Kalli01] [Luk01]. It cannot, therefore, be assumed that the *XPR* is always constant due to varying frequency and environment. Further to this there is no concrete evidence shown to date that *XPR* is reciprocal such that if a vertical

source was transmitted, there would be 6dB *XPR* on average at the mobile. It can only be assumed here therefore that the *XPR* is 6dB although varying its effect on diversity will be investigated in further chapters since it has to be considered as an input variable given the circumstances shown.

2.5 Examples of Mobile Terminal Diversity Antennas

A number of mobile terminal antennas have been implemented in many different ways and tested or evaluated for their diversity performance. Results do indicate that significant diversity performance can be achieved at the mobile in different ways, which will be presented here from literature studied. Further to this the effects of the human body and usage in different propagation environments will have considerable effects as well, which are discussed here. Mobile terminal diversity antennas occur not only on mobile handsets but also on other mobile equipment as well so they will also be discussed.

2.5.1 Dual antenna handsets

Mobile handsets can have two antennas implemented onto them in a number of ways in order that each of the two antennas can pick up independent fading signals in an urban fading environment. Different methods can be used such as two monopoles that can be placed on a handset [Leath96] and dual helix antennas [James00] although such antennas are bulky in size and not so appropriate for the style of a mobile handset. Given this problem, a typical diversity solution consists of a whip or helix antenna as a main antenna complemented by a Planar Inverted-F Antenna (PIFA) as shown in Figure 2-5 (a) [Ped97] [Ogawa97] [Coulb98] [Braun99] [Jen94]. Therefore the PIFA is internal and does not affect the aesthetics of the handset. Simulations [Jen94] [Ogawa97], antenna measurements [Ped97] [Braun99] and to some extent actual propagation measurements [Coulb98] have indicated that there is suitably low correlation and possibly some diversity gain with this antenna arrangement.

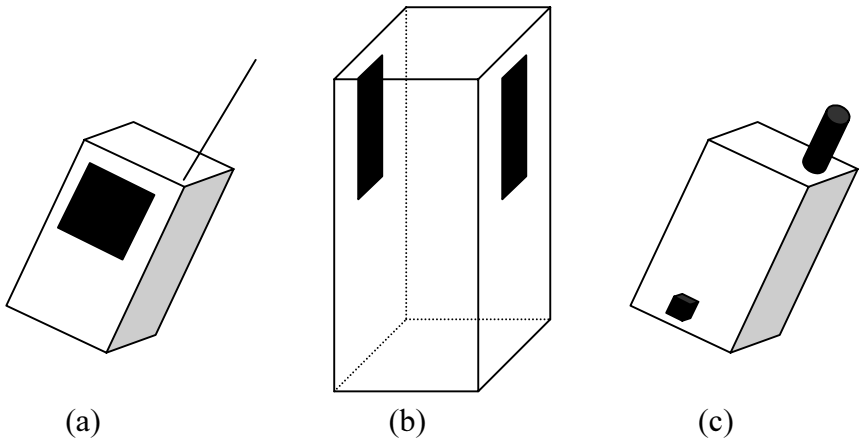

Figure 2-5 Examples of typical mobile terminal antenna handsets; (a) whip and helix antenna; (b) dual PIFA antenna; (c) helix and chip antenna

Similar experimentation [Coulb98] [Jen94] has been carried out on other antennas such as dual PIFA antennas shown in Figure 2-5 (b) where the arrangement has a reduced profile. Many other ideas exist such as L-antennas [Erät97] and dual patch antennas [Doug98]. In recent days, particularly for PDC handsets, the size restrictions have often required the designer to use a small meander antenna or chip antenna inside the terminal as shown in Figure 2-5 (c) [James00].

Although some evidence indicates that the mobile terminal antennas have some diversity it is not at all clear how. There are a number of reasons why this might be the case:

1. Different antenna patterns can implement angular diversity.
2. Antennas will have differing polarisations to implement some polarisation diversity.
3. Possibly some spatial diversity exists with the mutual coupling present.
4. The antennas will interact with each other so that they will affect their field patterns, polarisations and efficiency.
5. Further changes will occur when in talk position.

It is therefore necessary to have a method to evaluate theoretically how the antennas have diversity gain and how antenna properties affect different types of diversity. This knowledge will help direct the designer to optimise a mobile terminal diversity antenna given the design specifications set including size restrictions and frequency. Optimisation of diversity may happen at the expense of reduced efficiency; hence it is also important for the designer to be aware of how the efficiency is maximised.

2.5.2 Switched parasitic elements and single diversity antennas

Use of dual antennas at the mobile is one way of achieving diversity. Another method is to use a single antenna that has switched parasitic elements [Vaug99]. An example of switched parasitic elements is shown in Figure 2-6. By switching the parasitic elements differently with diode switches or similar to change their load impedances, the antenna field pattern can be changed. Therefore when switch 1 is closed, it will generate pattern 1 and likewise switch 2 is closed it will generate pattern 2. It is assumed in both cases that the other switch is open when one is closed. In the general case, angular diversity is being deployed here since the parasitic elements are often arranged to do so. It is also possible the spatial diversity might be implemented in some form or other since the phase centre could be moved when different parasitic elements are used. Polarisation diversity is also a possibility in some cases since the polarisations could be changed. A number of different designs have been implemented using this principle [Sib97] [Scott99] [Fass00] [Schlub00].

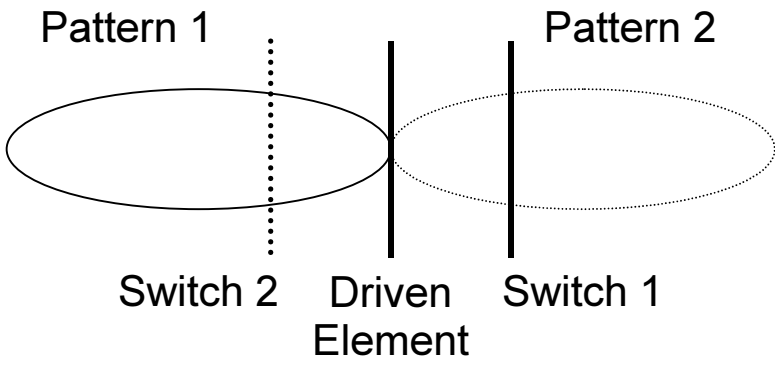

Figure 2-6 Diagram showing a typical example of switched parasitic elements

Another way to implement diversity with a single antenna structure is to use purpose built pattern diversity antennas [Ko01] [Hos94] [Paul92] [Mur01] [Kuga96]. In such cases a single antenna often has two feeds, which can steer the antenna beam as opposed to using parasitic elements. Again angular diversity is achieved mainly here although spatial and polarisation diversity could be taking place for the same reasons.

Finally it is important to mention that some antennas have been developed for polarisation diversity, which could be suitably implemented for a mobile terminal [Kuga98] [Fang00]. Development is still limited in this area although it could become an attractive option given the size limitations present at the mobile.

Like dual antennas at the mobile, the spatial, angular and polarisation diversity still needs to be evaluated when a single diversity antenna is implemented since they cannot be considered as purely angular diversity antennas. Modelling diversity at the mobile therefore needs to be considered with different applications in mind to assist the designer.

2.5.3 Effects of the human head

Evaluating diversity of a handset alone is insufficient since handsets are mainly used in talk position next to a human head. Therefore antenna characteristics and consequently the diversity potential are changed. Research in this area has been carried out to investigate the effects of the human head by 3D pattern measurements [Taka96] [Ped97] [Skjæ97] [Braun99], simulations [Doug98] and measurement trials [Green00].

Measurements indicate that the head does appear to improve correlation, which may be due to stronger coupling between the antennas or improved angular diversity. For many omni-directional antennas, however, the mean effective gain can reduce considerably in the presence of a person. It is also of no advantage when antennas placed inside a handset are covered by the hand during use. Further to this the mean effective gain when a handset is in use by different users in the order of 6-7dB according to measurements carried out by Pedersen [Correia01]. It can be seen here again, however, that it is still not known how the presence of a person changes the antennas and their diversity, which may help indicate what is happening when a human head is present.

2.5.4 Other mobile terminal antennas

Most of the antennas discussed so far are mainly used for a mobile handset. Looking to the future there are further designs that can be put forward for implementing diversity on other mobile terminals already discussed. Ideas have already been generated for applications such as notebook computers [Lieb97] [Mich96] [Lee01]. In these cases, the terminal may be larger and working at higher frequencies for Wireless Local Area Networks (WLAN) giving scope for more spatial diversity as mentioned earlier.

2.6 Conclusions

In this chapter, the key notations and terms used in diversity have been presented, which will be used throughout this thesis. Some considerations on diversity theory have also been presented that apply to the mobile terminal more so than at the base station and their importance has been emphasised. One of the key factors is how equal branch power and low correlation is optimised at

the expense of efficiency loss in the antennas. Therefore efficiency cannot be omitted when considering diversity performance.

As well as the antennas, diversity is influenced by the surrounding propagation environment being that of angle of arrival and the cross polarisation. As discussed there is limited information concerning this although appropriate models have been proposed that can be applied.

Research carried out does indicate there is some diversity from mobile terminal antennas and also the effects of the human body have been investigated. It is clearly the case that what diversity there is has been found out but it is still not apparent why there is diversity. Therefore this opens an avenue to investigate whether mobile terminal antennas have spatial, angular or polarisation diversity and how the antenna properties influence this in order to aid designing.

Chapter 3

3 Modelling Diversity at the Mobile

Having established in the previous chapter that it is not known exactly why mobile terminal antennas have diversity and how to evaluate it and optimise it, the three types of antenna diversity at the mobile will be investigated in this chapter. A number of scenarios have already been noted that are not present at the base station, which include mutual coupling between the antennas, a wider angle of arrival and also that the antennas interact with each other possibly forming different polarisations and angular field patterns.

After the theory behind mutual coupling, input impedance and other antenna theory is presented, new theoretical models are derived that consider the scenarios mentioned, which will then show how the antenna properties affect polarisation, spatial and angular diversity. A brief application of the theory is presented with measurements taken from two closely spaced monopoles to illustrate the interaction of spatial and angular correlation.

3.1 Antenna Properties at the Mobile

In this section the antenna properties are outlined that have effect on diversity and their definitions are explained with the appropriate mathematical formulae where necessary. Factors include the mutual coupling between the antennas, the way in which the antennas affect their field patterns, their polarisation and their Mean Effective Gain (MEG).

3.1.1 Two-port model of diversity antennas

In order to analyse the characteristics of two antennas operating as a diversity system, it is appropriate to model them as a two-port network. Figure 3-1 shows the two-port model for two mobile diversity antennas in the presence of each other. Each antenna has its own self impedance, Z_a, for antenna A and Z_b for antenna B in Ohms, Ω. Both antennas are loaded in series with a load impedance, Z_0 [Ω]. When the antennas are close together compared to a wavelength, as is likely to occur at the mobile terminal, then a mutual impedance will be present to determine the voltage transmitted from one antenna to the other. Further to this the mutual impedance is in series with

each of the antenna impedances. This allows the input impedance of each antenna to be determined in the presence of the other.

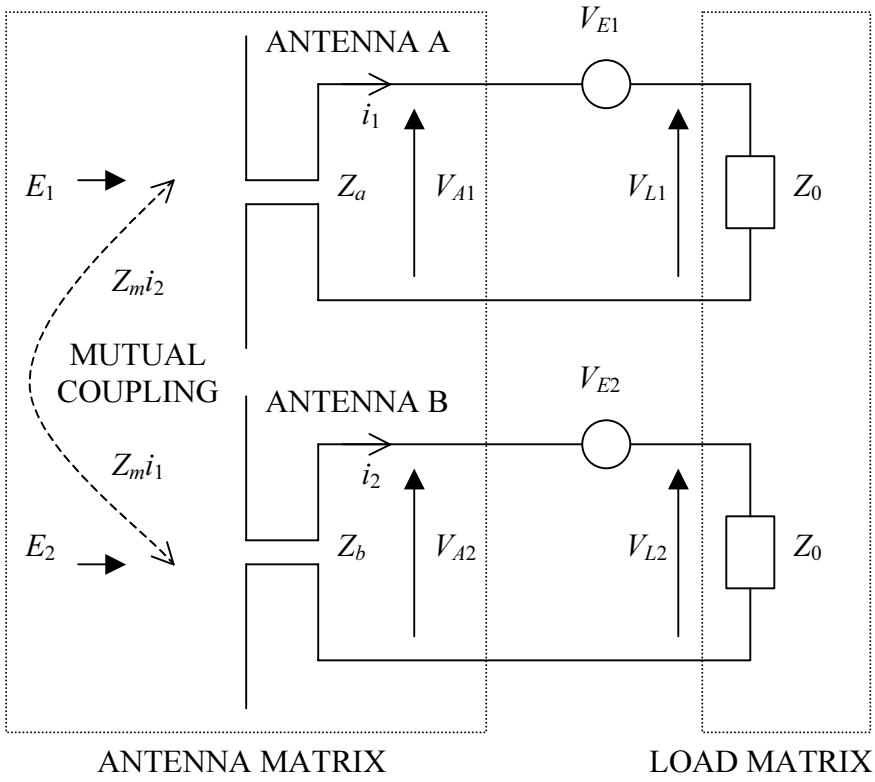

Figure 3-1 Diagram showing the two-port model of two diversity antennas

When the antennas are in receive mode, there will be an incident field on each of the two antennas, E_1 and E_2 [Vm^{-1}], as shown in Figure 3-1, which cause the two antennas to have source voltages V_{E1} and V_{E2} [V] respectively due to the induced current in the antennas, i_1 and i_2 [A]. By simple Ohm's law there will be load voltages V_{L1} and V_{L2} [V] and antenna voltages, V_{A1} and V_{A2} [V] as shown in Figure 3-1. Based on the model in Figure 3-1, each antenna can be modelled in circuit form like that in Figure 3-2, which represent antennas A and B respectively. Some of the source voltage is retained by each antenna due to the antenna self impedance and load impedance due to the mutual impedance, Z_m [Ω]. At the same time, however, voltage is gained from the other antenna represented by the current sources so voltage $Z_m i_2$ will transmit to antenna A and $Z_m i_1$ to antenna B.

The information presented here can be used to analyse the voltages induced in the antennas as will be shown in the following sections. It can be concluded at this point, however, that the impedance matrix of two diversity antennas, $\mathbf{Z}_A$, and the load impedance, $\mathbf{Z}_L$, are defined as follows:

$$\mathbf{Z}_A = \begin{pmatrix} Z_a + Z_m & Z_m \\ Z_m & Z_b + Z_m \end{pmatrix} = \begin{pmatrix} z_{11} & z_{12} \\ z_{21} & z_{22} \end{pmatrix} \tag{3.1}$$

$$\mathbf{Z}_L = \begin{pmatrix} Z_0 & 0 \\ 0 & Z_0 \end{pmatrix} \tag{3.2}$$

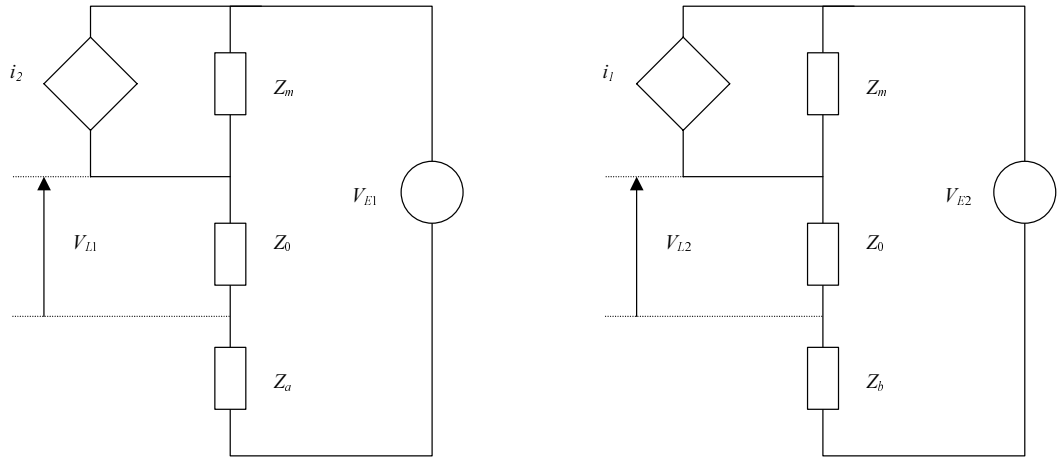

(a) (b)

Figure 3-2 Diagram showing a circuit model of two diversity antennas (a) Antenna A in Figure 3-1 and (b) Antenna B in Figure 3-1

3.1.2 Relation of impedance and scattering parameters

Since both S and Z parameters are applied in this thesis, it is important to note how they are related by using matrix conversions. To convert the Z parameters to S parameters, the following relations have been derived in linear form [Deane91]:

$$s_{11} = \frac{(z_{11} - Z_0)(z_{22} + Z_0) - z_{21}z_{12}}{(z_{11} + Z_0)(z_{22} + Z_0) - z_{21}z_{12}} \tag{3.3a}$$

$$s_{12} = \frac{2Z_0 z_{12}}{(z_{11} + Z_0)(z_{22} + Z_0) - z_{21}z_{12}} \tag{3.3b}$$

$$s_{21} = \frac{2Z_0 z_{21}}{(z_{11} + Z_0)(z_{22} + Z_0) - z_{21}z_{12}} \tag{3.3c}$$

$$s_{22} = \frac{(z_{11} + Z_0)(z_{22} - Z_0) - z_{21}z_{12}}{(z_{11} + Z_0)(z_{22} + Z_0) - z_{21}z_{12}} \tag{3.3d}$$

Likewise, the S parameters can be derived from the Z parameters as follows:

$$z_{11} = -Z_0\left(\frac{(s_{11}+1)(s_{22}-1)-s_{12}s_{21}}{(s_{11}-1)(s_{22}-1)-s_{12}s_{21}}\right) \tag{3.4a}$$

$$z_{12} = \frac{2s_{12}Z_0}{(s_{11}-1)(s_{22}-1)-s_{12}s_{21}} \tag{3.4b}$$

$$z_{21} = \frac{2s_{21}Z_0}{(s_{11}-1)(s_{22}-1)-s_{12}s_{21}} \tag{3.4c}$$

$$z_{22} = -Z_0\left(\frac{(s_{11}-1)(s_{22}+1)-s_{12}s_{21}}{(s_{11}-1)(s_{22}-1)-s_{12}s_{21}}\right) \tag{3.4d}$$

It must be noted that these equations depend on certain criteria. In the case of diversity antennas there is a reciprocity such that $z_{21} = z_{12} = Z_m$. Another criteria that must be met for equations (3.3) and (3.4) to be valid (which is true for two diversity antennas) is that:

$$Z_m < z_{11} \tag{3.5a}$$

$$Z_m < z_{22} \tag{3.5b}$$

3.1.3 Isolation and power transfer of antennas

Given the likelihood of significant mutual coupling between the antennas at the mobile there will be a low isolation between the antennas and impedance differences that will have an effect on diversity. This section therefore establishes the theory behind this, which will be applied to diversity computation. The mutual coupling and antenna effects have to be considered when:

1. The two antennas do not have the same impedance and are insufficiently matched (i.e. < 20dB return loss). Hence power transfer will be different at the two branches.
2. There is high mutual impedance (i.e < 20dB transmission loss) between the antennas that causes some power to be lost to the other antenna while power is also gained from the other antenna.

Applying the impedance matrices can determine both of these effects simultaneously and so they will be applied to diversity antennas. From Figure 3-1 it can be seen that the antenna and load networks are connected in series because of the position of the voltage source [Balab69 pp172]. Using fundamental theory of impedance networks connected in series [Balab69 pp173] then the

load voltage vector, $\mathbf{V}_L$, from Figure 3-1 can be related to the source voltage vector, $\mathbf{V}_E$, as used by Vaughan and Bach Andersen [Vaug87] by:

$$\mathbf{V}_L = \mathbf{V}_E \mathbf{Z}_L \left(\mathbf{Z}_A + \mathbf{Z}_L\right)^{-1} \tag{3.6}$$

where $\mathbf{V}_L$ and $\mathbf{V}_E$ are represented as vectors:

$$\mathbf{V}_E = \begin{pmatrix} V_{E1} \\ V_{E2} \end{pmatrix} \qquad \mathbf{V} = \begin{pmatrix} V_1 \\ V_2 \end{pmatrix} \tag{3.7}$$

Therefore by using standard two by two matrix algebra:

$$\mathbf{Z}_L \left(\mathbf{Z}_A + \mathbf{Z}_L\right)^{-1} = \frac{1}{\left(z_{11} + Z_0\right)\left(z_{22} + Z_0\right) - z_{12} z_{21}} \begin{pmatrix} \left(z_{22} + Z_0\right) Z_0 & -Z_0 z_{12} \\ -Z_0 z_{21} & \left(z_{11} + Z_0\right) Z_0 \end{pmatrix} \tag{3.8}$$

For the conjugate voltages the Hermitan transpose function is used [Vaug87]:

$$\left(\mathbf{Z}_L \left(\mathbf{Z}_A + \mathbf{Z}_L\right)^{-1}\right)^H = \frac{1}{\left(z_{11}^* + Z_0\right)\left(z_{22}^* + Z_0\right) - z_{12}^* z_{21}^*} \begin{pmatrix} \left(z_{22}^* + Z_0\right) Z_0 & -Z_0 z_{21}^* \\ -Z_0 z_{12}^* & \left(z_{11}^* + Z_0\right) Z_0 \end{pmatrix} \tag{3.9}$$

The resultant voltages can be derived by substituting equations (3.8) and (3.9) into (3.6) and further to this they can be simplified into S-Parameters when equation (3.3) is used. Therefore:

$$V_{L1} = V_{E1} \frac{s_{21}\left(z_{22} + Z_0\right)}{2 z_{21}} - V_{E2} \frac{s_{21}}{2} \tag{3.10}$$

$$V_{L2}^* = V_{E2}^* \frac{s_{12}^*\left(z_{11}^* + Z_0\right)}{2 z_{12}^*} - V_{E1}^* \frac{s_{21}^*}{2} \tag{3.11}$$

This creates a mutual coupling theory that can be used for calculating correlation and branch power ratios. The voltage transfer due to antenna matching and mutual coupling is best represented by a transfer matrix, $\mathbf{S}_T$:

$$\mathbf{V}_L = \begin{pmatrix} \frac{s_{21}\left(z_{22} + Z_0\right)}{2 z_{21}} & -\frac{s_{12}}{2} \\ -\frac{s_{21}}{2} & \frac{s_{12}\left(z_{11} + Z_0\right)}{2 z_{12}} \end{pmatrix} \mathbf{V}_E = \begin{pmatrix} s_{t1} & s_r \\ s_r & s_{t2} \end{pmatrix} \mathbf{V}_E = \mathbf{S}_T \mathbf{V}_E \tag{3.12}$$

The matrix therefore contains the isolation components, s_r, and the transfer components, s_{tn}. Another useful point to note is that when the antennas have the same impedance or when they are both matched then $s_{t1} = s_{t2} = s_t$. The Hermitan transpose can be used again to determine the conjugate voltages.

From equation (3.12) it can be concluded that when there is high mutual coupling, then both s_t and s_r are significant and when there are mismatches with low mutual coupling between the antennas then only s_t is significant.

As well as the transfer matrix, it is often useful to apply the inverse. Given that there is no cross coupling in the load matrix, $\mathbf{Z}_L$, and that reciprocity is maintained (i.e. $z_{12} = z_{21}$) then the following applies:

$$\mathbf{V}_E = \mathbf{Z}_L^{-1}(\mathbf{Z}_A + \mathbf{Z}_L)\mathbf{V}_L = \mathbf{S}_T^{-1}\mathbf{V}_L \tag{3.13}$$

Therefore:

$$\mathbf{S}_T^{-1} = \mathbf{Z}_L^{-1}(\mathbf{Z}_A + \mathbf{Z}_L) = \frac{1}{Z_0}\begin{pmatrix} z_{11}+Z_0 & z_{12} \\ z_{21} & z_{22}+Z_0 \end{pmatrix} = \frac{1}{s_{t1}s_{t2} - s_r^2}\begin{pmatrix} s_{t2} & -s_r \\ -s_r & s_{t1} \end{pmatrix} \tag{3.14}$$

Another useful matrix is that used to find the voltage at the output flange of the antennas, $\mathbf{V}_A$, in terms of the load voltage, $\mathbf{V}_L$. Again, under the assumption of reciprocity, this can be derived as follows:

$$\mathbf{V}_A = \mathbf{Z}_A(\mathbf{Z}_A + \mathbf{Z}_L)^{-1}\mathbf{V}_E = \mathbf{Z}_A(\mathbf{Z}_A + \mathbf{Z}_L)^{-1}\mathbf{Z}_L^{-1}(\mathbf{Z}_A + \mathbf{Z}_L)\mathbf{V}_L = \mathbf{Z}_A\mathbf{Z}_L^{-1}\mathbf{V}_L \tag{3.15}$$

By simple matrix algebra:

$$\mathbf{Z}_A\mathbf{Z}_L^{-1} = \frac{1}{Z_0}\begin{pmatrix} z_{11} & z_{12} \\ z_{21} & z_{22} \end{pmatrix} \tag{3.16}$$

3.1.4 Polarisation

It is common to have antennas at the mobile terminal which will have some significant cross polarisation often because the antennas are implemented in small sizes with imperfect ground planes. If two differing antennas are used then they will have different co-polar and cross-polar field patterns. Once the antennas are brought closer together then they will begin to interact with each other such that they can affect their polarisations. Therefore, to evaluate polarisation at the mobile the polarisations need to be calculated when the other antenna is present and then it may be the case that some polarisation diversity is present.

3.1.5 Antenna field patterns

More so than the relative polarisations, the field patterns will be affected on each antenna when in the presence of the other. It may be the case that the two field patterns become directional, which can create a significant angular diversity between the antennas.

3.1.6 Mean effective gain

The mean effective gain (MEG) is a measure of the average gain of an antenna in a mobile environment based on the angle of arrival (AOA) as used to evaluate complex correlation. This is an important feature of an antenna to determine how effective it will be in a mobile fading environment. In simple terms, MEG is defined as the power received by an antenna in a mobile fading environment with a given AOA compared to the power that would be received at the same point from an isotropic antenna. Therefore, a high MEG will occur if the antenna has high gain in the direction as where the majority of incoming signals are. Otherwise, the MEG will be low since the antenna will not receive many signals. This therefore shows how effective an antenna will be in a mobile fading environment regardless of whether it has a high gain or efficiency.

While having an antenna in the presence of the other there may be de-correlation due to the relative polarisations or field patterns but this can at the same time reduce the MEG of each antenna. Therefore reduced MEG will cause reduced system gain as explained in the previous chapter. It is therefore important to evaluate the mean effective gain of the antennas to determine how diversity will be affected. To evaluate the mean effective gain, the following equation is used [Taga90] in linear form:

$$\mathrm{MEG} = \int_0^{\pi}\int_0^{2\pi}\left(\frac{XPR}{1+XPR}G_\theta(\theta,\phi)p_\theta(\theta,\phi)+\frac{1}{1+XPR}G_\phi(\theta,\phi)p_\phi(\theta,\phi)\right)\sin\theta\, d\phi\, d\theta \tag{3.17}$$

The notations used in equation (3.17) are the same as the notations used in equation (2.5) only that the vertical and horizontal polarised gains $G_\theta(\theta,\phi)$ and $G_\phi(\theta,\phi)$ in linear form relative to an isotropic antenna are applied in this situation. The mean effective gain can be used to derive the signal to noise ratio factor, L, by substituting into equation (2.16) as follows:

$$L = \frac{\max(\mathrm{MEG}_1, \mathrm{MEG}_2)}{\mathrm{MEG}_0} \tag{3.18}$$

where MEG_1 and MEG_2 refer to antennas 1 and 2 respectively and MEG_0 is a reference used for the single antenna that would otherwise be present with no diversity. Also the branch power ratio, k, can be derived in linear form as follows by using equation (2.13) so that:

$$k = \min\left(\frac{\mathrm{MEG}_2}{\mathrm{MEG}_1}, \frac{\mathrm{MEG}_1}{\mathrm{MEG}_2}\right) \tag{3.19}$$

3.2 Polarisation Diversity at the Mobile

As explained in the previous chapter, research has been carried out in the past with regard to polarisation diversity antennas at the base station. Theoretical analysis has been undertaken by Vaughan [Vaug90] and Kozono [Koz84] although it is more applicable to the base station. Scenarios encountered at the mobile terminal including antenna effects and angle of arrival are not included in these two models so this section will present a new theoretical model suited to the mobile terminal. To begin with, the polarisation diversity in the fading environment will be considered and then the antenna effects will be introduced.

3.2.1 Polarisation diversity in the fading environment

Due to the scattering in the vertical and horizontal planes being different it is assumed that the vertical and horizontal polarisations in a fading environment are independent references. This gives scope to find de-correlated polarised sources. While they may be de-correlated, the cross polarisation power is often considerably weaker than the vertical so the low correlation is often at the expense of loss in efficiency.

Before resolving correlation and efficiency, polarisation angles need to be defined as shown in Figure 3-3. The polarisations are first of all spaced with an angular spacing, Ω [°], symmetrical to each other and then they are both rotated by angle, α [°], relative to the vertical; hence the line of rotation in Figure 3-3 is a line of symmetry between branches 1 and 2. Angle Ω is considered by Kozono [Koz84] only and angle α is considered by Vaughan [Vaug90] only. At the mobile it is necessary to integrate the two models together since the relative polarisations constantly change and also the terminal can be rotated. It is assumed also by both Vaughan and Kozono that there is one single arrival angle, which is by no means the case at the mobile.

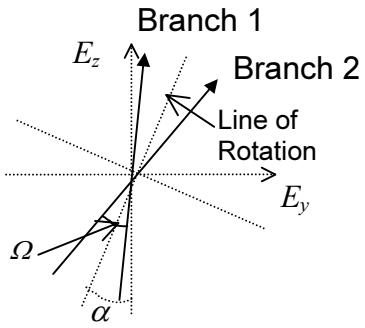

Figure 3-3 Diagram showing the polarisation angles for two polarisation diversity antennas

Referring to Figure 3-3, the voltage induced in the two linear polarisation branches can be made into a matrix shown in equation (3.20) to represent the *E*-fields in terms of relative vertical and horizontal fields, E_z and E_y [Vm^{-1}]. These fields have a Hertzian dipole field distribution proportional to $\sin\phi$ and $\sin\theta$ since any polarisation at a given point cannot distribute uniformly and needs an appropriate model. A third polarisation, E_x, does exist although with a uniform angle of arrival in azimuth it becomes irrelevant since the horizontal polarisation always adds up to the same value whatever the polarisation. Therefore the horizontal polarisation can be considered as E_y which can be determined by the cross polar ratio (*XPR*), creating a simpler model.

$$\begin{pmatrix} E_{\theta 1}(\theta,\phi) & E_{\phi 1}(\theta,\phi) \\ E_{\theta 2}(\theta,\phi) & E_{\phi 2}(\theta,\phi) \end{pmatrix} \equiv \begin{pmatrix} bf & ae \\ df & ce \end{pmatrix} \begin{pmatrix} E_z & 0 \\ 0 & E_y \end{pmatrix} \tag{3.20}$$

where:

$$a = \sin\left(\alpha + \frac{\Omega}{2}\right) \qquad c = \sin\left(\alpha - \frac{\Omega}{2}\right) \tag{3.21) (3.22}$$

$$b = \cos\left(\alpha + \frac{\Omega}{2}\right) \qquad d = \cos\left(\alpha - \frac{\Omega}{2}\right) \tag{3.23) (3.24}$$

$$e = \cos\phi \qquad f = \sin\theta \tag{3.25) (3.26}$$

The vectors can be resolved from equation (3.20) to give:

$$E_{\theta 1}(\theta,\phi) \equiv bfE_z \qquad E_{\theta 2}(\theta,\phi) \equiv dfE_z \tag{3.27) (3.28}$$

$$E_{\phi 1}(\theta,\phi) \equiv aeE_y \qquad E_{\phi 2}(\theta,\phi) \equiv ceE_y \tag{3.29) (3.30}$$

where:

$$E_z = e^{j(\omega t-\varphi_1)} \tag{3.31}$$

$$E_y = e^{j(\omega t-\varphi_2)} \tag{3.32}$$

Consequently equations (3.27) to (3.30) can be substituted into equation (2.5) to give:

$$\rho_{12} = \frac{\int_0^{\pi}\int_0^{2\pi}\left(XPR.\sin^2\theta p_\theta(\theta,\phi) + \tan\left(\alpha+\frac{\Omega}{2}\right)\tan\left(\alpha-\frac{\Omega}{2}\right)\cos^2\phi p_\phi(\theta,\phi)\right)\sin\theta d\phi d\theta}{\sqrt{\left(\int_0^{\pi}\int_0^{2\pi}\left(XPR.\sin^2\theta p_\theta(\theta,\phi) + \tan^2\left(\alpha+\frac{\Omega}{2}\right)\cos^2\phi p_\phi(\theta,\phi)\right)\sin\theta d\phi d\theta\right)\left(\int_0^{\pi}\int_0^{2\pi}\left(XPR.\sin^2\theta p_\theta(\theta,\phi) + \tan^2\left(\alpha-\frac{\Omega}{2}\right)\cos^2\phi p_\phi(\theta,\phi)\right)\sin\theta d\phi d\theta\right)}} \tag{3.33}$$

given that $E_z E_z^* = 1$ and $E_y E_y^* = 1$ from equations (3.31) and (3.32). It is interesting to note here that the envelope correlation, ρ_e, is in agreement with both Vaughan [Vaug90, eq. (21)] and Kozono [Koz84, eq. (13)] when the angles are set appropriately. In the case of Vaughan, the angle of arrival is set to a single incoming angle normal to the antennas so $p_\theta(\theta,\phi) = p_\phi(\theta,\phi) = \delta(\phi)\delta(\theta)$ and then Ω is fixed at 90°. The envelope correlation, given a Rayleigh environment resolves to be:

$$\rho_e = \frac{\left(XPR + \tan(\alpha+45)\tan(\alpha-45)\cos^2\phi_0\right)^2}{\left(XPR + \tan^2(\alpha+45)\cos^2\phi_0\right)\left(XPR + \tan^2(\alpha-45)\cos^2\phi_0\right)} \tag{3.34}$$

In the case of Kozono, the incoming angle is at a fixed angle in azimuth, ϕ_0, so that the angle of arrival is changed to $\delta(\phi-\phi_0)\delta(\theta)$, α is fixed at 0°. Therefore the envelope correlation becomes:

$$\rho_e = \left(\frac{\tan^2\left(\frac{\Omega}{2}\right)\cos^2\phi_0 - XPR}{\tan^2\left(\frac{\Omega}{2}\right)\cos^2\phi_0 + XPR}\right)^2 \tag{3.35}$$

Equation (3.33) is plotted in Figure 3-4 as complex correlation versus angle Ω for fixed values of α. In this situation, the complex correlation has only a real part so no imaginary component is plotted. The angle of arrival explained in chapter 2 is assumed here, uniform in azimuth and Gaussian in elevation. To help visualise the orientation of the two polarisations some diagrams have been added. The ±45° configuration is found when angle Ω is 90° and angle α is either 0° or 90°. In the latter case, the correlation is not the same but inverse as can be seen in Figure 3-4 because at such an orientation the two polarisations are in antiphase. The antennas are in V/H

configuration when Ω is 90° and α is 45°. In this case, the correlation is zero since the vertical and horizontal polarisations are indipendent.

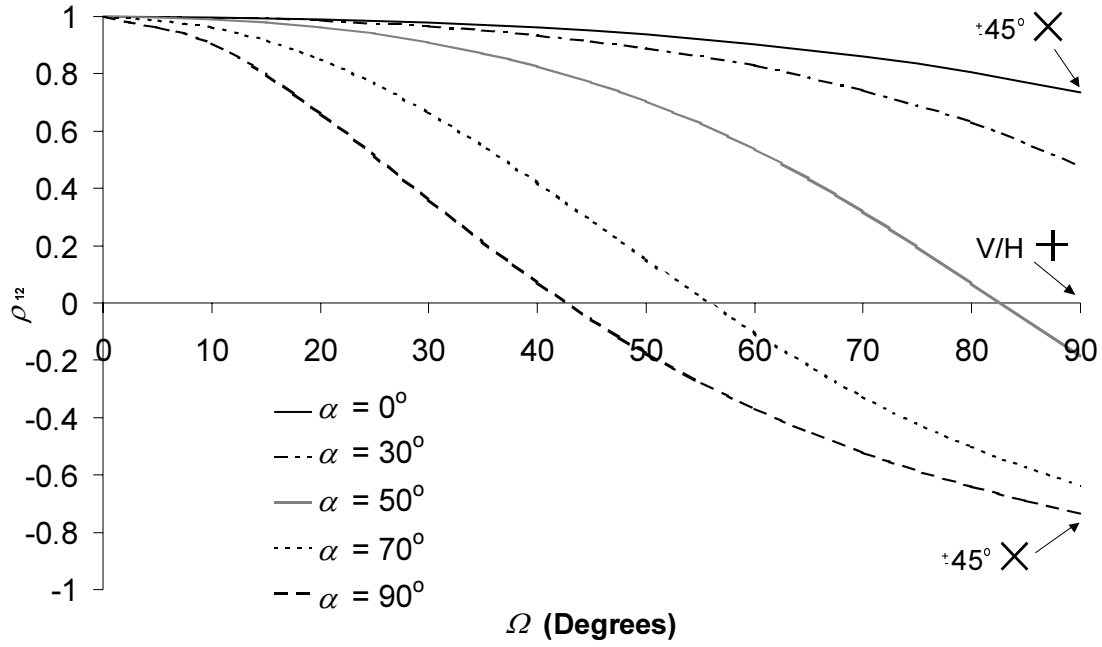

Figure 3-4 Graph showing the polarisation correlation at relative polarisations in space at the mobile with variable angular difference, Ω, and fixed values of rotation, α

As can be seen in Figure 3-4, there is total de-correlation at different angles of rotation and spacing. Not all of these points will necessarily give maximum diversity gain since the branch power ratio and the efficiency loss still need to be considered. To find these two quantities it will be necessary to calculate the MEG given the information used for correlation.

Therefore, to derive the relative gain in linear form based on *E*-fields:

$$G_{\theta 1}(\theta,\phi) = E_{z1}E_{z1}^{*} = b^2 f^2 \qquad G_{\phi 1}(\theta,\phi) = E_{y1}E_{y1}^{*} = a^2 e^2 \tag{3.36) (3.37}$$

$$G_{\theta 2}(\theta,\phi) = E_{z2}E_{z2}^{*} = d^2 f^2 \qquad G_{\phi 2}(\theta,\phi) = E_{y2}E_{y2}^{*} = c^2 e^2 \tag{3.38) (3.39}$$

Substituting into equation (3.38) to resolve the MEG on both branches, it is then possible to resolve the branch power ratio, *k*, using equation (3.39). As with correlation in Figure 3-4, *k* is plotted in Figure 3-5 and this shows that *k* is 0dB when α is 0° or 90°. It can also be noted that *k* is unity at the ±45° configuration and there is a maximum branch power ratio of 14dB when in the V/H configuration.

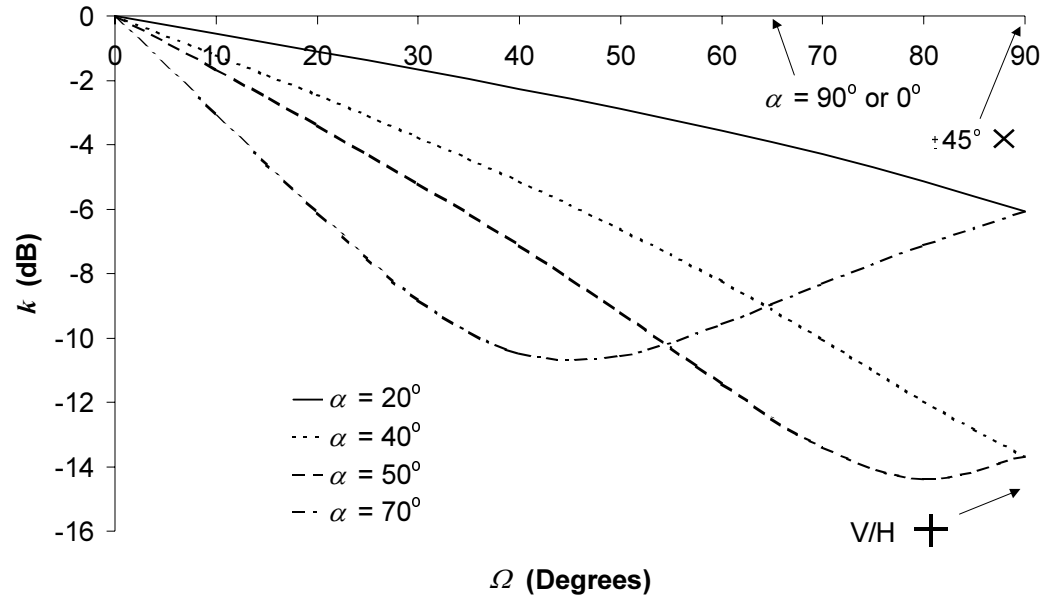

Figure 3-5 Graph showing the branch power ratio at relative polarisations in space at the mobile with variable angular difference, Ω, and fixed values of rotation, α

It is possible to also derive the efficiency loss, L, once a reference is defined for MEG_0 in equation (3.40). At the base station, the reference has often been considered as the vertical. At the mobile, this is not particularly useful since the mobile terminal may not necessarily be typically vertical. Therefore it would be appropriate to define an appropriate reference angle, α_0, from the vertical as in Figure 3-3. The relative gain can therefore be defined as:

$$G_{\theta 0}(\theta,\phi) = E_{z0}E_{z0}^{*} = \cos^2\alpha_0 f^2 \qquad G_{\phi 0}(\theta,\phi) = E_{y0}E_{y0}^{*} = \sin^2\alpha_0 e^2 \tag{3.40) (3.41}$$

Using equations (3.40) and (3.41) it is now possible to derive L for all angles and plot the results as with k and correlation in Figure 3-6. The same angle of arrival model as used for correlation is used here. An arbitrary value of α_0 is chosen as 60^o similar to a typical angle at talk position.

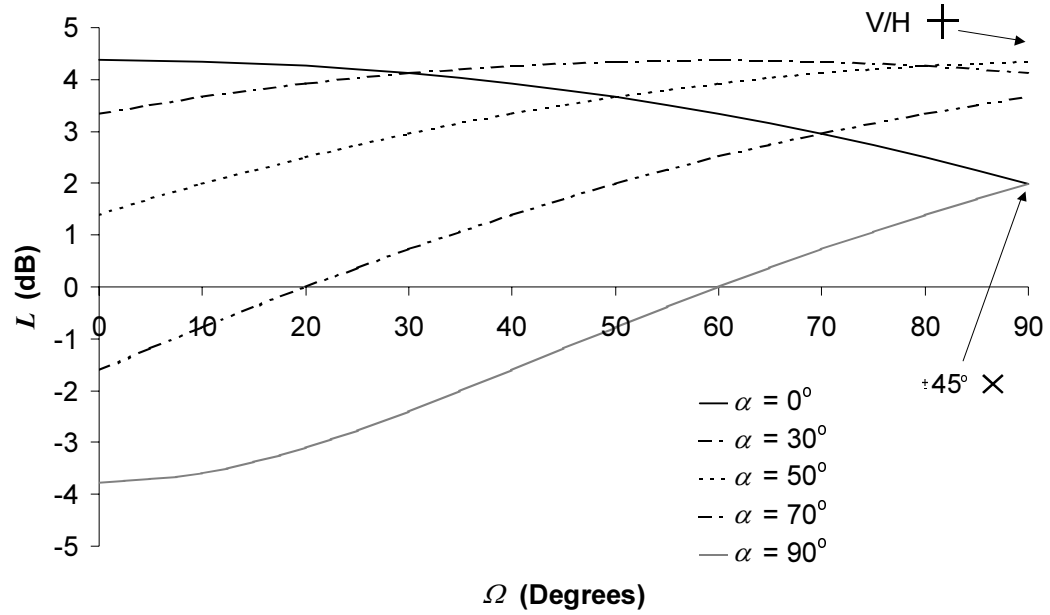

Figure 3-6 Graph showing the efficiency loss at relative polarisations in space at the mobile with variable angular difference, Ω, and fixed values of rotation, α

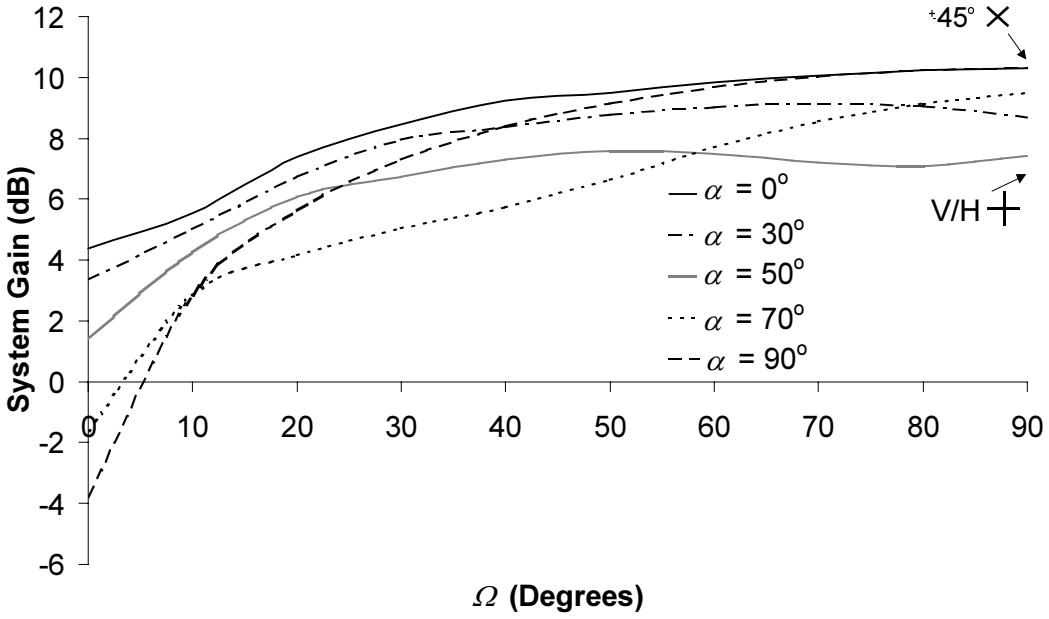

Figure 3-7 Graph showing the system gain at relative polarisations in space at the mobile with variable angular difference, Ω, and fixed values of rotation, α

It is therefore possible to plot system gain in the same format in Figure 3-7 when in talk position so that α_0 is arbitrarily chosen to be 60^o. Similar characteristics occur when other angles of α_0 are used although if they are near the vertical, then there will be a drop in maximum diversity gain as much as 2.5dB. Figure 3-7 is a useful graph to illustrate the difference between system gain and diversity gain explained in section 2.1.5. For example, when Ω is 0^o then the gain is by no means

diversity gain since the branches are correlated in this case. In such a case, the diversity gain is unity as the diversity combiner is dormant. At different angles of rotation, α, the maximum branch signal in one of the branches is either greater than or less than the reference at α_o. Consequently, L is either a gain or a loss which is equal to the resulting system gain in this case. Another point to note is that the system gain is over 10dB at $\pm 45^o$, which is the maximum theoretical diversity gain for a selection diversity combiner in Figure 2-2. This is due to the fact that the diversity gain in this case is 8.3dB, due to non zero correlation and L is 1.98dB so that adding these two together gives an overall system gain of 10.28dB.

In conclusion, the maximum system gain occurs when there is $\pm 45^o$ configuration (i.e $\Omega = 90^o$ and $\alpha = 90^o$ or 0^o). It must be noted, however, that in this configuration, the diversity combiner is not working to its full performance because there is not total de-correlation. For this to be true Ω needs to be closed up to 55^o with α at 90^o (i.e. $\pm 62.5^o$ configuration). This shows an important case, that although the output is maximum at $\pm 45^o$, the diversity combiner is not performing its full potential. Therefore, the improved system performance is partly due to the diversity system, but also the increase MEG from a dual antenna system. This method distinguishes the two contributions.

3.2.2 Effects of cross-polar ratio on polarisation diversity

Before going further and considering antenna effects it is important to note that polarisation diversity is heavily dependent on the cross polar ratio, *XPR*. As already discussed, it is assumed to be 6dB although this could vary considerably depending on the fading environment. In the case of polarisation diversity it is necessary to have as much cross polarisation as possible (i.e. *XPR* is as low as possible). In suburban and rural environments, *XPR* is likely to increase and so there is a maximum *XPR* to achieve polarisation diversity. For *XPR* lower than 6dB, diversity improves although when increased there is still some scope for diversity until the *XPR* has reached 15dB in order to achieve a suitable de-correlation, a reasonable branch power ratio and signal to noise ratio loss. Beyond this point the signal to noise ratio loss reduces below –3dB at $\pm 45^o$ configuration, resulting in an output that has no gain above the original reference. Therefore polarisation diversity is not suitable for rural environments that have such *XPR* characteristics.

3.2.3 Effects of angle of arrival on polarisation diversity

It has already been emphasised that the standard deviation on the angle of arrival model can change rapidly when building heights vary [Taga90] although the mean value does not change considerably. To identify the scale by which correlation changes Figure 3-8 shows the correlation

for fixed rotation angle, α, when the standard deviation, σ_A, is 20°, 40° and 80°. As can be seen there is little change in the correlation so the effects of varying angle of arrival can be assumed negligible. Branch power ratio and efficiency loss, L, will not be affected since the mean effective gain of the antennas will both change by the same factor. Therefore there will be negligible effect on the overall system gain due to change in AOA.

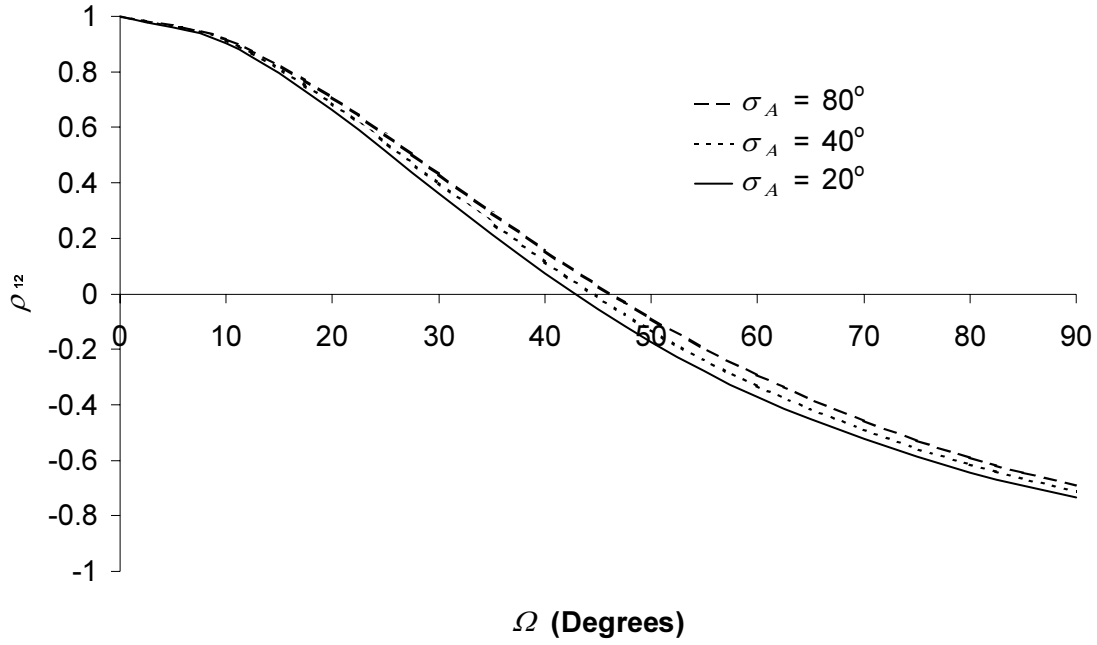

Figure 3-8 Graph showing the angle of arrival effects on correlation with the angle of rotation, α, fixed at 90° and variable angular difference, Ω

3.2.4 Antenna effects on polarisation diversity characterisation

In the case of measuring the polarisation diversity in the fading environment, there are antenna properties to consider, which will affect what correlation is measured at the receiver. Further to this the antennas may have different mean effective gain, which will affect branch power ratio and efficiency. A useful way to measure polarisation diversity effectively is by using a loop antenna for the horizontal polarisation (since it only has E_ϕ polarisations to measure E_y) and a vertical dipole with only E_θ components to measure E_z [Cox86]. The two antennas can be attenuated at the output as necessary to change their relative polarisations as in Figure 3-3. Measurement of the *XPR* can also be found from such measurements.

For the measurement scenario, it is necessary to derive the load matrix below by combining equations (3.20) and equations (3.12):

$$\begin{pmatrix} E_{L\theta 1}(\theta,\phi) & E_{L\phi 1}(\theta,\phi) \\ E_{L\theta 2}(\theta,\phi) & E_{L\phi 2}(\theta,\phi) \end{pmatrix} \equiv \mathbf{S}_T \begin{pmatrix} bf & ae \\ df & ce \end{pmatrix} \begin{pmatrix} E_z & 0 \\ 0 & E_y \end{pmatrix} \tag{3.42}$$

which makes equation (3.33) for the complex correlation become:

$$\rho_{12} = \frac{\int_0^{\pi}\int_0^{2\pi} \begin{pmatrix} XPR.(s_{t1}b + s_r d)(s_{t2}^* d + s_r^* b) f^2 p_\theta(\theta,\phi) \\ +(s_{t1}a + s_r c)(s_{t2}^* c + s_r^* a) e^2 p_\phi(\theta,\phi) \end{pmatrix} \sin\theta d\phi d\theta}{\sqrt{\left(\int_0^{\pi}\int_0^{2\pi} \left(XPR.|s_{t1}b + s_r d|^2 f^2 p_\theta(\theta,\phi) + |s_{t1}a + s_r c|^2 e^2 p_\phi(\theta,\phi)\right)\sin\theta d\phi d\theta\right)} \sqrt{\left(\int_0^{\pi}\int_0^{2\pi} \left(XPR.|s_{t2}d + s_r b|^2 f^2 p_\theta(\theta,\phi) + |s_{t2}c + s_r a|^2 e^2 p_\phi(\theta,\phi)\right)\sin\theta d\phi d\theta\right)}} \tag{3.43}$$

When the isolation, s_r, is greater than –20dB then it will have significant impact on measurement of the correlation. Complexity arises when the isolation and possibly matching conditions for s_{t1} and s_{t2} change when the respective polarisations change. Low isolation will change the correlation due to power being exchanged between branches. If there is negligible mismatch, with return loss below –20dB, and if s_r is below –20dB then equation (3.43) will reduce to equation (3.33).

Another helpful item to note is that the antennas are not necessarily polarisation pure (i.e. there is a significant cross polar component that is not negligible compared to the co polar component.) Like isolation it will create further changes to the optimum configuration resulting in further complexities within the structure since the polarisations of one antenna change in the presence of the other. If the two antennas have the same polarisation impurity then the following matrix, **M**, could be applied:

$$\mathbf{M} = \begin{pmatrix} 1 & V_{XP}/V_{CP} \\ V_{XP}/V_{CP} & 1 \end{pmatrix} = \begin{pmatrix} 1 & m \\ m & 1 \end{pmatrix} \tag{3.44}$$

where V_{CP} is the co polar voltage of the antenna field and V_{XP} is the cross polar voltage. It is then possible to multiply the matrix **M** by $\mathbf{S}_T$ in equation (3.42) and then complex correlation becomes:

$$\rho_{12} = \frac{\int_0^{\pi}\int_0^{2\pi} \begin{pmatrix} XPR.(s_{t1}(b+am) + s_r(d+cm))(s_{t2}^*(d+cm) + s_r^*(b+am)) f^2 p_\theta(\theta,\phi) \\ +(s_{t1}(a+bm) + s_r(c+dm))(s_{t2}^*(c+dm) + s_r^*(a+bm)) e^2 p_\phi(\theta,\phi) \end{pmatrix} \sin\theta d\phi d\theta}{\sqrt{\int_0^{\pi}\int_0^{2\pi} \begin{pmatrix} XPR.|s_{t1}(b+am) + s_r(d+cm)|^2 f^2 p_\theta(\theta,\phi) \\ +|s_{t1}(a+bm) + s_r(c+dm)|^2 e^2 p_\phi(\theta,\phi) \end{pmatrix} \sin\theta d\phi d\theta} \sqrt{\int_0^{\pi}\int_0^{2\pi} \begin{pmatrix} XPR.|s_{t2}(d+cm) + s_r(b+am)|^2 f^2 p_\theta(\theta,\phi) \\ +|s_{t2}(c+dm) + s_r(a+bm)|^2 e^2 p_\phi(\theta,\phi) \end{pmatrix} \sin\theta d\phi d\theta}} \tag{3.45}$$

If the two antennas have different polarisation impurities then the mathematics are very complex so they are not shown for clarity.

Branch power ratio and efficiency are affected by the gain patterns of the antennas and the fact that power is being exchanged between them. Therefore equations (3.34) to (3.37) can be modified as follows in order to account for antenna effects in this situation.

$$G_{\theta 1}(\theta,\phi) = E_{zL1}E_{zL1}^{*} = \left|s_{t1}b + s_r d\right|^2 f^2 G_{P\theta 1}(\theta,\phi) \tag{3.46}$$

$$G_{\phi 1}(\theta,\phi) = E_{yL1}E_{yL1}^{*} = \left|s_{t1}a + s_r b\right|^2 e^2 G_{P\phi 1}(\theta,\phi) \tag{3.47}$$

$$G_{\theta 2}(\theta,\phi) = E_{zL2}E_{zL2}^{*} = \left|s_{t2}d + s_r b\right|^2 f^2 G_{P\theta 2}(\theta,\phi) \tag{3.48}$$

$$G_{\phi 2}(\theta,\phi) = E_{zL2}E_{zL2}^{*} = \left|s_{t2}c + s_r a\right|^2 e^2 G_{P\phi 2}(\theta,\phi) \tag{3.49}$$

where $G_{P\theta n}$ and $G_{P\phi n}$ represent the gain patterns of the antennas at a given angle when in the presence of the other antenna.

In terms of evaluating polarisation diversity of two mobile terminal antennas, this section does not have any direct application since typical mobile antennas have E_θ and E_ϕ components rather than vertical and horizontal polarisations. Therefore a different method of evaluation has to be used that is inherent within angular diversity, which will be discussed in the next chapter. The purpose of presenting this section is purely in the interests of showing when measuring the polarisation diversity in a fading environment and how antennas used would affect that. Evaluating the polarisation diversity performance of two mobile terminal antennas will be presented in the next chapter.

3.2.5 Third polarisation for non uniform azimuth AOA

Since there is a uniform azimuth AOA, the third polarisation, E_x, is not relevant although with a non uniform angle of arrival the third polarisation will have a different mean power to that of E_y so therefore some *XPR* will exist in the horizontal plane to give some diversity. Measurement of this *XPR* is complicated and cannot be achieved with antenna models available. Therefore it can only be derived based on simulations from AOA statistics in the azimuth plane and summing the signals as appropriate for the two polarisations. Using this third polarisation will mean that the resultant polarisation correlation will vary with the azimuth angle at which the antenna is positioned in.

3.3 Spatial and Angular Diversity at the Mobile Terminal

Although spatial and angular diversity are two separate types of diversity in their own right, it is difficult to ignore the two in most mobile terminal applications since it is often the case that there is always an element of both spatial and angular diversity working simultaneously in mobile terminal diversity antennas. Therefore this section will show how both spatial and angular diversity are defined at the mobile and how they work together.

3.3.1 Spatial diversity in the fading environment

As with polarisation diversity, spatial diversity can be considered in the fading environment without the antenna effects. It is well known, as explained in the previous chapter, that the theoretical complex correlation for antennas horizontally spaced by distance, d, is $J_0(\beta d)$. In the case of mobile handsets and many other mobile terminals the antennas are not only horizontally spaced but vertically spaced also. Given that there is not a uniform AOA distribution in elevation the correlation needs to be modelled differently since the derivation of $J_0(\beta d)$ assumes a uniform AOA. Figure 3-9 shows a modified version of the spatial separation of two diversity branches in space [Saund99] with the vertical separation, h, taken into account as well as the horizontal separation, d.

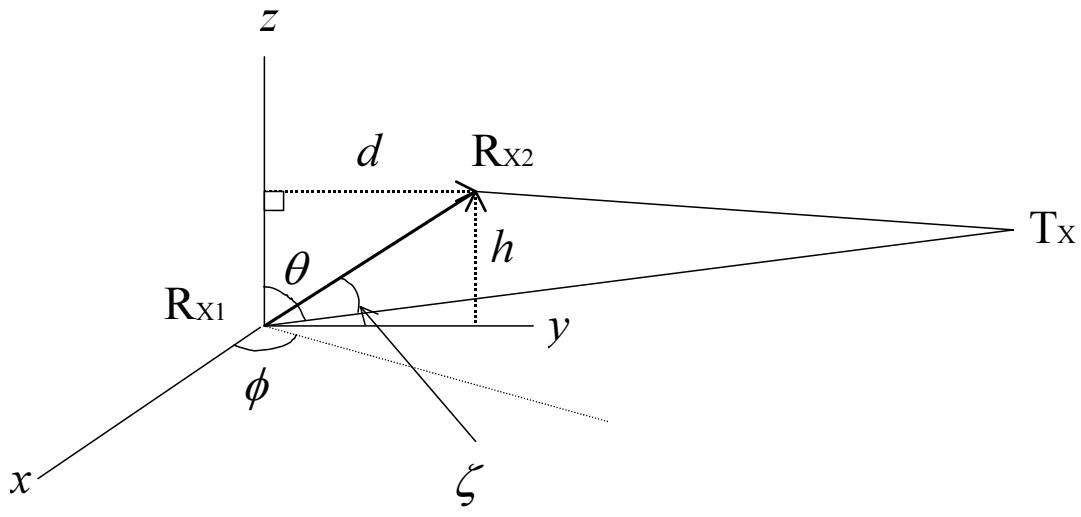

Figure 3-9 Diagram showing the vertical and horizontal separation for spatial diversity at the mobile

By simple trigonometry shown in Figure 3-9 it is possible to derive the phase difference between the branches versus angle ζ assuming d and h are negligible compared to the distance from the

scatterers or the Tx point as shown in Figure 3-9. If only the vertical polarisation is chosen (although polarisation of the antennas does not matter as long as they are both the same) then, the *E*-field matrix can be defined in terms of relative *E*-fields [Vm^{-1}] with spacing for a single polarisation:

$$\begin{pmatrix} E_{\theta 1}(\theta,\phi) & E_{\phi 1}(\theta,\phi) \\ E_{\theta 2}(\theta,\phi) & E_{\phi 2}(\theta,\phi) \end{pmatrix} \equiv \begin{pmatrix} 1 & 0 \\ e^{j\beta\left(\sqrt{d^2+h^2}\right)\cos\zeta} & 0 \end{pmatrix} \begin{pmatrix} E_{\theta}(\theta,\phi) & 0 \\ 0 & E_{\phi}(\theta,\phi) \end{pmatrix} \tag{3.50}$$

Therefore:

$$E_{\theta 1}(\theta,\phi) = E_{\theta}(\theta,\phi) \tag{3.51}$$

$$E_{\theta 2}(\theta,\phi) = E_{\theta}(\theta,\phi) e^{j\beta\left(\sqrt{d^2+h^2}\right)\cos\zeta} \tag{3.52}$$

where β With equations (3.51) and (3.52) substituted into equation (2.5) the complex correlation becomes:

$$\rho_{12} = \int_0^{\pi}\int_0^{2\pi} e^{j\beta\left(\sqrt{d^2+h^2}\right)\cos\zeta} p(\theta,\phi)\sin\theta d\phi d\theta \tag{3.53}$$

Derivation of ζ can be found in Appendix C in terms of angles θ and ϕ as follows:

$$\cos\zeta = \sin(\theta + \delta\theta \operatorname{sgn}\phi)\sin\phi \tag{3.54}$$

Where:

$$\delta\theta = \tan^{-1}\left(\frac{h}{d}\right) \tag{3.55}$$

By considering only horizontal separation (i.e. h = 0) it is possible to simplify equation (3.53) further [Abm72]:

$$\rho_{12} = \int_0^{\pi} J_0(\beta d \sin\theta) p_{\theta}(\theta)\sin\theta d\theta \tag{3.56}$$

If h is equal to zero and $P_{\theta}(\theta,\phi)$ is made equal to $\delta(\theta)$ then equation (3.53) reduces to $J_0(\beta d)$ as would be expected. Figure 3-10 shows a comparison with the Bessel function of the correlation versus d when there is 20° standard deviation and 40° standard deviation. As can be seen there is negligible difference resulting in no significant change to the diversity gain.

However, when there is vertical separation, $J_0(\beta d)$ no longer holds as an approximation when referring to Figure 3-11 where correlation magnitude is plotted versus d for fixed values of h. The

standard deviation is at 20^{o} in this case. There are imaginary parts in the complex correlation due to the non-uniform elevation AOA. In the general case, however, vertical spacing helps to reduce the correlation when combined with horizontal spacing although there are occurrences where it increases by a negligible amount.

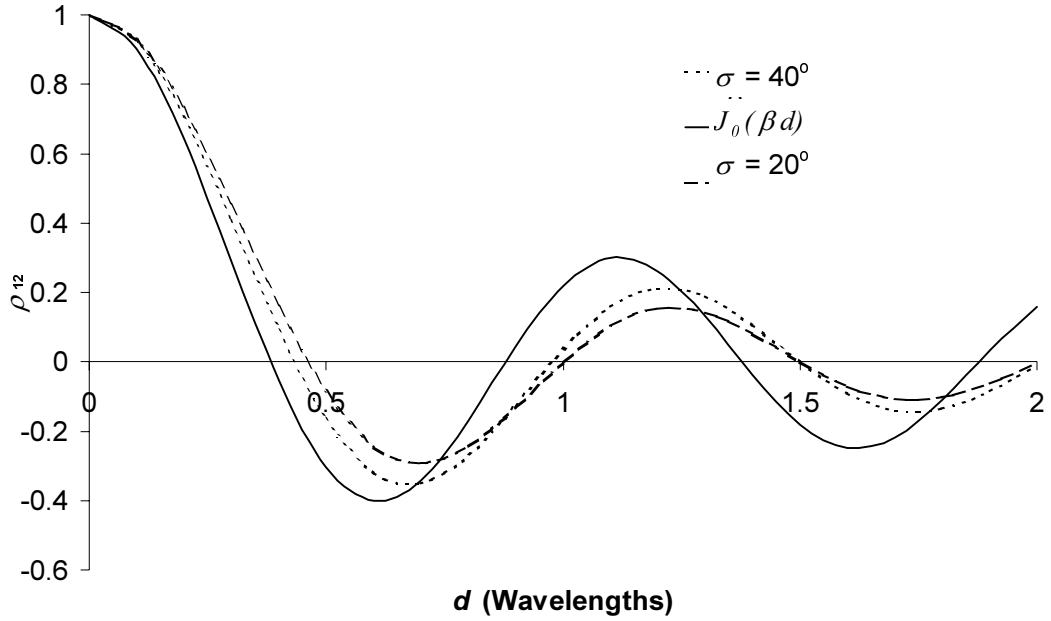

Figure 3-10 Graph showing a comparison of the horizontal spatial correlation when elevation angle of arrival is considered

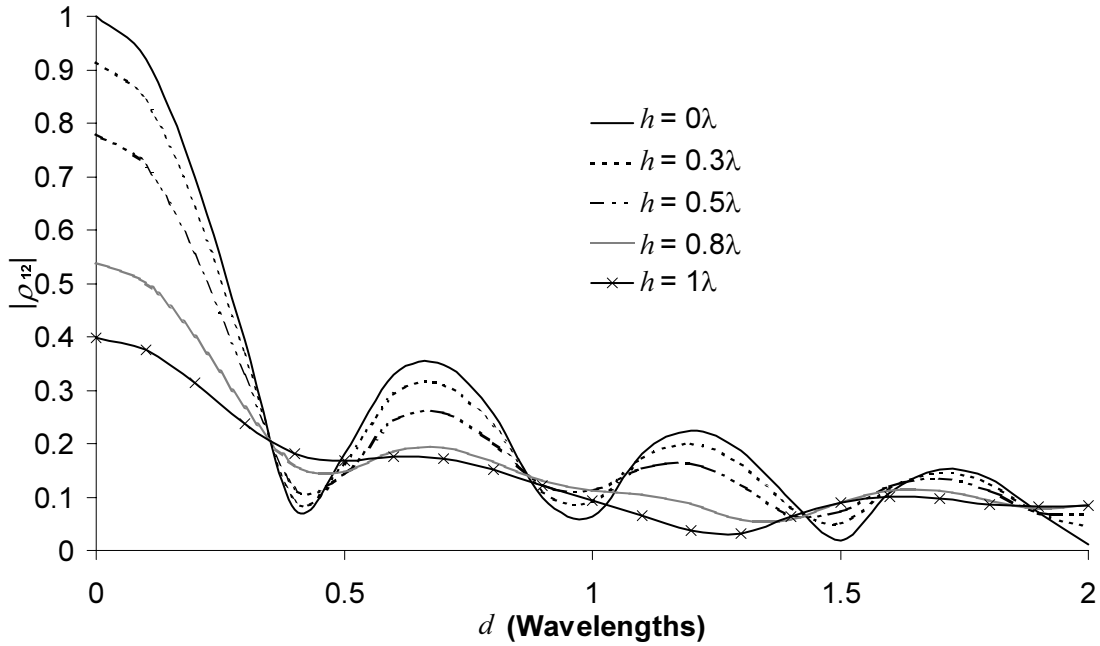

Figure 3-11 Graph showing correlation versus horizontal spacing at different fixed values of vertical spacing

3.3.2 Spatial diversity for non uniform angle of arrival in azimuth

When the angle of arrival is uniform in azimuth, it does not matter at what azimuth angle the two points in space are orientated. However, for non-uniform azimuth angle of arrival this does matter so therefore another offset angle, $\delta\phi$, needs to be considered. Use of this angle is explained in Appendix D.

3.3.3 Antenna effects on spatial diversity

The effects of mutual coupling can be applied to the spatial fields in a similar way to that of polarisation diversity although the spatial components are obviously different. Equation (3.50) can be combined with equation (3.12) so that the effects of mutual coupling can be resolved as follows:

$$\begin{pmatrix} E_{L\theta 1}(\theta,\phi) & E_{L\phi 1}(\theta,\phi) \\ E_{L\theta 2}(\theta,\phi) & E_{L\phi 2}(\theta,\phi) \end{pmatrix} \equiv \mathbf{S}_T \begin{pmatrix} 1 & 0 \\ e^{j\beta\left(\sqrt{d^2+h^2}\right)\cos\zeta} & 0 \end{pmatrix} \begin{pmatrix} E_\theta(\theta,\phi) & 0 \\ 0 & E_\phi(\theta,\phi) \end{pmatrix} \tag{3.57}$$

Therefore, for a single polarisation:

$$E_{\theta 1}(\theta,\phi) = \left(s_{t1} + s_r e^{j\beta\left(\sqrt{d^2+h^2}\right)\cos\zeta} \right) E_\theta(\theta,\phi) \tag{3.58}$$

$$E_{\theta 2}(\theta,\phi) = \left(s_r + s_{t2} e^{j\beta\left(\sqrt{d^2+h^2}\right)\cos\zeta} \right) E_\theta(\theta,\phi) \tag{3.59}$$

After substituting into equation (2.5), the complex correlation becomes:

$$\rho_{12} = \frac{s_{t1}s_r^* + s_{t2}^* s_r + \left(s_{t1}s_{t2}^* + |s_r|^2\right)\int_0^\pi\int_0^{2\pi} e^{j\beta\left(\sqrt{d^2+h^2}\right)\cos\zeta}\, p_\theta(\theta,\phi)\sin\theta\, d\phi\, d\theta}{\sqrt{\left(\left(|s_{t1}|^2 + |s_r|^2\right) + 2\Re\left\{ s_{t1}s_r^* \int_0^\pi\int_0^{2\pi} e^{j\beta\left(\sqrt{d^2+h^2}\right)\cos\zeta}\, p_\theta(\theta,\phi)\sin\theta\, d\phi\, d\theta \right\}\right)} \sqrt{\left(\left(|s_{t2}|^2 + |s_r|^2\right) + 2\Re\left\{ s_{t2}s_r^* \int_0^\pi\int_0^{2\pi} e^{j\beta\left(\sqrt{d^2+h^2}\right)\cos\zeta}\, p_\theta(\theta,\phi)\sin\theta\, d\phi\, d\theta \right\}\right)}} \tag{3.60}$$

Where $\Re$ denotes the real part. Again, in this situation, the effects are negligible when s_r is below –20dB and when there are negligible mismatches giving return loss of less than –20dB. In cases where antennas are closely spaced, then low isolation will result. As a consequence, the coupling does cause some degree of increase in correlation since the high coupling makes it harder for the receiver distinguish the difference between the signals in the two branches when spatially separated.

3.3.4 Angular diversity generated by antennas

With the two antennas closely spaced, there is a correlation between the two field patterns that can be evaluated while the antennas are in the presence of each other. It is especially important that the presence of the second antenna is considered when closely spaced since it will act as a parasitic element. This will give scope for angular diversity if the antennas have similar mean effective gain and still maintain their efficiency when brought closer together.

To evaluate the angular correlation, the three dimensional field patterns of the antennas are required either from simulations or from measurements. To remove the spatial effects it is important that the antenna field patterns are each measured at their respective phase centres, which are often around the feed point. If the two antenna patterns are then correlated with each other, they are compared as if they were coherent with each other so that the angular diversity can be evaluated.

To obtain a true measure of the angular correlation, the effects of any impedance changes, which can introduce a further phase shift at the output, need to be removed. Therefore the correlation from angular contributions should be measured from the voltage vector at the output flanges of the antennas as in Figure 3-1. Therefore, by using equation (3.15), the correct *E*-fields at the antenna outputs can be derived from the complex antenna amplitude patterns (i.e. the complex voltage at the output from each angle of the antenna), $A_\theta(\theta,\phi)$ and $A_\phi(\theta,\phi)$, as follows:

$$\begin{pmatrix} E_{\theta A1}(\theta,\phi) & E_{\phi A1}(\theta,\phi) \\ E_{\theta A2}(\theta,\phi) & E_{\phi A2}(\theta,\phi) \end{pmatrix} \equiv \mathbf{Z}_A \mathbf{Z}_L^{-1} \begin{pmatrix} A_{\theta 1}(\theta,\phi) & A_{\phi 1}(\theta,\phi) \\ A_{\theta 2}(\theta,\phi) & A_{\phi 2}(\theta,\phi) \end{pmatrix} \tag{3.61}$$

In the case of angular diversity, the two branches act as a parasitic element to each other to affect their angular field patterns. The patterns are measured when coherent so mutual coupling has no meaning. Therefore z_{12} and z_{21} become zero effectively for evaluating angular contribution. The E_θ and E_ϕ components in this case are therefore:

$$E_{\theta A1}(\theta,\phi) = \frac{z_{11} A_{\theta 1}(\theta,\phi)}{Z_0} \tag{3.62}$$

$$E_{\theta A2}(\theta,\phi) = \frac{z_{22} A_{\theta 2}(\theta,\phi)}{Z_0} \tag{3.63}$$

$$E_{\theta \phi 1}(\theta,\phi) = \frac{z_{11} A_{\phi 1}(\theta,\phi)}{Z_0} \tag{3.64}$$

$$E_{\theta\phi 2}(\theta,\phi)=\frac{z_{22}A_{\phi 2}(\theta,\phi)}{Z_0} \tag{3.65}$$

By substituting equations (3.62) through to (3.65) into equation (2.5), the angular complex correlation can be resolved as shown in equation (3.66). The impedance in equation (3.66) results in being a phasor. This phasor will not affect the magnitude of the angular correlation but only the phase. If both antennas are well matched then impedance has negligible affect on correlation.

$$\rho_{12}=\frac{z_{11}z_{22}^{*}\int_0^{\pi}\int_0^{2\pi}\left(XPRA_{\theta 1}(\theta,\phi)A_{\theta 2}^{*}(\theta,\phi)p_{\theta}(\theta,\phi)+A_{\phi 1}A_{\phi 2}^{*}p_{\phi}(\theta,\phi)\right)\sin\theta d\phi d\theta}{|z_{11}||z_{22}|\sqrt{\int_0^{\pi}\int_{-\pi}^{2\pi}\left(XPR|A_{\theta 1}(\theta,\phi)|^2 p_{\theta}(\theta,\phi)+|A_{\phi 2}(\theta,\phi)|^2 p_{\phi}(\theta,\phi)\right)\sin\theta d\phi d\theta}\sqrt{\int_0^{\pi}\int_0^{2\pi}\left(XPR|A_{\theta 2}(\theta,\phi)|^2 p_{\theta}(\theta,\phi)+|A_{\phi 2}(\theta,\phi)|^2 p_{\phi}(\theta,\phi)\right)\sin\theta d\phi d\theta}} \tag{3.66}$$

3.3.5 Angular and spatial diversity from two monopoles

An example of spatial and angular contributions is shown in Figure 3-12 from measurements of the field patterns of closely spaced quarter wavelength monopoles undertaken in an anechoic chamber. The measurements were undertaken at 900MHz appropriately matched to provide a return loss greater than 10dB by removing 5% of the quarter wavelength wire off the end. The monopole that was not driven was loaded with 50Ω. Both of the monopoles were fed with coaxial cable with ferrite rings to prevent any current imbalance. Also a 3dB pad attenuator was used at the driving input to prevent any impedance mismatch. Sufficient ground plane (0.3x0.6m) was also used such that at least a quarter wavelength radius of ground plane was surrounding both of the monopoles whatever distance apart they were moved to. A series of holes were drilled in the ground plane to re-solder the monopoles according to the distance apart required.

Elevation patterns were of the monopoles were then measured and correlation was evaluated based on methods that are explained in the next chapter. The S parameters were also used to evaluate the spatial correlation. When the antennas were closer than half a wavelength, isolation was low, greater than –10dB so spatial correlation was affected.

As would be expected as shown in Figure 3-12, the angular complex correlation decreases as the dipoles get closer together. When they are spaced beyond 0.5 wavelengths the spatial complex correlation reduces where as the angular correlation gets closer to unity. Further to this the spatial correlation increases as the antennas get closer and increase in coupling. Therefore as the antennas get closer, the angular correlation needs to be optimised such that it can achieve better overall

decorrelation. As the distance increases, there is less need for angular contribution since there is sufficient spatial decorrelation.

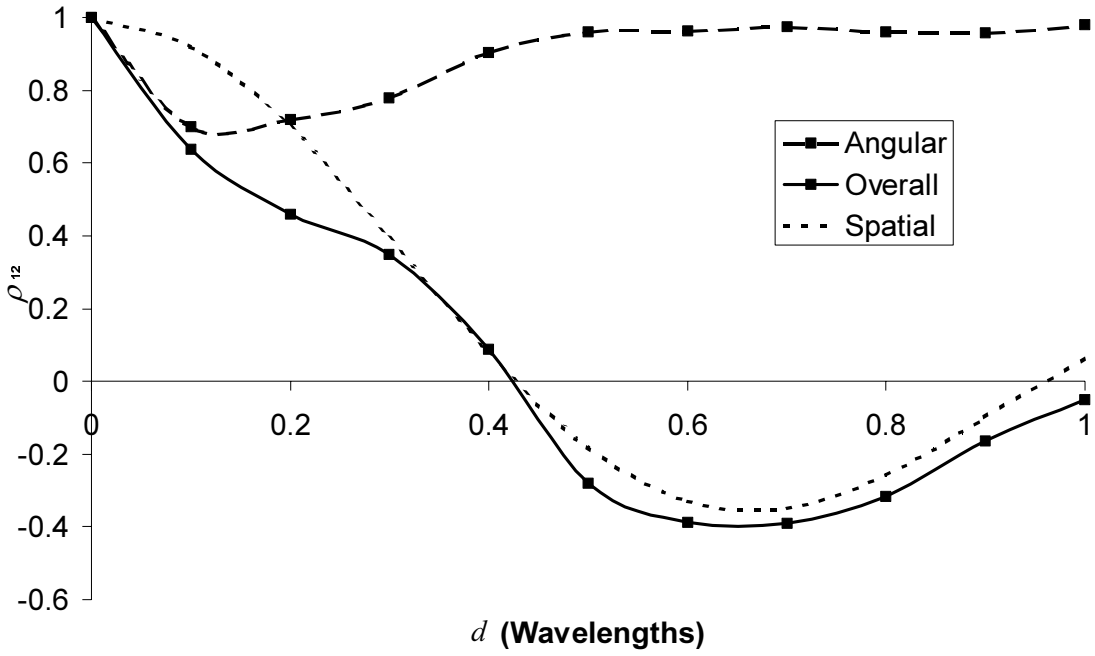

Figure 3-12 Graph showing the interaction of angular and spatial diversity on two closely spaced monopoles

Understanding spatial, angular and polarisation diversity in a mobile diversity system requires correct interpretation when results are presented. More of this will be presented in the following chapter when the method for analysing antenna diversity performance is explained in order to determine why antennas have diversity.

3.3.6 Effects of angle of arrival and cross polar ratio on angular diversity

As with spatial and polarisation correlation, the angular correlation is compared in Figure 3-13 when the standard deviation on the elevation angle of arrival is varied. As can be seen there is negligible difference between the curves so the effects of angle of arrival can be ignored. Cross-polar ratio, *XPR*, cannot be changed to show its effect on the correlation since monopoles are only vertically polarised. Results shown in following chapters, however, will show the effects of *XPR* since there will be a cross-polar component involved.

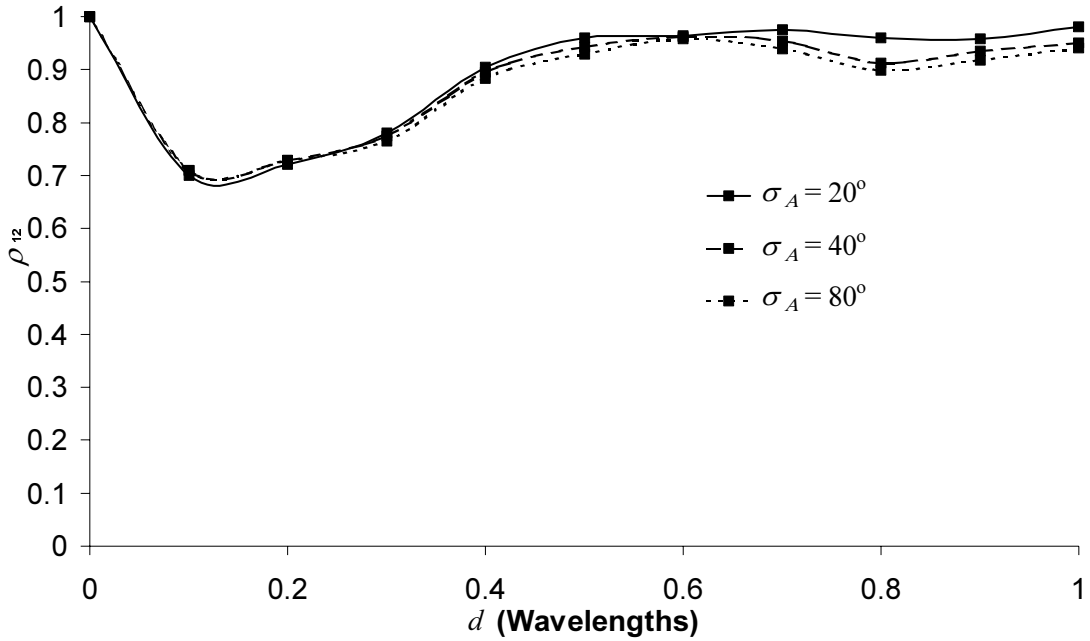

Figure 3-13 Graph showing comparisons of the angular correlation with different angle of arrival statistics based on results taken from closely spaced monopoles

3.3.7 Efficiency loss from angular diversity

Although closely spaced monopoles may achieve increased angular diversity, this does come at the expense of reduction in efficiency. As can be seen from Figure 3-14, the mutual resistance, r_{12}, increases dramatically below 0.5λ spacing and the input resistance (r_{11}) and input reactance (x_{11}) of each monopole is affected as well. Therefore in such cases of close spacing, where the high mutual coupling causes a significant amount of current to be drained in the loaded parasitic element, then power is lost.

Losing such power results in a loss of efficiency consequently reducing the MEG as well. Figure 3-15 shows the MEG plotted versus spatial distance, *d*, and it shows that the MEG reduces significantly as the monopoles get closer together below 0.5λ due to the increase in coupling. The MEG in this case was evaluated using methods explained in chapter 4.

3.3.8 Diversity performance of two closely spaced monopoles

Knowing the correlation and MEG, the comparison between diversity gain and system gain versus spatial distance can be seen in Figure 3-16 where the diversity gain is reasonably constant since the spatial and angular correlation complement each other to give a low overall correlation. However, the efficiency loss does give a lower output system gain when the monopoles are close although it is still a reasonable system gain.

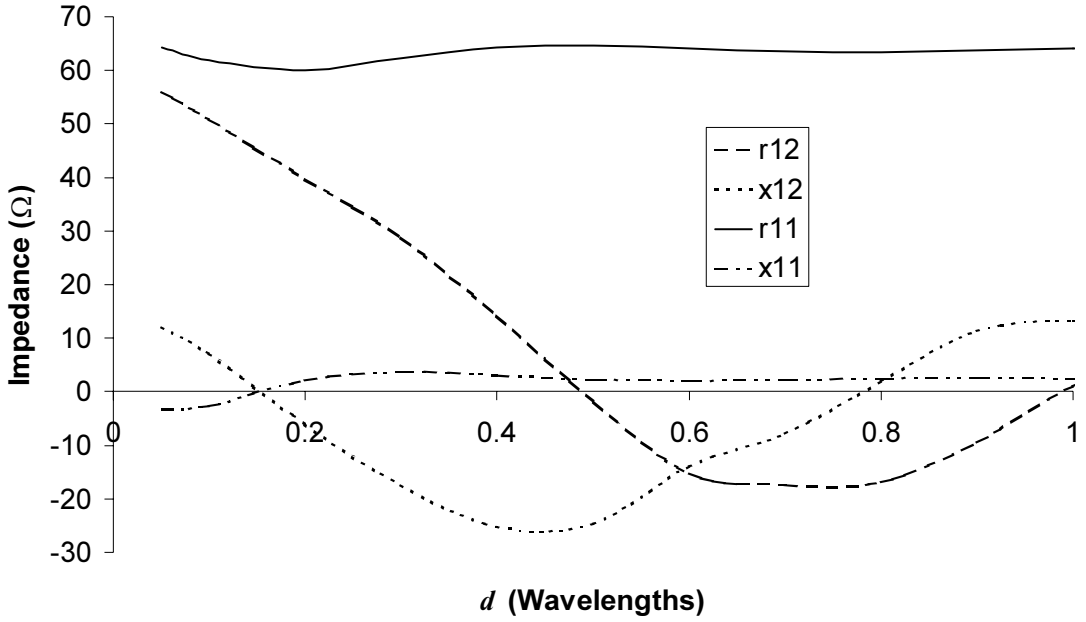

Figure 3-14 Graph showing the self impedance and mutual impedance between two closely spaced monopoles

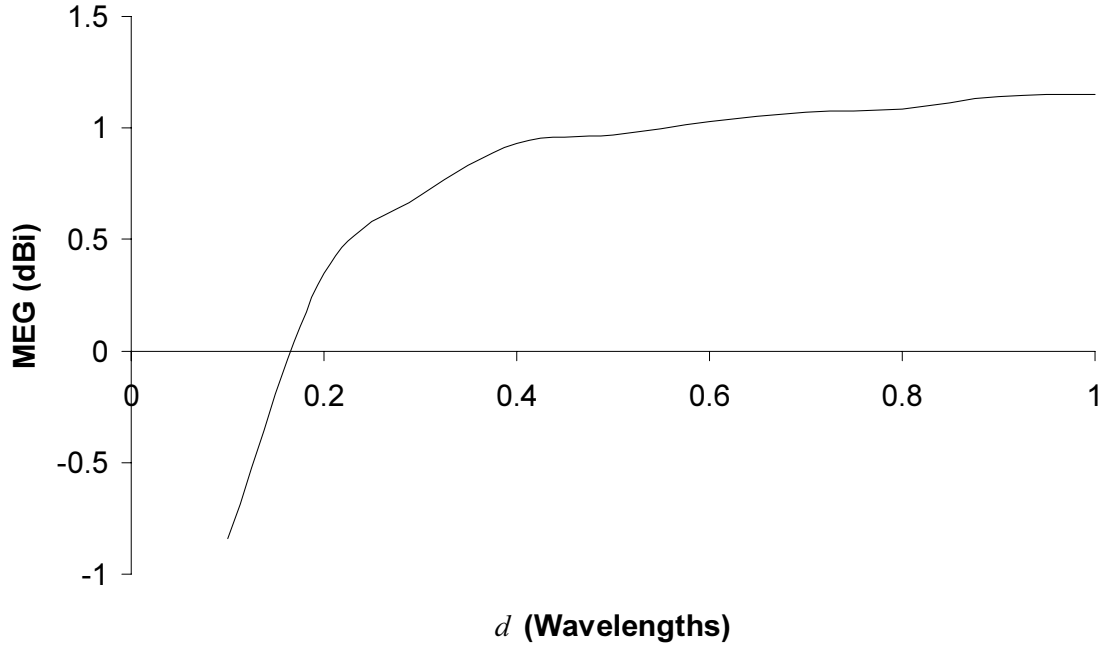

Figure 3-15 Graph showing Mean Effective Gain (MEG) for two closely spaced monopoles versus spatial distance

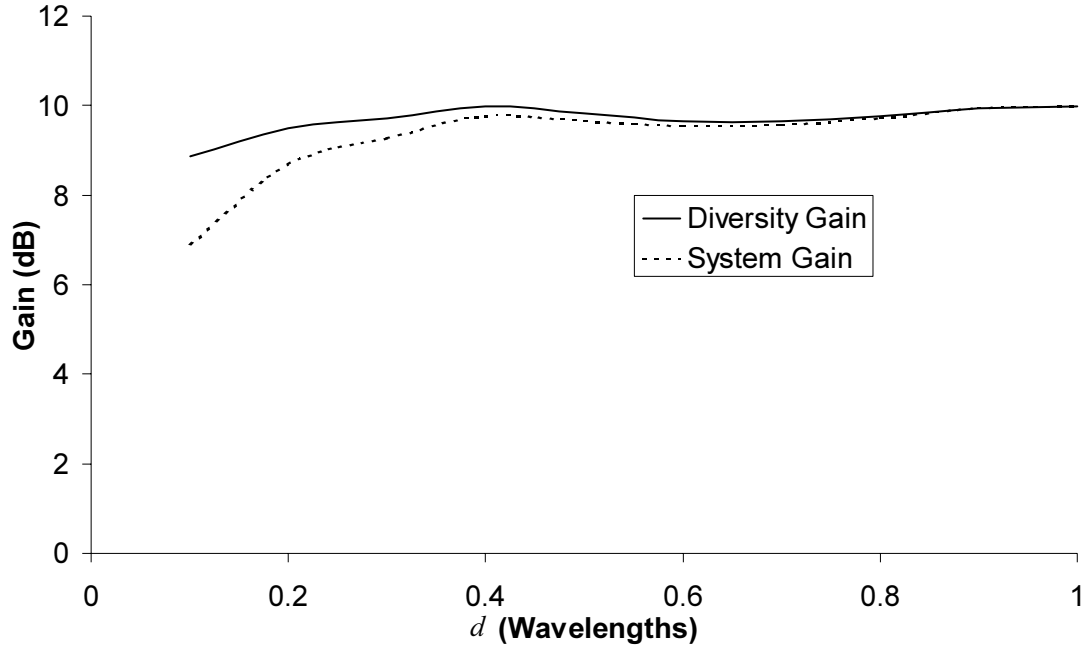

Figure 3-16 Graph showing the comparison between diversity gain and system gain for two closely spaced monopoles

3.4 Conclusions

The three main forms of diversity being spatial, angular and polarisation diversity at the mobile have been presented using new theoretical models considering effects of the antenna, the AOA and XPR at the mobile. The relevant antenna properties including MEG, polarisation, mutual and self-impedances have been presented and it is shown how they are integrated into diversity.

New models presented for polarisation diversity show how the diversity combiner performs best at the $\pm 62.5^{o}$ configuration because there is equal mean power between the branches and total de-correlation. However, due to signal losses in each branch compared to a reference branch at 60^{o} from the vertical, $\pm 45^{o}$ configuration does give a better output because the branches have gain in power. The spatial diversity model includes consideration of vertical spacing, horizontal spacing and diagonal spacing, which is encountered at the mobile.

Considering these new models, it has been shown how integrating the effects of antenna impedances does affect the spatial and polarisation correlation seen at the receiver when antennas are closely spaced. High mutual impedance causes an increase in correlation since the two branches cannot be easily compared at the receiver in such cases. For angular correlation, impedance affects only the phase and so the angular field patterns can be correlated when in the presence of each other. Although closely spaced antennas may be able to generate significant

angular correlation, it does come at the expense of losing some efficiency, so the two need to be compared to see how the overall output is affected.

The next chapter will apply these concepts to analyse why mobile terminal antennas have diversity to help the designer determine how they can be appropriately optimised. Further to this the next chapter will show how spatial, angular and polarisation correlation integrate together to produce an overall correlation. From this the designer can identify the significant contributions to diversity and how they interact.

The work presented for polarisation diversity was compiled into a journal paper, "Characterisation of Polarization Diversity at the Mobile", awaiting submission. The work presented for spatial and angular diversity was compiled into another journal paper, "Analysis of Mobile Terminal Diversity Antennas" also awaiting submission Similar conference publications have also been produced including "Modelling Polarisation Diversity at the Mobile Terminal", presented at the *International Conference of Antennas and Propagation (ICAP)*, April 2001 and "Spatial Diversity of Two Closely Spaced Dipoles", presented at the *Postgraduate Research in Electronics, Photonics, Communications and Software (PREP)* conference in April 2001.

Chapter 4

4 Method for Evaluating Diversity at the Mobile Terminal

In the previous chapter, theoretical models for the main forms of antenna diversity at the mobile terminal were presented. The effects of the antenna field patterns, mutual coupling and matching properties were also presented. To evaluate diversity of actual mobile terminal antennas, the measurements or simulations need to be appropriately carried out and processed as explained in this chapter using the theory explained in chapter 3. All mobile terminal diversity antennas will consist of spatial, angular and polarisation correlation components which unfortunately cannot be simply multiplied or added together to evaluate the overall correlation. It is important therefore that the correlation values are correctly interpreted to understand the spatial, polarisation and angular contributions. This will indicate why the mobile terminal antennas have diversity to assist the designer. Further to this, it can be analysed how the antennas might be appropriately optimised for maximum diversity performance and efficiency.

4.1 General Variables

For all forms of correlation, it is necessary to use the cross-polar power ratio, *XPR* (except in spatial), the mean angle of arrival, $\overline{\theta}$, and the standard deviation of the angle of arrival, σ_A. As discussed in chapter 2 the *XPR* is assumed to be 6dB, $\overline{\theta}$ and σ_A are also assumed to be 20^o for the purpose of the analysis presented in this chapter. Therefore the effects of changing their figures should be noted as appropriate although they are shown to have little effect on diversity in the general case.

4.2 Evaluating Spatial Correlation

The simplest correlation to evaluate is the loaded spatial correlation where the appropriate parameters can be found to evaluate the complex correlation from equation (3.60). First of all the transfer matrix, $\mathbf{S}_T$, can be calculated by taking two port S-parameter measurements from a vector

network analyser when the antennas are in the presence of each other in free space. The respective Z-parameters can likewise be calculated from the S-parameters using equations (3.4a) to (3.4d).

The other parameter that needs to be known when evaluating spatial diversity is the distance between the antennas, $\sqrt{d^2+h^2}$, and their respective argument, $\delta\theta$, used in equation (3.55). In the case of mobile terminal antennas the spatial distance is strictly the distance between the antenna phase centres when the antennas are positioned into their relative places. Care must be taken when measuring the distances between phase centres since the phase centre of an antenna can possibly be moved when in the presence of the other.

For antennas such as horns and dipoles, finding the phase centre is simple since it is the point at which the phase is constant at every angular point in azimuth. In real terminal antennas, their structure does not allow them to have a constant phase at any point since often the ground plane is used with an irregular current distribution. In such cases the phase centre is normally defined as the position where the phase is moderately constant especially within the main lobes of the field pattern [Bal97]. Therefore the phase centre will be determined by this position. The position of the antenna must also be noted so that the horizontal spacing, d, the vertical spacing, h, and their relative argument, $\delta\theta$, can be quantified.

4.3 Evaluating Angular Correlation

Having found the phase centres of the two antennas for the spatial correlation, the three dimensional amplitude patterns can be measured or simulated at the phase centres to evaluate the angular correlation. For suitable resolution and accuracy, pattern cuts in 10^o steps can be used [Sulo02] so that equation (3.66) can be evaluated in discrete form as in equation (4.1) knowing the $\mathbf{S}_T$ matrix.

Correctly positioning the antennas at their appropriate phase centres can be difficult since once the first antenna has been measured or simulated, the mobile terminal has to be carefully repositioned so that it is at the phase centre of the second antenna. Further to this, the second antenna still needs to be measured or simulated when the first antenna is at its phase centre so as to evaluate the overall correlation. Therefore three full three-dimensional patterns have to be measured or simulated, which is time consuming. Another method can ease this problem by only having to evaluate two three dimensional patterns. First of all, the first antenna is measured or simulated at its phase centre whilst the second antenna terminated with a 50Ω load to obtain the field pattern, $A_1(\theta,\phi)$ [V]. Following this, the feed can be moved over to the second antenna and swapped with the 50Ω load to measure or simulate its field pattern while the first antenna is still at

its phase centre. This field pattern can be given the notation $A_{2A}(\theta,\phi)$ [V]. Therefore $A_1(\theta,\phi)$ would be correlated with $A_{2A}(\theta,\phi)$ in order to obtain the overall complex correlation of the antennas.

$$\rho_{12} = \frac{z_{11}z_{22}^{*}\sum_{i=1}^{N}\sum_{j=1}^{M}\left(XPRA_{\theta 1ij}A_{\theta 2ij}^{*}p_{\theta}(\theta_i,\phi_j)+A_{\phi 1ij}A_{\phi 2ij}^{*}p_{\phi}(\theta_i,\phi_j)\right)\sin\theta_i}{|z_{11}||z_{22}|\sqrt{\sum_{i}^{N}\sum_{j}^{M}\left(XPR\left|A_{\theta 1ij}\right|^2 p_{\theta}(\theta_i,\phi_j)+\left|A_{\phi 1ij}\right|^2 p_{\phi}(\theta_i,\phi_j)\right)\sin\theta_i \sum_{i}^{N}\sum_{j}^{M}\left(XPR\left|A_{\theta 2ij}\right|^2 p_{\theta}(\theta_i,\phi_j)+\left|A_{\phi 2ij}\right|^2 p_{\phi}(\theta_i,\phi_j)\right)\sin\theta_i}} \tag{4.1}$$

To obtain the angular correlation, the complex phasor used to derive spatial correlation in equation (3.52) can be applied to remove the spatial phase delay inherent in $A_{2A}(\theta,\phi)$. Therefore if this phase delay is removed then $A_{2A}(\theta,\phi)$ becomes $A_2(\theta,\phi)$ as if it was measured or simulated at its own phase centre. Therefore:

$$A_2(\theta,\phi) = A_{2A}(\theta,\phi)e^{-j\beta\sqrt{(d^2+h^2)}\sin(\theta+\delta\theta\,\mathrm{sgn}\,\phi)\sin\phi} \tag{4.2}$$

This can therefore be applied to both polarisations, A_θ and A_ϕ, so that the angular correlation is simplified to only needing two three dimensional pattern measurements.

4.4 Evaluating Polarisation Correlation

Having evaluated the angular field patterns, $A_1(\theta,\phi)$ and $A_2(\theta,\phi)$, for both polarisations, they can be used to likewise evaluate the relative polarisations at each angle of the antennas and therefore determine the polarisation correlation. As discussed in the previous chapter, the polarisation diversity of an antenna can only be evaluated in terms of E_θ and E_ϕ polarisations since the incident fields can still encounter E_θ components even when the antenna is horizontally orientated (e.g. a horizontal dipole). Therefore these polarisations are strictly different from the vertical and horizontal polarisations, E_x and E_y, in a fading environment.

Figure 4-1 shows the polarisations of an antenna being measured or simulated at a fixed angle. The polarisations relative to each other can be determined by the absolute values of E_θ and E_ϕ. Correlation can be evaluated based on the averaging of the relative polarisations at each angle. This will yield significantly different results to that of the polarisation correlation of the fading environment discussed in chapter 3. Phase has no consideration as far as relative polarisation of

the antennas is concerned so therefore the reactive (or lossless) impedance effects do not need to be taken into account as is the case with angular diversity.

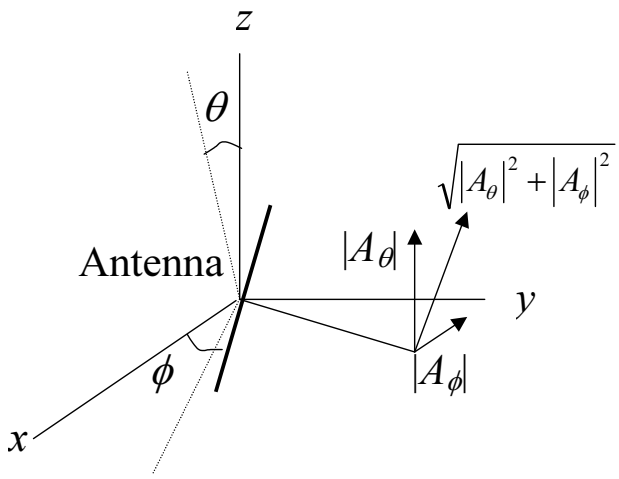

Figure 4-1 Diagram showing the relative polarisations determined from the *E*-fields of the antennas

Relative polarisation is defined as the proportion of total field strength magnitude in the A_θ and A_ϕ cases. Referring to Figure 4-1, the total amplitude in any given direction is derived by using Pythagoras' theorem. The proportion of $|A_\theta|$ is therefore derived as a ratio of $|A_\theta|$ to the total amplitude. Therefore it will be unity when there is only an $|A_\theta|$ component and zero if there is none. The same is true for $|A_\phi|$ in vice versa. Therefore, the *E*-fields are therefore derived as follows in terms of relative polarisations in linear form:

$$E_{\theta 1}(\theta,\phi) \equiv \frac{|A_{\theta 1}(\theta,\phi)|}{\sqrt{|A_{\theta 1}(\theta,\phi)|^2 + |A_{\phi 1}(\theta,\phi)|^2}} \quad E_{\phi 1}(\theta,\phi) \equiv \frac{|A_{\phi 1}(\theta,\phi)|}{\sqrt{|A_{\theta 1}(\theta,\phi)|^2 + |A_{\phi 1}(\theta,\phi)|^2}} \qquad (4.3)\ (4.4)$$

$$E_{\theta 2}(\theta,\phi) \equiv \frac{|A_{\theta 2}(\theta,\phi)|}{\sqrt{|A_{\theta 2}(\theta,\phi)|^2 + |A_{\phi 2}(\theta,\phi)|^2}} \quad E_{\phi 2}(\theta,\phi) \equiv \frac{|A_{\phi 2}(\theta,\phi)|}{\sqrt{|A_{\theta 2}(\theta,\phi)|^2 + |A_{\phi 2}(\theta,\phi)|^2}} \qquad (4.5)\ (4.6)$$

The polarisations for E_θ and E_ϕ fields can be substituted into equation (2.5) and expressed in discrete form for evaluation purposes as shown in equation (4.7). This can be used to compare whether the two antennas have similar E_θ and E_ϕ polarisations or not. If there is low correlation, it can indicate to the designer that there is significant polarisation contribution within the angular correlation.

$$\rho_{12} = \frac{\sum_{i=1}^{N}\sum_{j=1}^{M}\left(XPR.\frac{\left|A_{\theta 1ij}\right|\left|A_{\theta 2ij}\right|}{\sqrt{\left(\left|A_{\theta 1ij}\right|^2+\left|A_{\theta 1ij}\right|^2\right)\left(\left|A_{\theta 2ij}\right|^2+\left|A_{\theta 2ij}\right|^2\right)}}p_\theta(\theta_i,\phi_j) + \frac{\left|A_{\phi 1ij}\right|\left|A_{\phi 2ij}\right|}{\sqrt{\left(\left|A_{\theta 1ij}\right|^2+\left|A_{\theta 1ij}\right|^2\right)\left(\left|A_{\theta 2ij}\right|^2+\left|A_{\theta 2ij}\right|^2\right)}}p_\phi(\theta_i,\phi_j)\right)\sin\theta_i}{\sqrt{\left(\sum_{i=1}^{N}\sum_{j=1}^{M}\left(XPR.\frac{\left|A_{\theta 1ij}\right|^2}{\left|A_{\theta 1ij}\right|^2+\left|A_{\theta 1ij}\right|^2}p_\theta(\theta_i,\phi_j) + \frac{\left|A_{\phi 1ij}\right|^2}{\left|A_{\theta 1ij}\right|^2+\left|A_{\theta 1ij}\right|^2}p_\phi(\theta_i,\phi_j)\right)\sin\theta_i\right)\times \left(\sum_{i=1}^{N}\sum_{j=1}^{M}\left(XPR.\frac{\left|A_{\theta 2ij}\right|^2}{\left|A_{\theta 2ij}\right|^2+\left|A_{\theta 2ij}\right|^2}p_\theta(\theta_i,\phi_j) + \frac{\left|A_{\phi 2ij}\right|^2}{\left|A_{\theta 2ij}\right|^2+\left|A_{\theta 2ij}\right|^2}p_\phi(\theta_i,\phi_j)\right)\sin\theta_i\right)}} \tag{4.7}$$

4.5 Mean Effective Gain

Using the three dimensional gain patterns at the phase centres, equation (3.17) can be evaluated in discrete form as shown in equation (4.8) and used to derive the branch power ratio, *k*, and any efficiency loss, *L*. It must be noted that when the two antennas are in the presence of each other they could affect their respective mean effective gains (MEGs) and become a disadvantage to diversity. An example of this has already been seen in section 3.37 where two closely spaced monopoles have a loss in MEG of up to 3dB when spaced less than 0.5 wavelengths apart. This is an example of how closely spaced monopoles may have improved angular diversity but this comes at the expense of losing efficiency. Therefore a compromise is necessary to obtain optimum output system gain.

$$\mathrm{MEG} = \sum_{i=1}^{N}\sum_{j=1}^{M}\left(\frac{XPR}{1+XPR}G_{\theta 1ij}(\theta_i,\phi_j)p_\theta(\theta_i,\phi_j) + \frac{1}{1+XPR}G_{\phi 1ij}(\theta_i,\phi_j)p_\phi(\theta_i,\phi_j)\right)\sin\theta_i \tag{4.8}$$

4.6 Interpretation of Correlations

The methods used for deriving spatial, angular and polarisation correlation have been presented to this point although they have no significance unless their meanings are correctly interpreted so

that the designer can determine how the three correlations affect the overall correlation and likewise contribute to diversity. This section will therefore present results from simulations undertaken to illustrate how the three correlations interact based on the proposed angle of arrival model.

4.6.1 Horizontal spatial correlation integrated with angular correlation in azimuth

To begin with, the antenna model used for this analysis is presented in Figure 4-2 where two vertically polarised isotropes are manipulated in a way that the spatial and angular correlations can be changed independently of each other. Looking at the plan view in Figure 4-2, there is horizontal spacing, d, which can be adjusted to change the spatial correlation as necessary and made zero to remove it. Angular correlation is adjusted by varying the angles ψ, $\delta\phi_1$ and $\delta\phi_2$. Both antennas have always have the same sector size, ψ, removed at any one time. The sectors in the two antennas can be offset differently by angles $\delta\phi_1$ and $\delta\phi_2$ respectively. This allows the possibility of many combinations of spatial and angular correlation for analysis. Whatever the sector size, the phase pattern is 0^o and the magnitude is always unity where there is no sector cut away. For evaluating correlation, the magnitude does not need to be normalised according to the sector size. It is important to note that the antenna patterns used in this section are idealised and not necessarily realisable. However, they are chosen as examples of typical antenna patterns used at the mobile terminal so the designer can extrapolate from the results to determine how their particular design will have optimum de-correlation, MEG and resulting system gain.

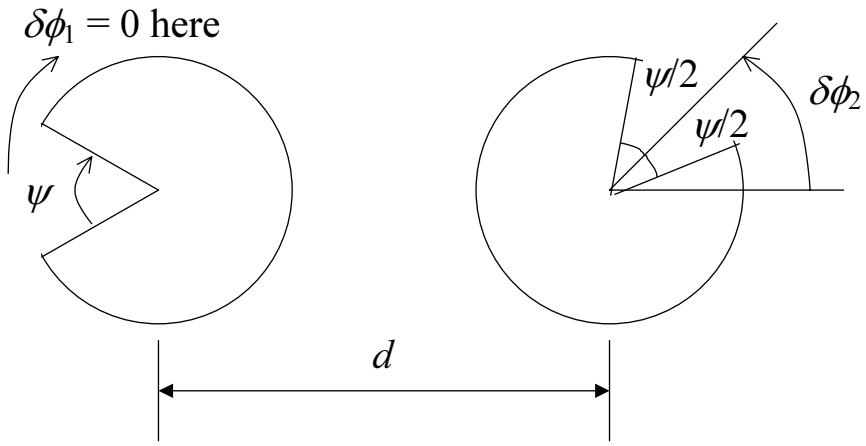

Figure 4-2 Diagram showing the plan view of the antenna model used

The first set of results in Figure 4-3 show how angular correlation integrates with spatial correlation in the case of a large overlap of the two antenna patterns. The varying angle is ψ in this case and is on the *y*-axis of the mesh plots. The spatial distance, *d*, is plotted on the *x*-axis and the resulting complex correlation magnitude on the *z*-axis. The only difference between the three mesh plots is that the angle, $\delta\phi_1$, is adjusted which does have some impact on the results when *d* is non-zero as can be seen from comparing Figure 4-3 (a), (b) and (c). It is important to note at this point that angular correlation and the spatial correlation could be placed on the *x* and *y* axis to try and find a link between the angular and spatial correlation. However, there are cases where this does cause ambiguity since there are cases where the angular and spatial correlation values can yield two different resulting for overall correlation values. Therefore, the mesh plot would have two layers in some places.

The spatial correlation can be noted from the curve where $\psi = 0^o$ and the angular correlation can be noted from the curve versus ψ where $d = 0\lambda$ to see the interaction of spatial and angular correlation. Clear indications are shown from Figure 4-3 in all three cases that around $d = 1\lambda$ varying angular correlation will increase the spatial correlation in some cases and in other cases decrease it. Also in Figure 4-3 it can be seen that the same angular correlation from different antenna orientations will change the spatial correlation differently. Otherwise, all three mesh plots would have little difference. An important point to note is that the angular correlation goes to zero in Figure 4-3 (a) only since this is the only case where the antenna patterns have no overlap to make this possible. Angular correlation in this case is therefore a measure of how much overlap there is between the two antenna patterns but this is not true in other cases as will be seen. Finally it must be noted that the magnitude of the correlation is plotted which does have imaginary components when the spacing is non-zero. This is due to the fact that the angular patterns will add up the real and imaginary parts differently and so the resultant signals at the two antenna branches have a phase shift between them when they are compared.

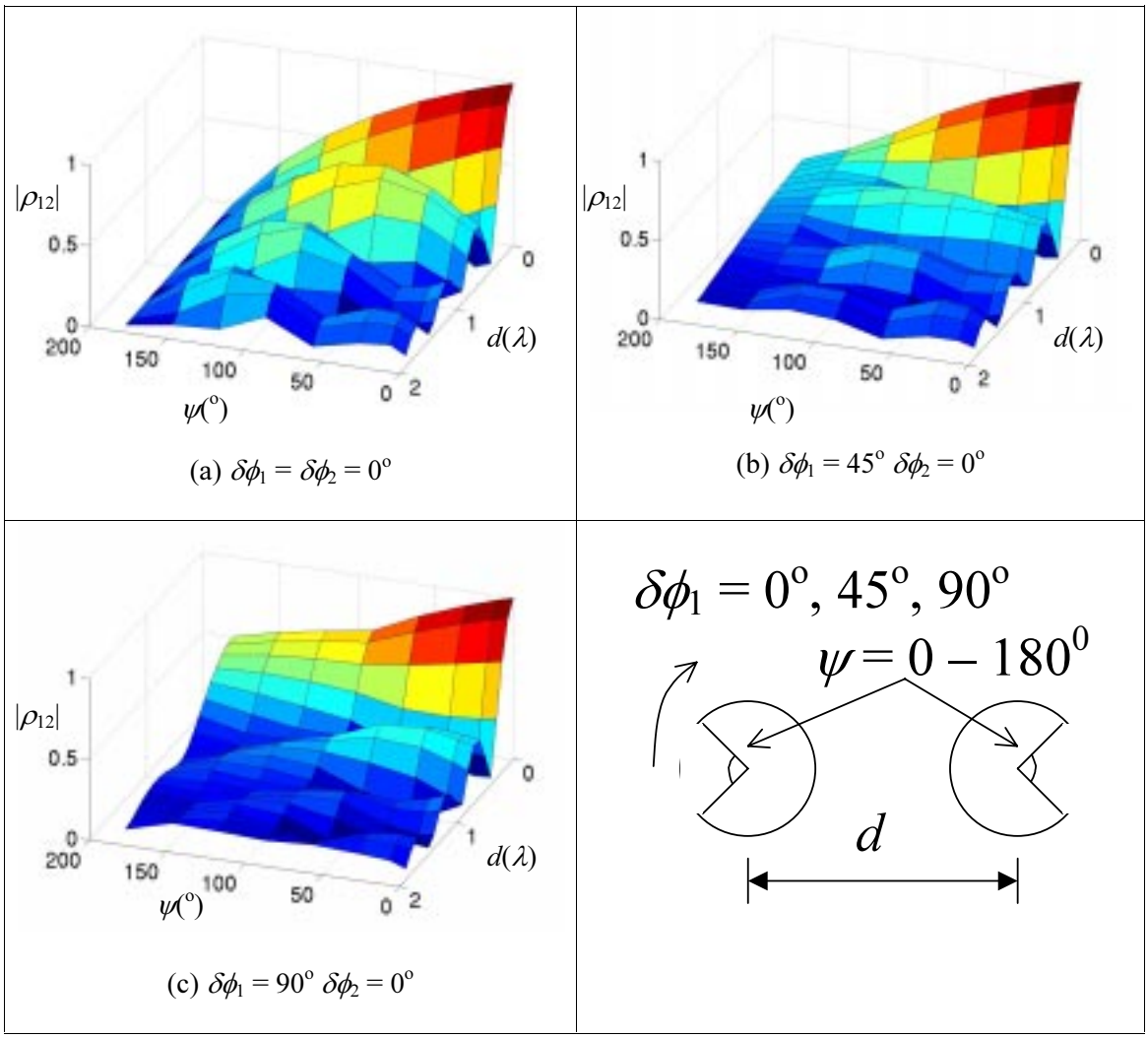

Figure 4-3 Interaction of angular and horizontal spatial correlation with a large overlap

Figure 4-4 presents the results in the same way as in Figure 4-3 with adjustments to make the antennas semi directive. This time, $\delta\phi_2$, is the varying angle with ψ fixed to 180° and $\delta\phi_1$ fixed at 0°, -30° and -60°. As can be seen $\delta\phi_2$ is normalised relative to $\delta\phi_1$ in each case from –180° to +180° (i.e. the region where the antennas overlap) and Figure 4-4 (a) is symmetrical around $\delta\phi_2$ + 180 + $\delta\phi_1$ = 0° where as the others are not since the real and imaginary parts of the spatial components do not add up to the same value when the symmetrically opposite angle is used. It is again quite clear from comparisons of Figure 4-4 (a), (b) and (c) that the same angular correlation in the three cases effects the spatial correlation differently.

Figure 4-5 presents the same results as Figure 4-4 only the sector size, ψ, is increased to 270°. Therefore in this case the antennas are more directive and $\delta\phi_2$ needs to only range from –90° to +90° when relative to $\delta\phi_1$. The nature of the results are much the same as those in Figure 4-4 only angular correlation decreases more rapidly since the antennas are more directive.

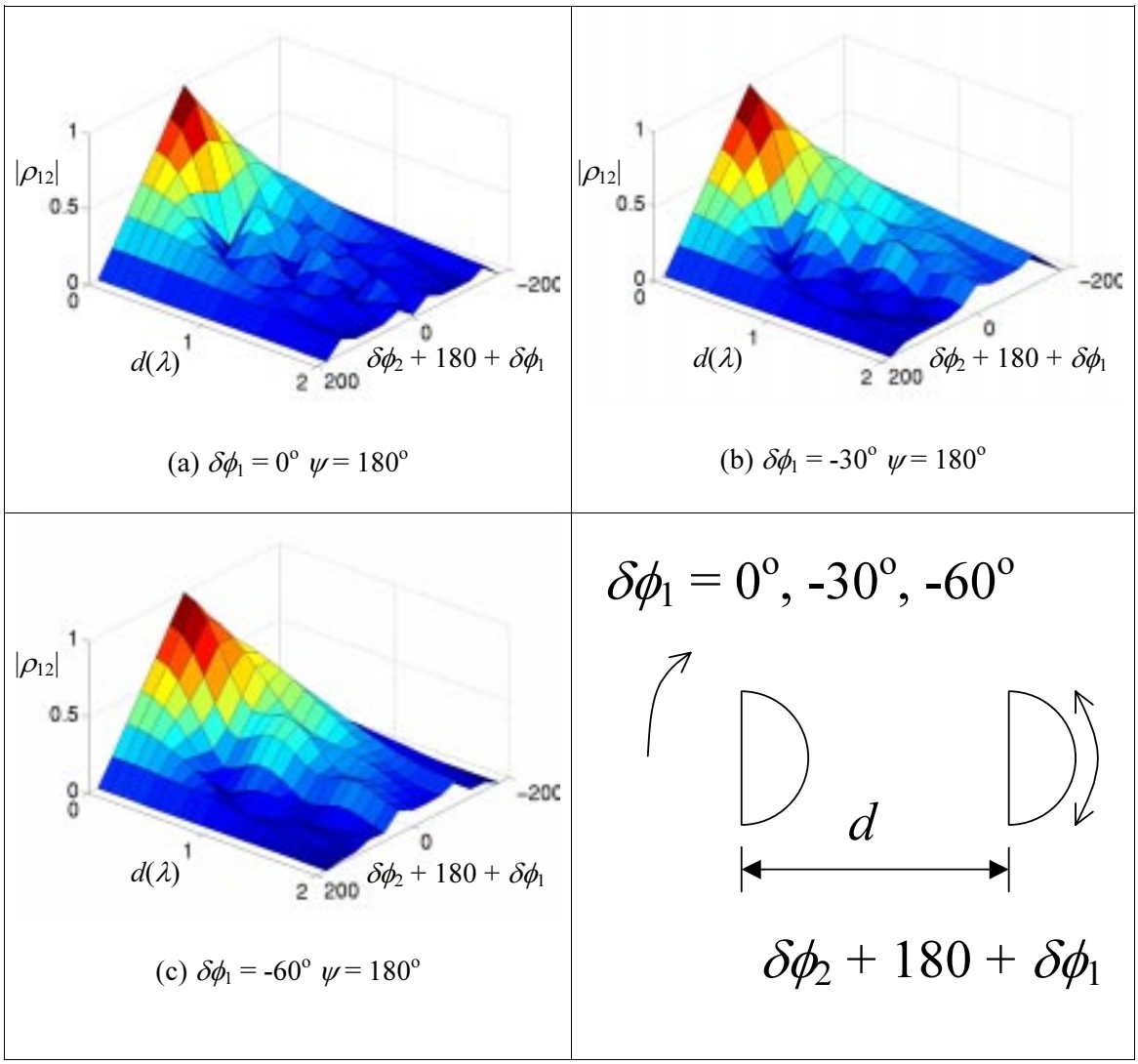

Figure 4-4 Interaction of angular and horizontal spatial correlation with two semi directive patterns

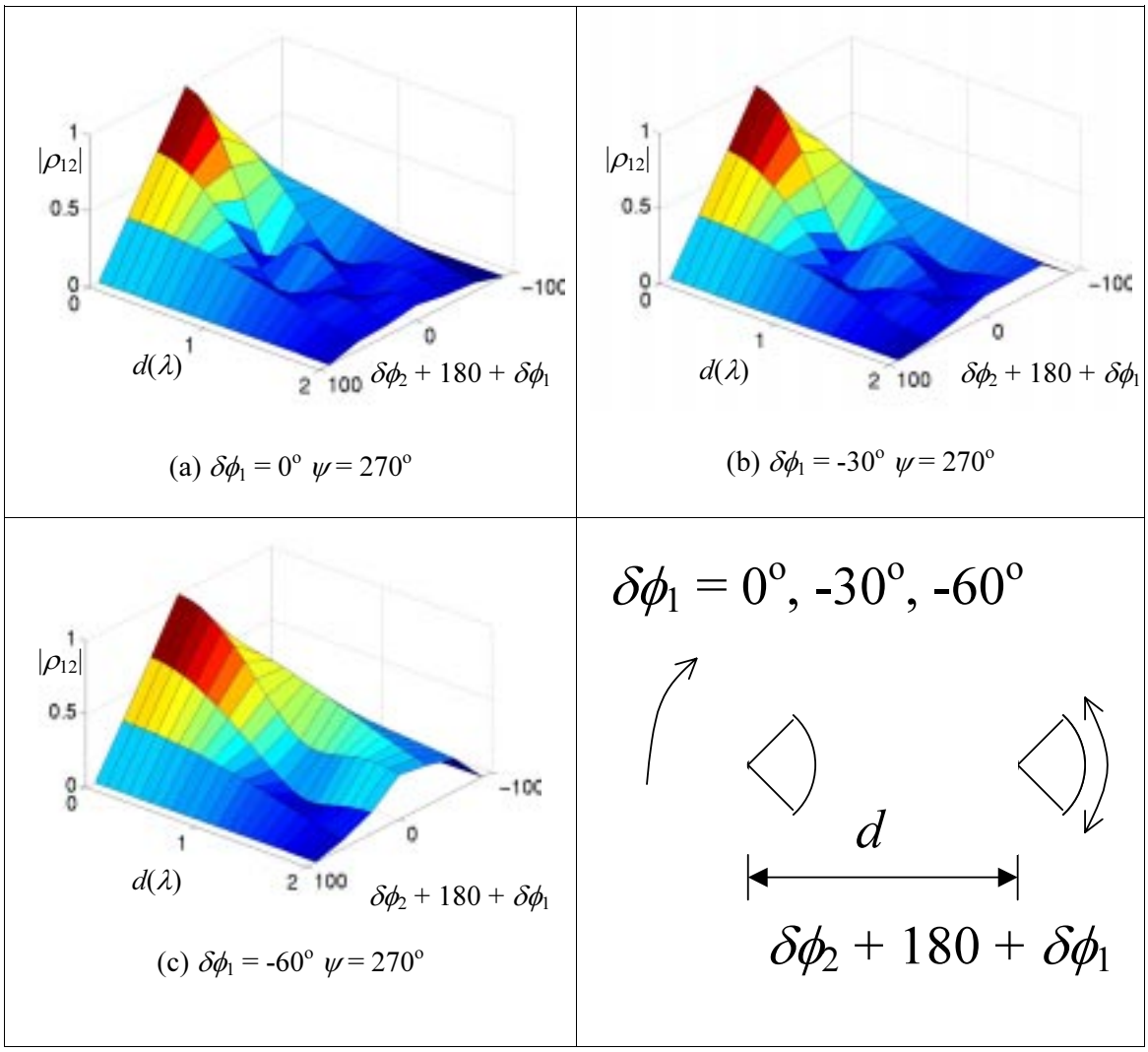

Figure 4-5 Interaction of angular and horizontal spatial correlation with two directive patterns

Finally, Figure 4-6 shows the interaction of an omni directional antenna with a semi directive antenna (Figure 4-6 (a) and (c)) and a directive antenna (Figure 4-6 (b) and (d)). In this case, $\delta\phi_1$ remains zero and only $\delta\phi_2$ changes in either case. Angle ψ only applies to the second antenna in this situation being 180^o in the first case and 270^o in the other. Varying $\delta\phi_2$ does make some difference to the overall correlation. Therefore, similar to that of two directional antennas, the correlation will increase or decrease depending on the direction that the directive antenna is pointing in. A final point to note here is that in this scenario, angular correlation is not a measure of overlap.

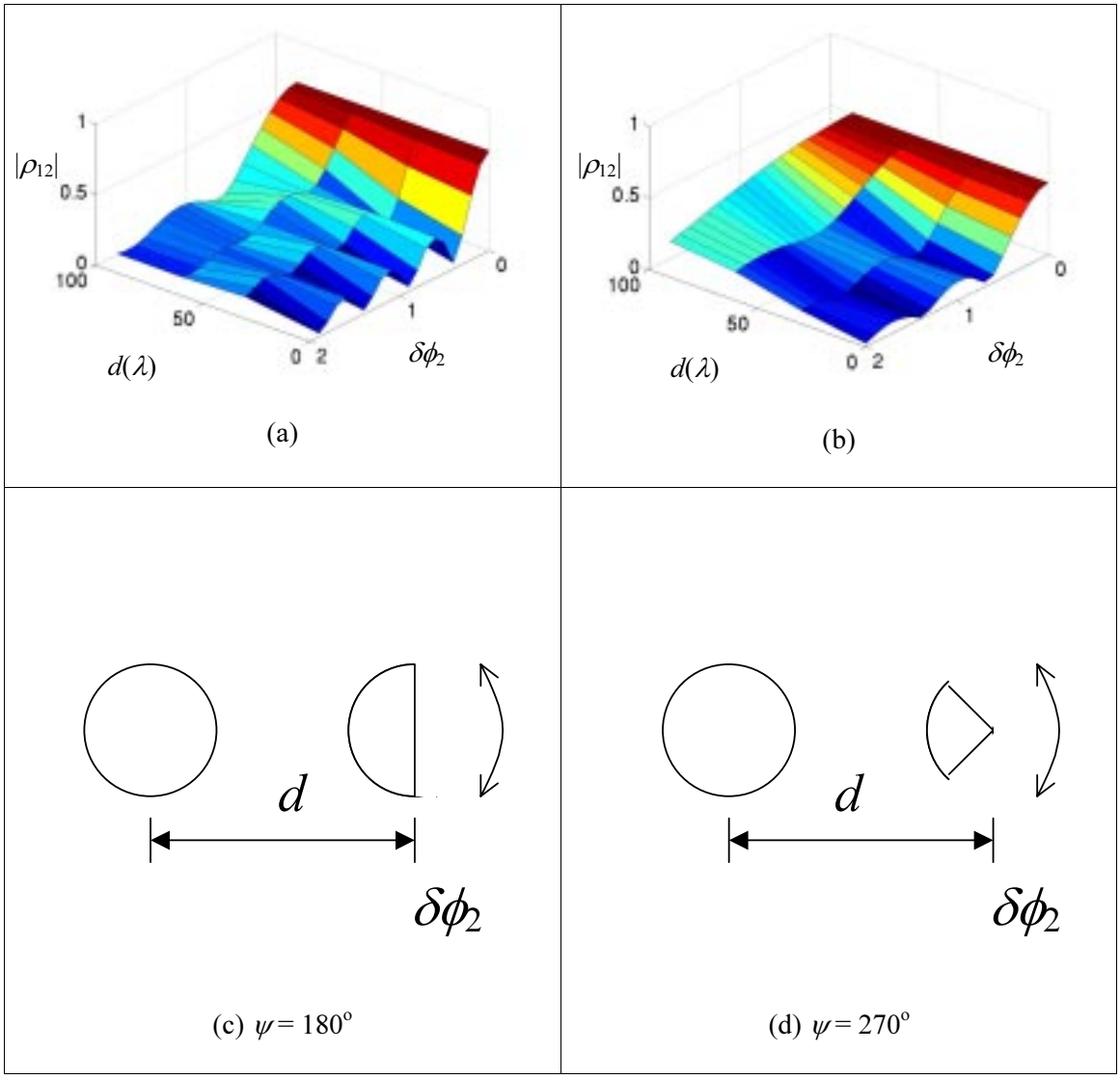

Figure 4-6 Interaction of angular and horizontal spatial correlation with an omni directional antenna and a semi directive antenna ((a) and (c)), and a directional antenna ((b) and (d))

Having presented the results of different scenarios for angular and spatial diversity, it can be seen that knowledge of the angular and spatial correlation alone is not sufficient enough to determine how they affect the overall correlation. Knowledge of the distance between the antennas and the antenna patterns is required to give appropriate comment. Figure 4-7 shows a set of correlation curves taken from Figure 4-3 that illustrate how the same angular correlation (0.66) from different antenna configurations used in the results affects the spatial correlation differently.

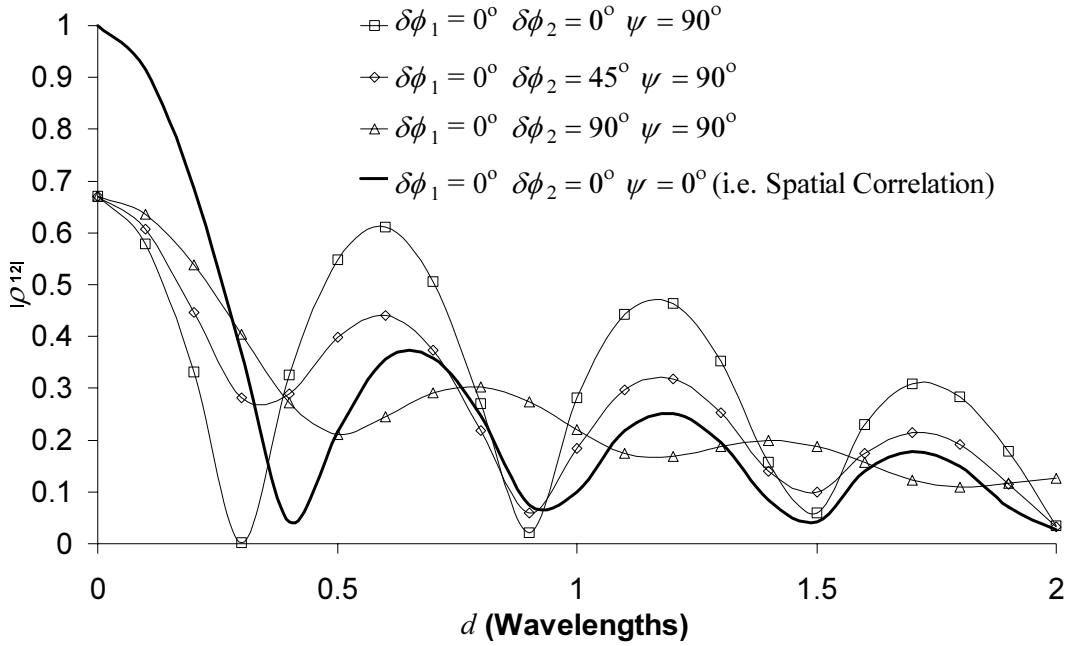

Figure 4-7 Comparison of how the same angular correlation affects spatial correlation in different scenarios for the horizontally separated antennas with small directionality

The same was carried out taking results from Figure 4-4 and Figure 4-5 in Figure 4-8 and Figure 4-9 respectively where again the same angular correlation affects the spatial correlation differently.

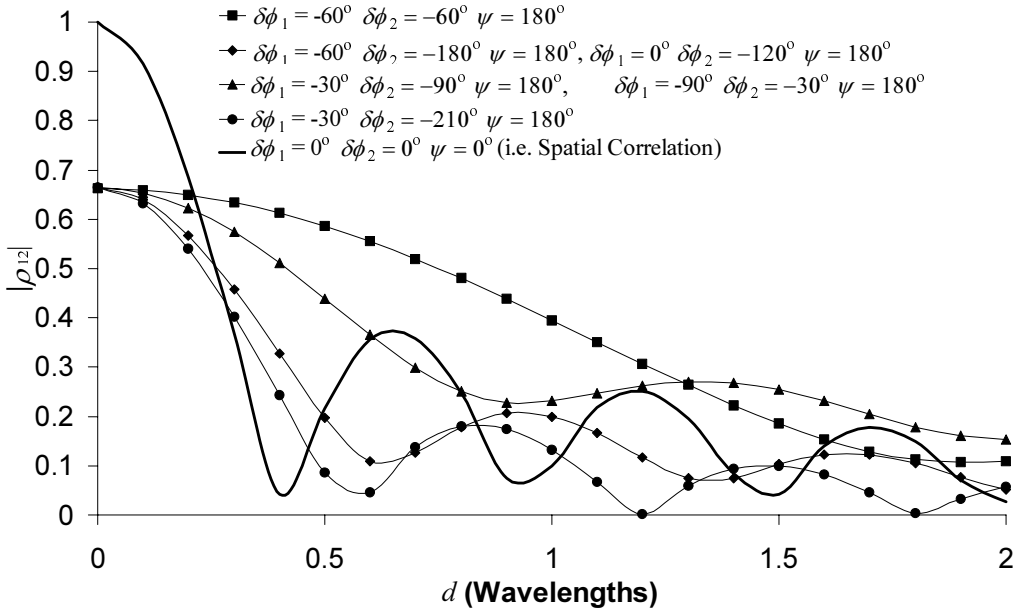

Figure 4-8 Comparison of how the same angular correlation affects spatial correlation in different scenarios for the horizontally separated antennas with semi directionality

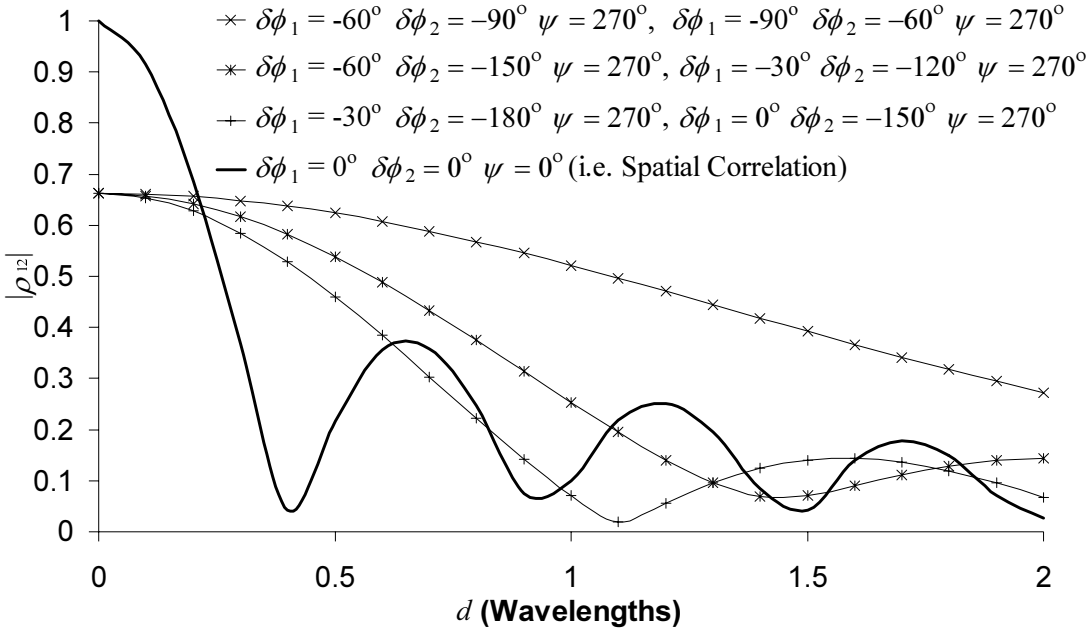

Figure 4-9 Comparison of how the same angular correlation affects spatial correlation in different scenarios for the horizontally separated antennas with high directionality

For the omni directional antenna with directional antenna case, the results from Figure 4-6 (a) are plotted in Figure 4-10 and results from Figure 4-6 (b) are plotted in Figure 4-11.

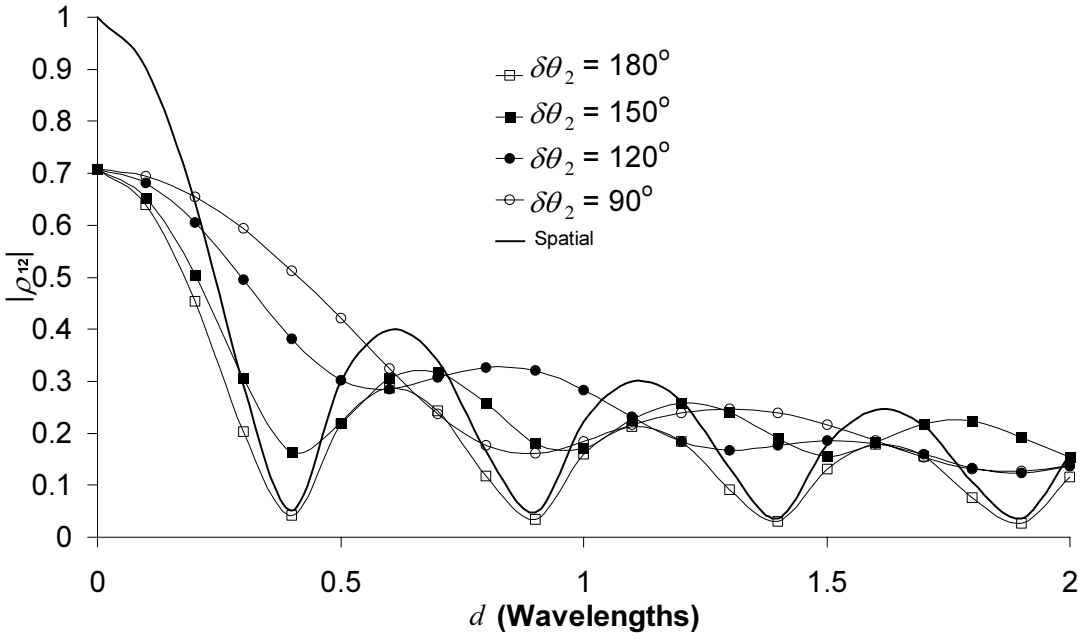

Figure 4-10 Comparison of how the same angular correlation affects spatial correlation in different scenarios for the horizontally separated antennas with one omni directional and one semi directional antenna

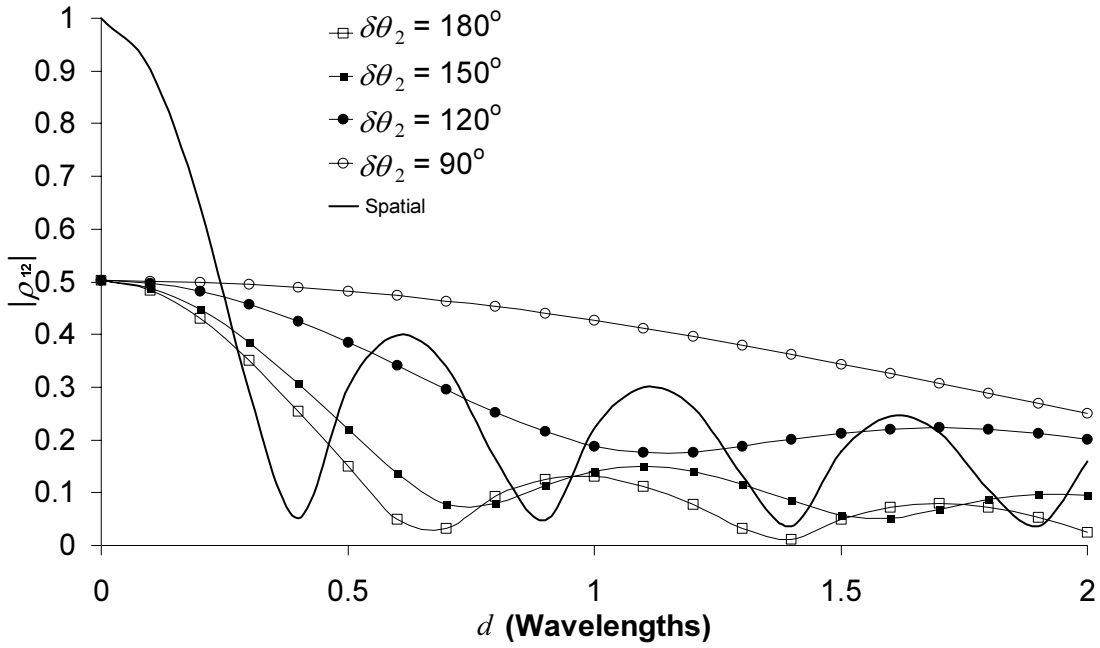

Figure 4-11 Comparison of how the same angular correlation affects spatial correlation in different scenarios for the horizontally separated antennas with one omni directional and one directional antenna

Angular correlation has varying effects on spatial correlation depending on the directivity of the antennas and the directions that they are pointing in. It is therefore necessary for the designer to analyse the azimuth patterns and determine whether there are significant angular contributions for closely spaced antennas. Figure 4-7 indicates that when antennas of low directionality are mainly radiating in opposite directions, then there will be a rapid increase or decrease in correlation depending on the spatial distance. If they are radiating orthogonal to each other or closer together, there is less rapid change to the spatial correlation. Semi directive antennas, as illustrated in Figure 4-8, consist of 120° sector overlaps between the antennas although they point in different directions. From this analysis, when the 120° sectors are pointing closer towards $\phi = \pm 90^{\circ}$ the correlation is increased where as when they are pointing closer towards $\phi = 0^{\circ}$ and $\phi = \pm 180^{\circ}$ then the correlation decreases. In all cases the angular correlation and antenna overlap is the same, although the spatial correlation is affected differently in each case due to the azimuth direction the two antennas are pointing in.

The same principle is true for 90° radiating antennas from analysis of Figure 4-9; this time though it is a 60° overlapping sector. Since the antennas are more directional in this case, the overlapping region is narrower which means in the general case the correlation decreases less rapidly when compared with Figure 4-8.

Like the case of two directional antennas, the omni directional and directional antenna scenarios in Figure 4-10 and Figure 4-11 show that the effects on overall correlation are due to the direction the directive element is pointing in similar to that of two directive elements. If the antenna is pointing towards $\phi = \pm 90^{o}$ then the correlation is increased but if it points towards $\phi = 0^{o}$ or 180^{o} then the correlation reduces.

4.6.2 Vertical spatial correlation integrated with angular correlation in elevation

The previous section presented analysis for cases of horizontal spacing only. Similar analysis was carried out for vertical spacing of isotropes separated by vertical distance *h*. All the angles shown in Figure 4-2 are applied the same way; however, distance *d* becomes distance *h* and angles $\delta\phi_1$ and $\delta\phi_2$ become $\delta\theta_1$ and $\delta\theta_2$ respectively. The results from these simulations are presented in Figure 4-12 for 180^{o} sectors, Figure 4-13 for 90^{o} sectors and Figure 4-14 for omni-directional and directional antennas. Their outcome differs to the horizontal case due to the non-uniform angle of arrival in elevation. Further to this, the angular correlation is not a measure of overlap between the antennas affecting the results dramatically. More so, angular correlation is a measure of overlap within the AOA region. Antennas with lower directionality have not been presented here since they do not produce significant results without a uniform angle of arrival.

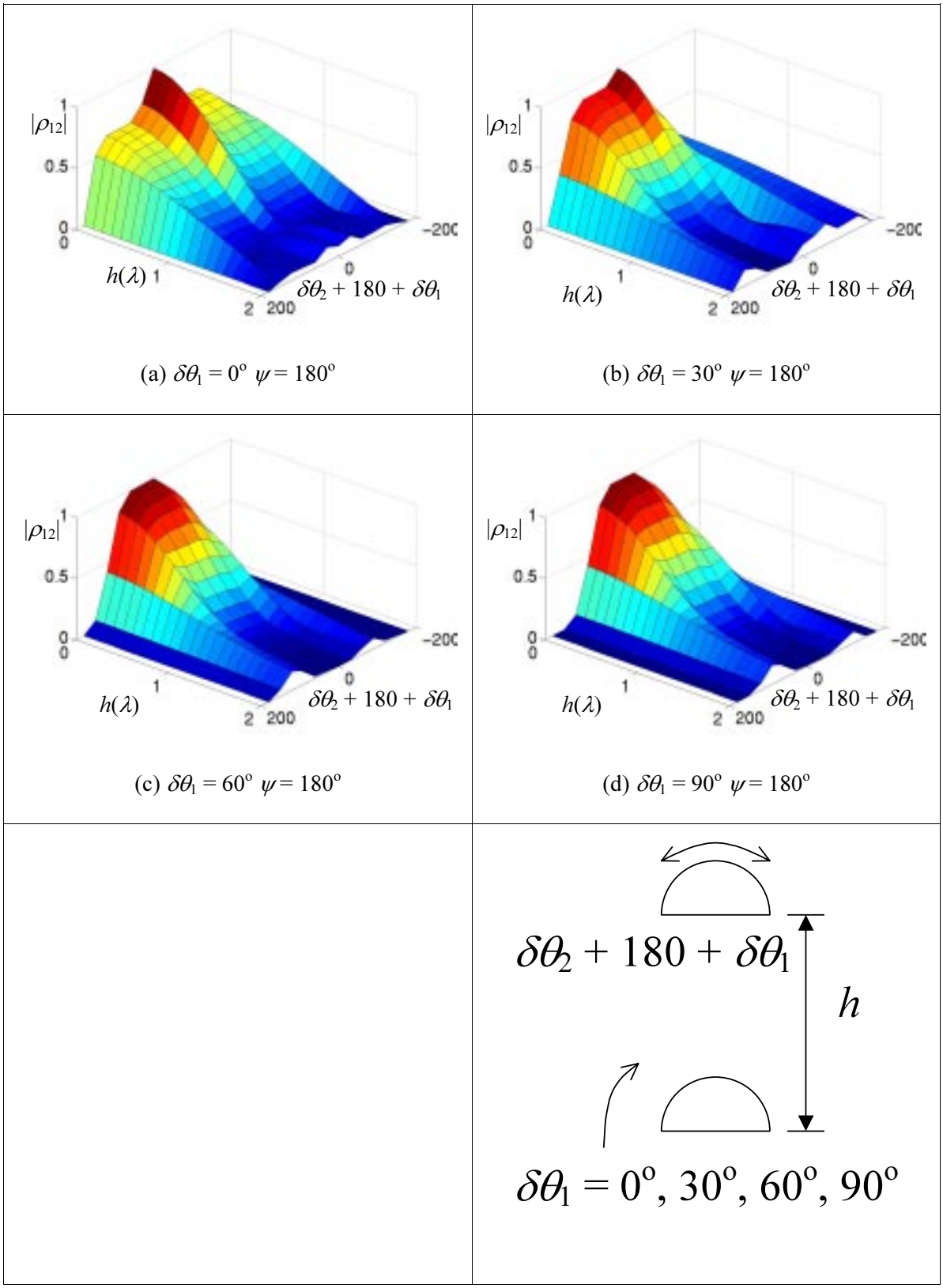

Figure 4-12 Interaction of angular and vertical spatial correlation with two semi directive patterns

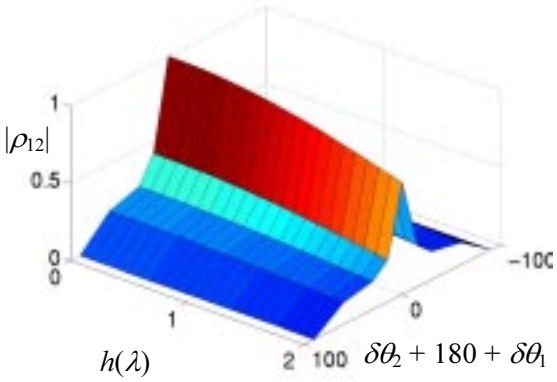

(a) $\delta\theta_1 = 0^o$ $\psi = 180^o$

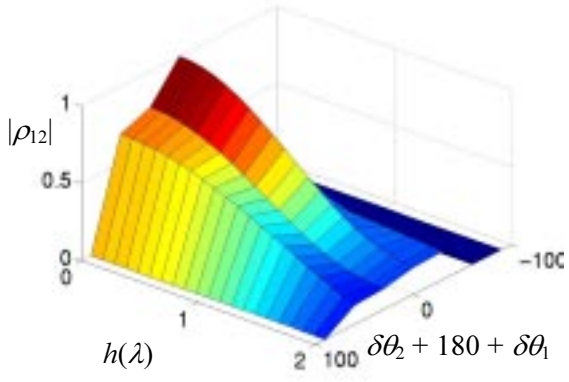

(b) $\delta\theta_1 = 30^o$ $\psi = 180^o$

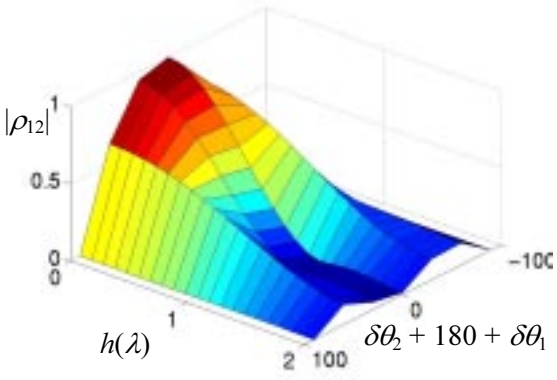

(c) $\delta\theta_1 = 60^o$ $\psi = 180^o$

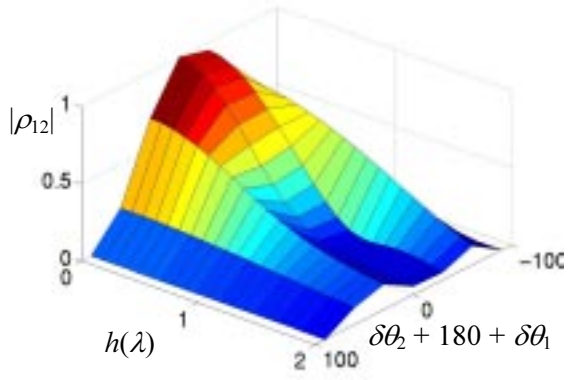

(a) $\delta\theta_1 = 90^o$ $\psi = 180^o$

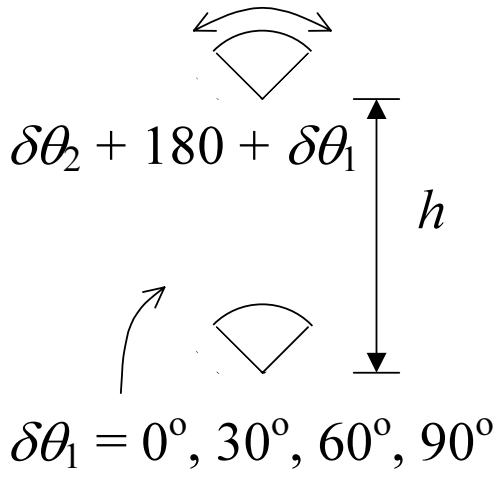

Figure 4-13 Interaction of angular and vertical spatial correlation with two directive patterns

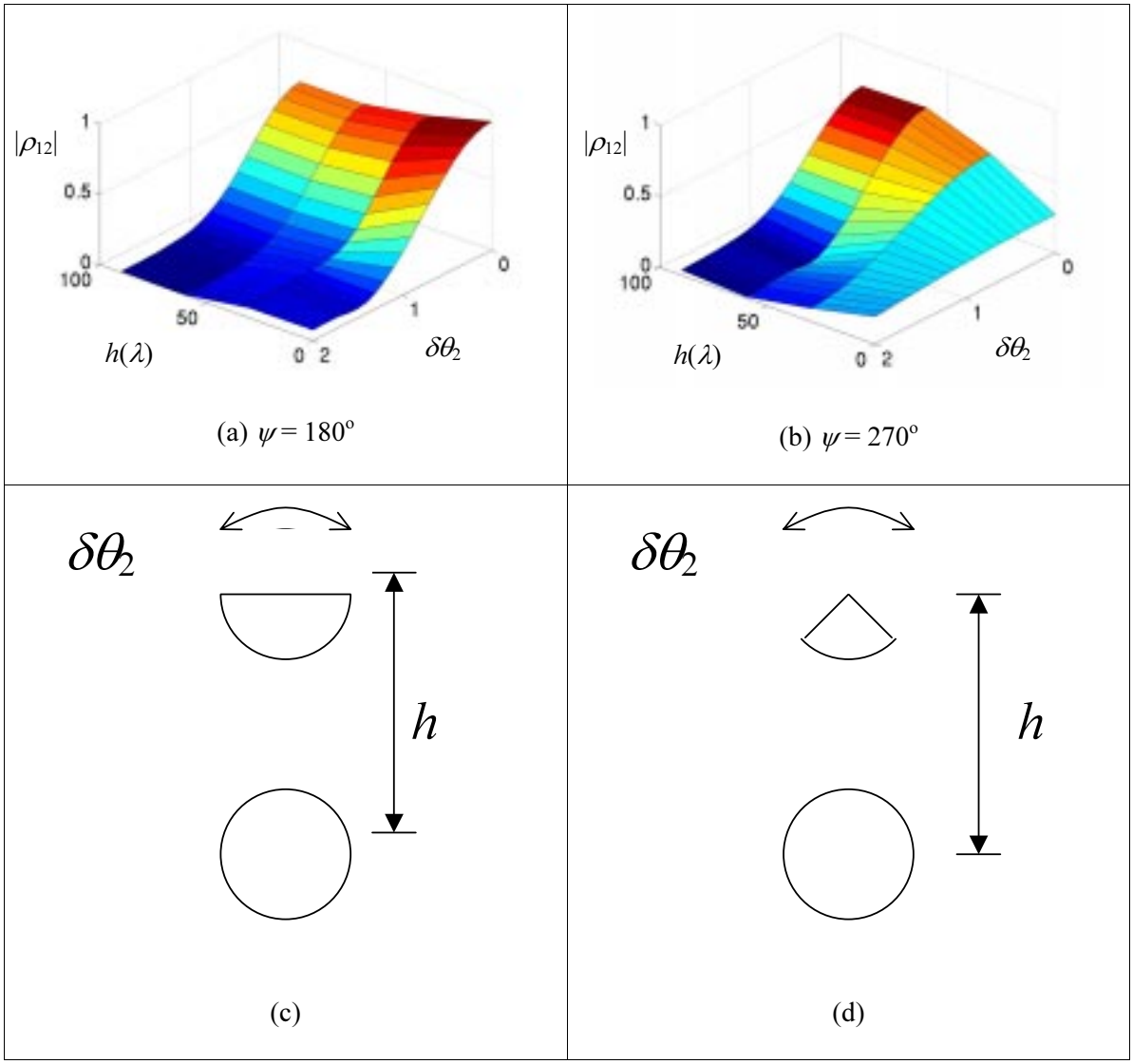

Figure 4-14 Interaction of angular and horizontal spatial correlation with an omni directional antenna and a semi directive antenna ((a) and (c)), and a directional antenna ((b) and (d))

Again, graphs have been plotted in Figure 4-15 and Figure 4-16 to illustrate the effects from the same correlation on the spatial diversity for 180° sectors and 270° sectors respectively. Following this graphs have been plotted in Figure 4-17 and Figure 4-18 to illustrate the angular correlation effects on spatial diversity when there is an omni directional antenna and a 180° sector and a 90° sector respectively.

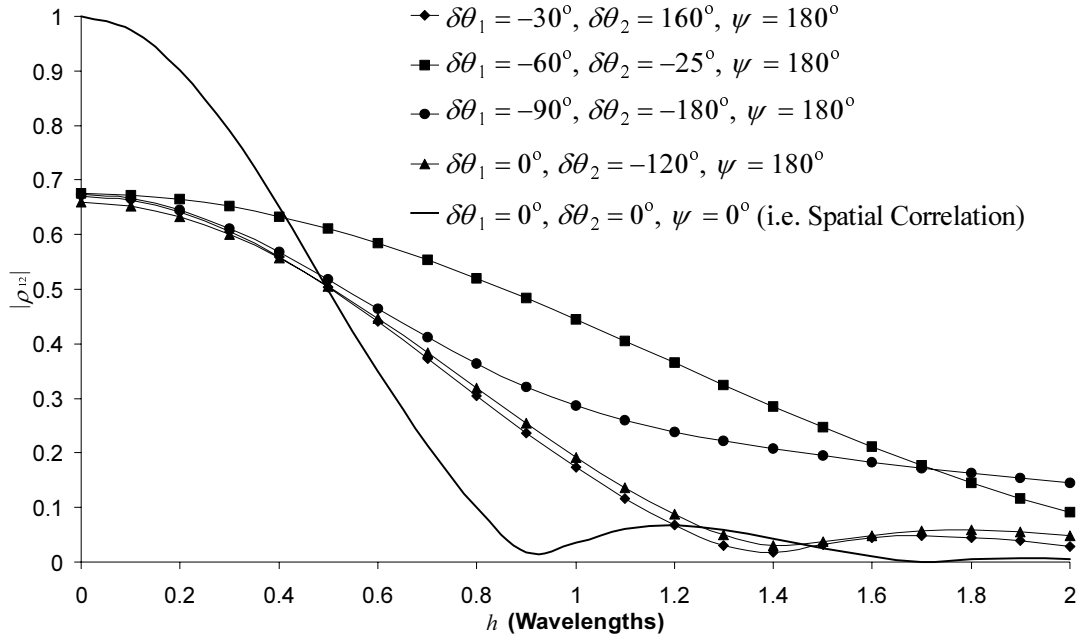

Figure 4-15 Comparison of how the same angular correlation affects spatial correlation in different scenarios for the vertically separated antennas with semi directionality

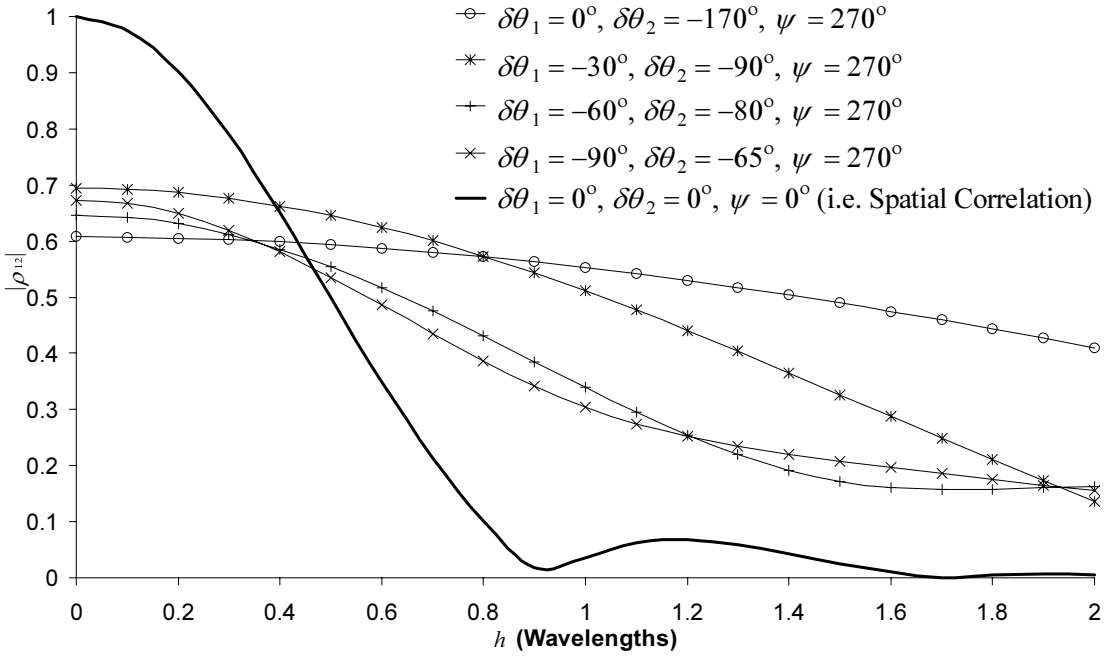

Figure 4-16 Comparison of how the same angular correlation affects spatial correlation in different scenarios for the vertically separated antennas with high directionality

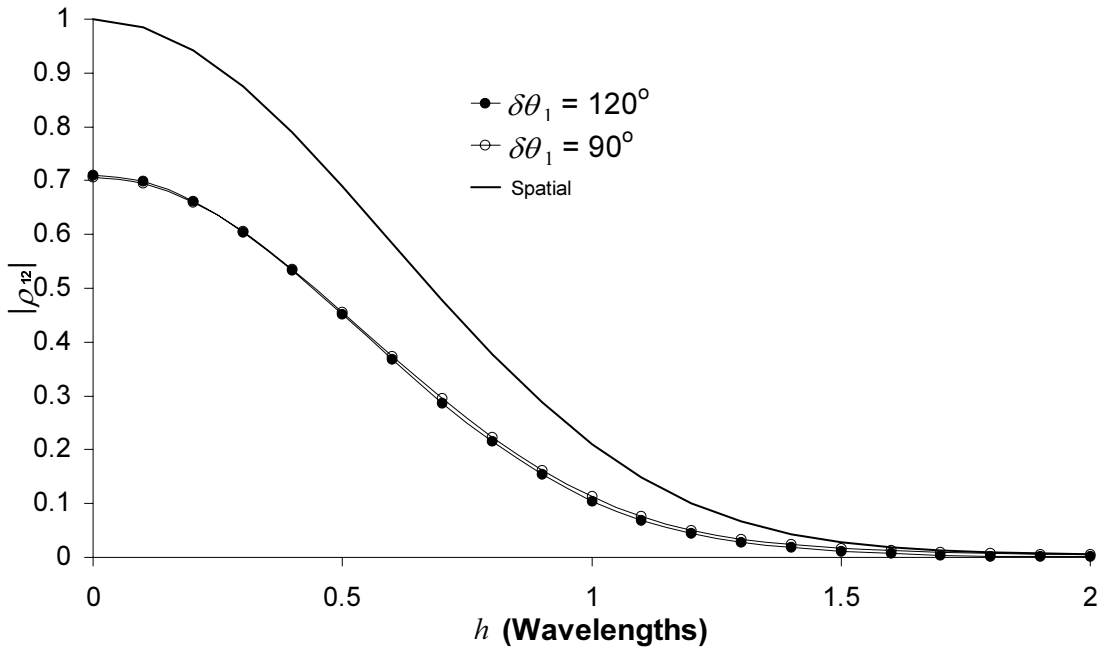

Figure 4-17 Comparison of how the same angular correlation affects spatial correlation in different scenarios for the vertically separated antennas with an omni directional antenna and a semi directional antenna

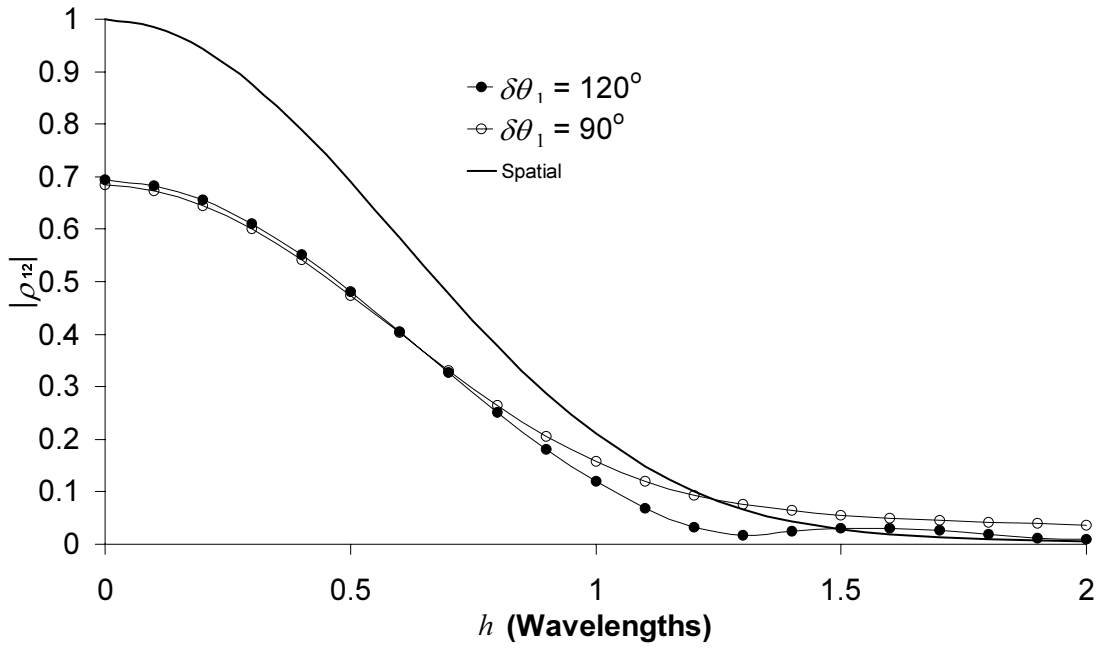

Figure 4-18 Comparison of how the same angular correlation affects spatial correlation in different scenarios for the vertically separated antennas with an omni directional antenna and a directional antenna

Analysis of Figure 4-15 and Figure 4-16 shows that when the overlapping part of the two sectors is outside of the angle of arrival region (i.e. $\theta = 30^{o}$ to 100^{o}) there is not such a rapid decrease on

the spatial correlation, however, within the angular region there is a more rapid decrease in comparison. In both cases, the limited angle of arrival means that below 2 wavelengths, directive antennas will increase the correlation and become a disadvantage unlike azimuth angular contributions. In the case of an omni-directional and directional antenna in Figure 4-17 and Figure 4-18, there is not a significant change to the spatial correlation from the same angular correlation due to the limited angle of arrival. For the best MEG, it is desirable that the directional antenna is pointing within the angle of arrival region.

4.6.3 Other effects of angular correlation

The only other two correlation interactions so far not discussed are the effects of elevation pattern on the horizontal spacing and the effects of azimuth pattern on elevation. These scenarios are not so complex and can be explained briefly. For vertical spacing, de-correlation due to the azimuth pattern will always reduce the overall correlation; therefore an angular contribution is made in all cases.

In the case of elevation pattern effects on horizontal correlation this is the same as if the elevation angle of arrival was altered in any way. Referring to Figure 1-10 in the chapter 3, it can be seen that elevation angle of arrival has little effect on horizontal spatial correlation as long as there is omni-directionality in azimuth. Therefore only azimuth changes can have any significant effect on horizontal spatial correlation. However, it must be noted that when elevation patterns are different, there will often be an implication that the azimuth patterns are different as well.

A final point to note is that the analysis has been carried out for antennas with the same polarisation. Analysis has shown that different polarisations do not make any significant effect on the way in which the angular correlation affects the spatial correlation. Therefore the polarisation correlation explained in section 4.4 can be used as a measure of how much polarisation contribution there is within the angular correlation.

4.6.4 Principles of interaction of spatial and angular correlation

Having presented results of the effects of angular correlation on spatial correlation, some conclusions need to be drawn for the designer to determine how angular correlation will affect the spatial correlation. There are cases where it will be not necessary to carry out detailed analysis of the azimuth and elevation patterns:

1. When the spacing is greater than 2λ, there is usually total spatial de-correlation in the majority of cases apart from exceptional cases such as Figure 4-13 (a), which do not often occur. Therefore in such circumstances it is not necessary to have angular correlation. It

would be more sensible in this situation for the antennas to be omni-directional at the mobile.

2. When the spacing is less than 0.1λ, there is little spatial contribution so the angular correlation will be comparable with the overall correlation. Therefore it would not be necessary to consider the effects of angular correlation on spatial correlation here.
3. If the angular correlation is negligible (less than 0.2) then the overall correlation will remain low regardless of spacing. Therefore in this case, it is an angular diversity system.
4. If the angular correlation is high (greater than 0.9) then the overall correlation will be comparable with the spatial correlation except in non-typical circumstances such as in Figure 4-13 (a). Therefore in this case it is a spatial diversity system.

When the spacing is between 0.1 and 2 wavelengths and the angular correlation is between 0.2 and 0.9 a more careful analysis of the azimuth and elevation patterns is required to determine whether the angular characteristics are beneficial to the diversity. This is clearly outlined in Figures 4-7 to 4-10 and 4-15 to 4-16 where the angular correlation may increase or decrease the spatial correlation. From the analysis carried out in this section the following can be concluded:

4.6.4.1 For horizontally spaced antennas

If the antennas have horizontal spacing then only the azimuth patterns need to be analysed. Patterns with low directivity will contribute some degree of de-correlation if their main lobes are closer together rather than opposite to each other where there will not necessarily be as much angular de-correlation. More directivity from the azimuth patterns pointing in different directions will contribute better de-correlation on average but this depends on the specific directions that the antennas are radiating in.

4.6.4.2 For vertically spaced antennas

Vertical spacing creates more complexity than the horizontal case since the angle of arrival is non-uniform. Both the azimuth and elevation patterns will have to be analysed in this case. Directivity in azimuth will reduce vertical correlation in all cases so it is therefore better to have contrasting azimuth patterns rather than elevation patterns. Analysis shows that de-correlation in the elevation plane is better achieved from angular contributions when the overlapping region of the two antenna patterns is within the angular region of incoming signals (i.e. $\theta = 30\text{-}100^{o}$). This will also achieve better MEG.

4.6.4.3 For both vertically and horizontally spaced antennas

In this case the criteria set out in sections 4.6.4.1 and 4.6.4.2 are both applicable in terms of how the overall correlation can be affected.

4.6.4.4 Summary of results

In conclusion these guidelines are set on the assumption of a uniform AOA in azimuth with Gaussian elevation AOA is assumed. Other angle of arrival models will be used in the future so it will be necessary to adapt these principles as they emerge. Further to this high directivity has been considered although it is still assumed that the beamwidth is reasonably wide, at least 90^{o} which is normally the case at the mobile. The designer could therefore extrapolate from these results to determine how the spatial and angular contributions in a given case will interact. The theory would not necessarily be applicable to narrower beamwidths so further analysis would be necessary.

4.6.4.5 Effect of antenna directivity on mean effective gain

Increasing the directivity of the antennas may significantly reduce the angular correlation although this can come at the expense of reduction in MEG. This section shows briefly how increasing the directivity can degrade the MEG. To begin with, this is not relevant in the horizontal case since the MEG in fact remains constant. As ψ is increased the gain is normalised appropriately (which did not need to be done to evaluate the correlation) and consequently the MEG still averages out to the same value in the case of uniform angle of arrival in azimuth.

In the elevation case, however, the situation is different due to the non-uniform AOA. Figure 4-19 shows the MEG for the semi-directional and directional antennas used in section 4.6.2 when the angle $\delta\theta_1$ is varied. In the first case, the $\psi = 180^{o}$ sector has maximum MEG when $\delta\theta_1$ is zero since the sector covers the most of the angle of arrival region in elevation, given uniform azimuth angle of arrival. For the $\psi = 270^{o}$ sector, the MEG is at a maximum when $\delta\theta_1$ is 70^{o} since this is the case where the antenna is covering as much of the AOA region as possible. Therefore, it can be concluded in elevation that maximum MEG is achieved when the antennas are radiating within as much of the angle of arrival region as possible. This is beneficial to diversity since section 4.6.4.2 concluded that the overlapping region of the antennas are also required to be within the angular region. Therefore optimum diversity will be achieved when the antennas are within the angular region.

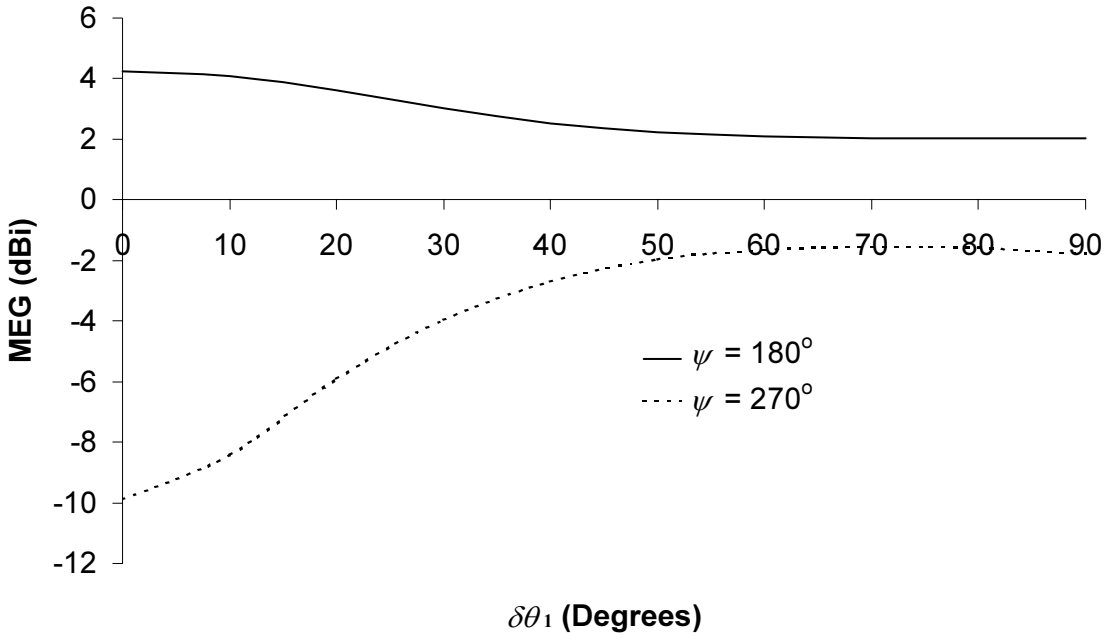

Figure 4-19 Graph showing change in Mean Effective Gain (MEG) versus sector shift angle in elevation for vertically spaced isotropes

4.6.5 Polarisation correlation within angular correlation

Using the method of polarisation correlation evaluation in equation (4.7) the results can be used to find how different the polarisations are within an angular diversity system. If there is a difference, it can be concluded that there is some contribution of polarisation diversity to the overall system. Figure 4-20 shows two cases of dipoles used, where angles φ and ε are self-explanatory.

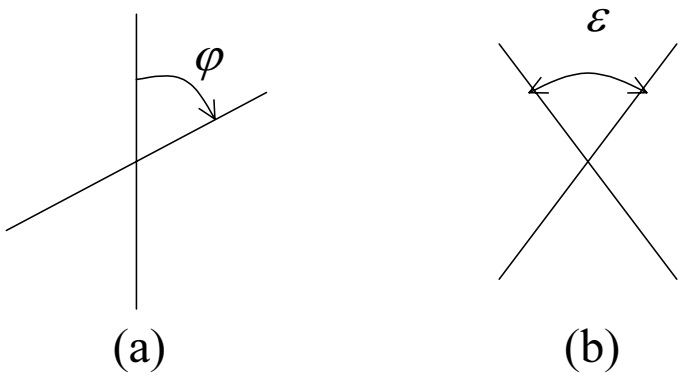

Figure 4-20 Diagram showing two examples of polarisation correlation used to show inherent polarisation correlation

Results from the setup in Figure 4-20 (a) are presented in Figure 4-21 and results from Figure 4-20 (b) are presented in Figure 4-22. In both cases, there is significant difference between the correlation of the antenna polarisations and the fading environment polarisations. In Figure 4-21, the correlation is lowest when the antennas are cross-polarised although it is by no means zero. This is because there is still significant E_θ polarisation in the horizontal antenna, which increases the correlation. The same is true in Figure 4-22 regardless of angle ε because there are still considerable E_θ and E_ϕ components so that the polarisation correlation will only reduce by a small margin around 140°.

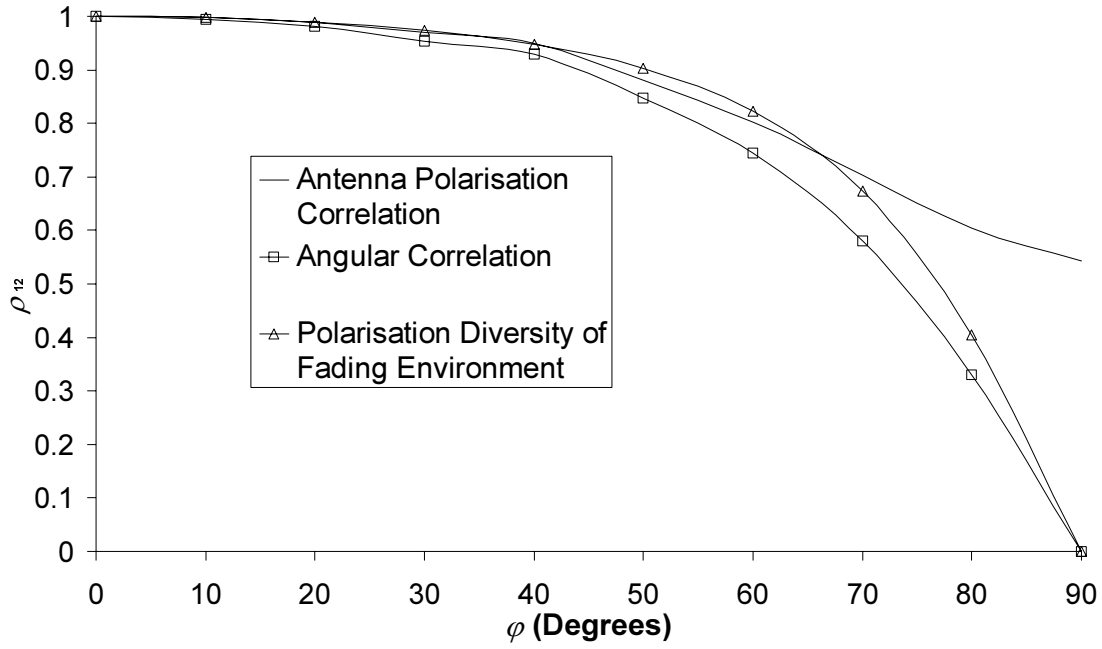

Figure 4-21 Polarisation correlation results from the setup in Figure 4-20 (a)

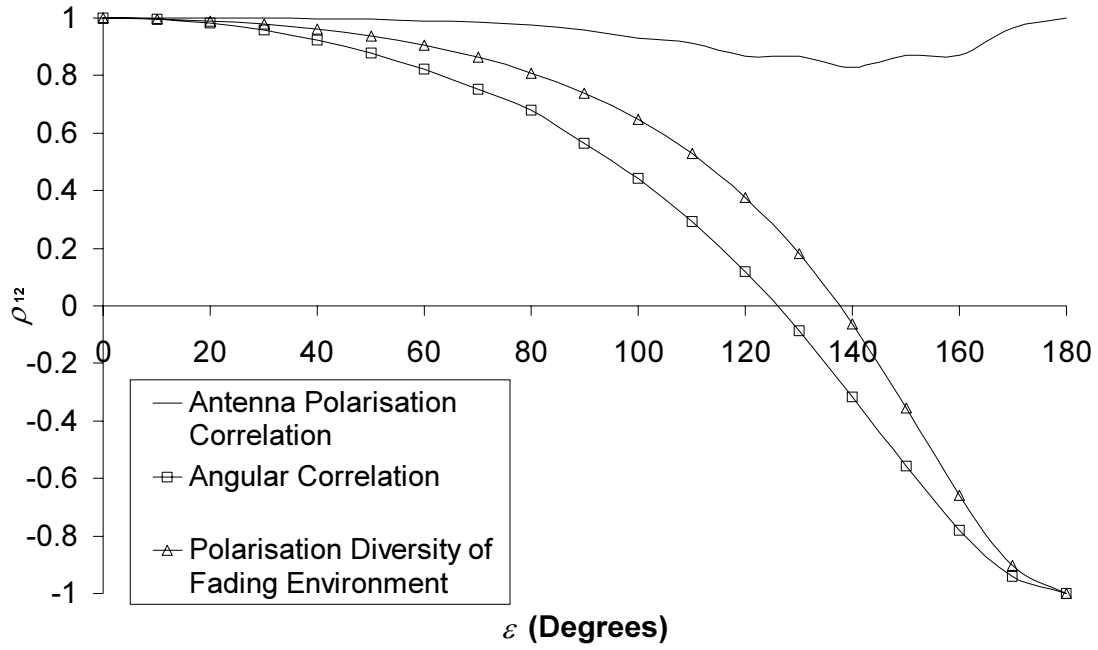

Figure 4-22 Polarisation correlation results from the setup in Figure 4-20 (b)

4.7 Effects of coupling and impedance in interpretation of results

At this point, effects of coupling and impedance have not been mentioned. However, it is important the coupling effects are taken into account so that the analysis can be carried out correctly. To begin with, the spatial correlation should be analysed with coupling present, which may change marginally if there is significant coupling since it is what is seen at the receiver. Angular diversity should be analysed at the output flange of the antenna, therefore impedance changes need to be taken into account, which will affect the phase as explained in chapter 3. In both cases, the angular and polarisation contributions can be evaluated correctly in the same way as if no coupling and impedance effects were considered.

4.8 Conclusion

The method for evaluating diversity at the mobile terminal has been presented to compute the spatial, angular and polarisation correlation based on antenna measurements. The antenna measurements include the angular field patterns, the spatial distance (including the direction) between the antennas and the S parameters. These results can be used to assist the designer to determine the diversity contributions of a mobile terminal.

The second part of the chapter investigated how the spatial, angular and polarisation contributions interact with each other. The first investigation considered how the spatial and angular correlation

integrated together to form an overall correlation by manipulating the spatial distance and field patterns of two isotropes. It was found that the angular correlation affected the spatial correlation differently depending on the antenna field patterns. Therefore the designer has to analyse the field patterns as well as the correlation results to determine whether the angular contribution has any benefit to the overall correlation. Results indicated that better angular contribution is achieved when the antennas have directive azimuth patterns and point in different directions although not far from each other. In elevation, the directive beams need to overlap within the angle of arrival region between 0^o and 30^o above the horizontal.

Antenna polarisation correlation was shown to be inherent within angular correlation. The value of polarisation correlation is a measure of whether the angular correlation is at all due to a polarisation contribution. If the antennas have similar polarisation then the polarisation correlation will be high.

Chapter 5

5 Case Study Measurements

Having established the method for evaluating the spatial, angular and polarisation diversity at the mobile, this will now be applied to two case studies. The first case study is a mobile handset terminal using a Planar Inverted-F Antenna (PIFA) as the main antenna and a meander line monopole as the second antenna. Some measurements were also carried out at talk position using a phantom head filled with appropriate sugar solution to analyse the effects of the head on spatial, angular and polarisation diversity. The second case study investigates the diversity potential of an Intelligent Quadrifilar Helix Antenna (IQHA), which simulations and measurements have shown to have as high as 23dB in system gain in an urban Rayleigh environment.

5.1 Handset and measurement specifications

Photographs of the handset are given in Figure 5-1 where it can be seen in (a) that there is a dual band PIFA designed for the *Nokia 3210* handset attached to a copper ground plane the same size as the normal handset. Secondly on the other side shown in Figure 5-1 (b) a meander line monopole antenna was added based on a design developed by Huang [Huan00].

(a) (b)

Figure 5-1 Pictures of the handset with a PIFA and meander line monopole

The dimensions of the PIFA dielectric are 40mm by 50mm in physical size attached to a ground plane 115mm by 45mm as is the size of the ground plane for the handset. The back piece of the

outer casing was used since this also had dielectric properties and it played a part in the impedance matching of the PIFA antenna. Without the casing, the PIFA was not matched. A male SMA connector with semi rigid cable was used to connect to the feed point for measurement purposes. As a dual band antenna, the PIFA is designed to work at GSM900 and GSM1800 bands so measurements were carried out at 920MHz and 1800MHz.

The meander line monopole, on the other hand, was not dual band so two separate meander line antennas were used for the 920MHz and 1800MHz measurements. For 920MHz, the total wire length was 189mm and meandered in a tapered fashion as shown in Figure 5-2 (a). The maximum length at the top is 18mm as shown, and then every line below reduces in length by 1mm as one progresses down the taper. The track width was 1mm with spacing of 2mm as shown. The meander was connected to a ground plane 30x35mm and the antenna was inclined 30^{o} above the ground plane. In the case of 1800MHz in Figure 5-2 (b) the design is exactly the same although this time it starts with a wire length of 11mm and not 18mm to constitute the reduction in wire length down to 78mm. The ground plane at 1800MHz was also different in size, 40x50mm.

At both frequencies, therefore, the meander monopole was not connected to the handset ground plane for the purposes of these measurements. To begin with, it was necessary to remove the meander line monopole to determine whether the antennas lose their mean effective gain (MEG) in any way when in the presence of each other. Therefore, disconnecting the soldering joint of the antenna would affect the results and they would not necessarily be repeatable since the return loss could be significantly different when the antenna was re-soldered. Further to this, it was therefore possible to carry out the tests at 1800MHz by replacing the 920MHz meander line monopole with a shorter meander line.

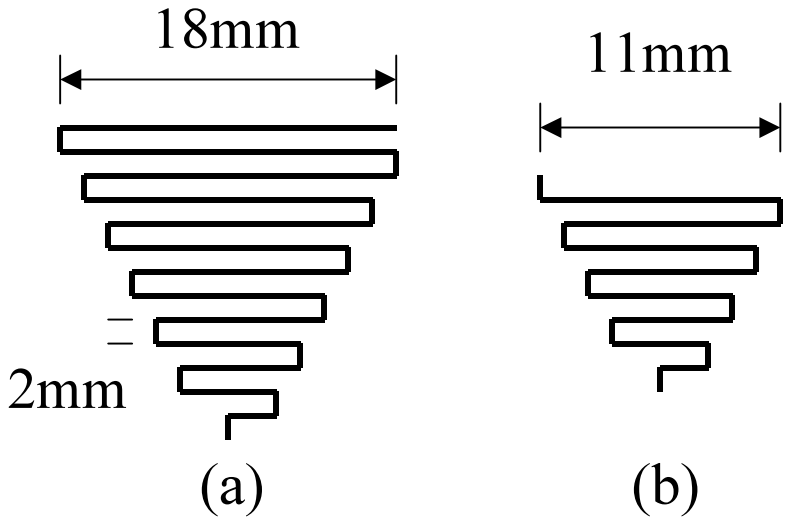

Figure 5-2 Diagram showing the construction parameters for the two meander line monopoles

The Z parameters of the antennas at the measurement frequencies are shown in Table 5-1. Both antennas have a reasonable match yielding at least 10dB return loss with low coupling, although not negligible, as shown by the S parameters in Table 5-2.

Frequency / MHz	z_{11}/Ω	$z_{12}/z_{21}/\Omega$	z_{22}/Ω
920	38.16 - j28.94	-12.63 + j18.02	31.08 - j9.60
1800	45.48 - j10.26	2.91 - j34.55	79.45 - j35.05

Table 5-1 Z-Parameters of the antennas at the two frequencies of measurement

Frequency / MHz	s_{11}/dB	s_{12}/s_{21}/dB	s_{22}/dB
920	-20.09	-8.48	-12.16
1800	-11.21	-12.51	-10.71

Table 5-2 S-Parameters of the antennas at the two frequencies of measurement

5.2 Correlation measurements on the handset

The antennas were measured with 10^o and 5^o step elevation cuts with the handset vertical in free space. This was done to verify that the 10^o steps were giving sufficiently accurate resolution to evaluate complex correlation using equation (4.1). In all cases, the comparison of the 10^o and 5^o cuts in Table 5-3 show sufficient accuracy for complex correlation; hence 10^o resolution is considered to be sufficient. The overall correlation is clearly lower at 1800MHz compared to 920MHz so the spatial, angular and polarisation correlations are evaluated to see why this is the case.

Angular correlation to begin with has been shown both when the impedance effects are applied and when they are not. By inspection it is clear that better definitions of the angular correlation are given when the impedance effects are taken into account. Angular correlation is considerably higher at 920MHz which can be explained when the azimuth and $\phi = 0^o$ elevation patterns are compared in Figure 5-3. As a point of reference, $\phi = 0^o$ is the point normal to the back of the handset, which is the boresight of the PIFA antenna. There is no significant difference in the elevation patterns, especially not in the angular region from $\theta = 30^o$ to 100^o where the elevation angle of arrival is mainly coming from. Therefore the elevation patterns cannot give a sufficient explanation of why there is reduction in angular correlation at 1800MHz. Azimuth patterns, on the other hand, are all similar apart from the PIFA antenna pattern at 1800MHz, which has greater directionality. This will account for a decrease in angular correlation since there is diversity from

an omni-directional antenna in comparison with a directional antenna. All plots in Figure 5-3 are E_θ plots since the E_ϕ patterns are negligible in magnitude and need not be considered.

Spatial correlation shown after angular correlation in Table 5-3 has some effect from coupling and is lower at 1800MHz, which would be expected since the spacing at 920MHz is only 0.23λ where it is 0.6λ at 1800MHz. The correlation at 920MHz is 1.02 in value when it should be less than or equal to 1 although this is due to computational and measurement error from limited decimal places. However, this is negligible error close enough to unity. At this point it shows how coupling increases the spatial correlation since the antennas begin to merge into one. At 1800MHz this is less so and the increased spacing is contributing to the reduction in overall correlation.

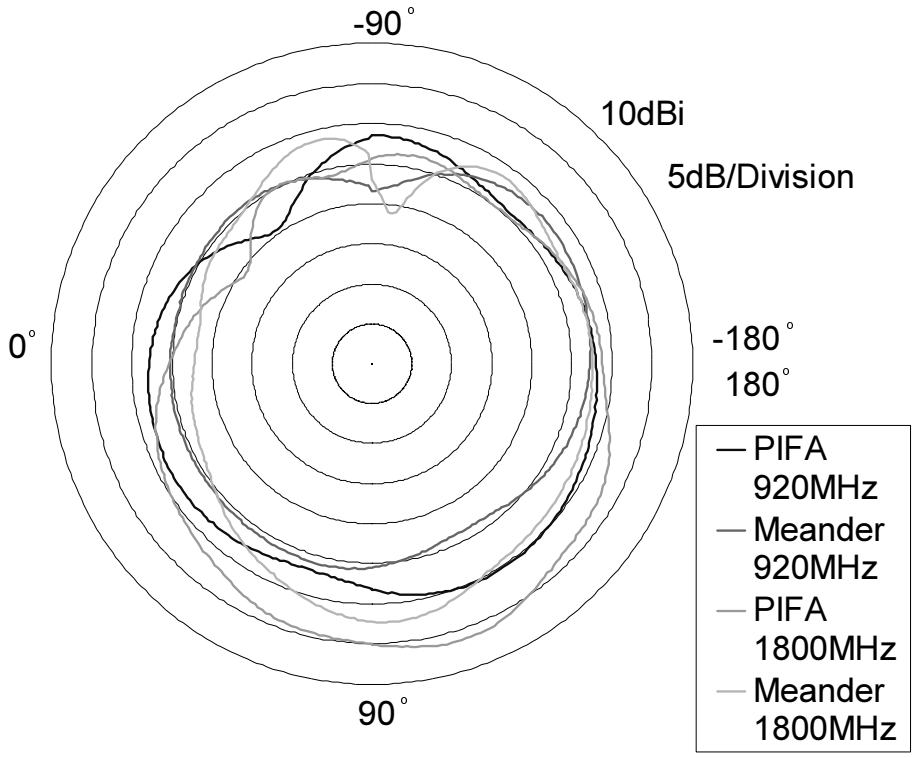

(a)

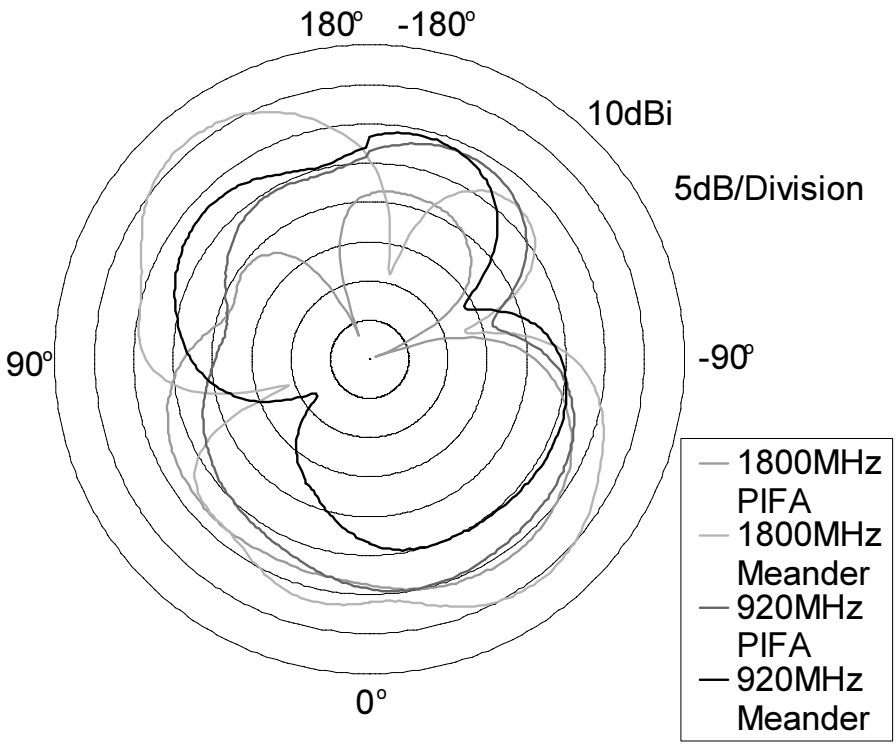

(b)

Figure 5-3 Comparison of the azimuth (a) and $\phi = 0^o$ elevation (b) patterns between the PIFA and meander

Type of Correlation	ρ_{12} at 920MHz	$\lvert\rho_{12}\rvert$ at 920MHz	ρ_{12} at 1800MHz	$\lvert\rho_{12}\rvert$ at 1800MHz
Overall				
10^o Cuts	-0.40 - j0.71	0.82	-0.29 – j0.75	0.37
5^o Cuts	-0.40 - j0.71	0.82	-0.29 – j0.76	0.38
Angular (Without Impedance Effects)				
10^o Cuts	-0.52 - j0.61	0.80	-0.51 – j0.31	0.59
5^o Cuts	-0.51 - j0.61	0.80	-0.51 - j0.30	0.60
Angular (With Impedance Effects)				
10^o Cuts	-0.69 - j0.40	0.80	-0.44 – j0.40	0.59
5^o Cuts	-0.69 - j0.41	0.80	-0.45 - j0.40	0.60
Spatial (No Coupling)	0.90 + j0.24	0.93	0.22 + j0.48	0.53
Spatial (With Coupling)	0.96 + j0.34	1.02	0.17 - j0.28	0.33
Polarisation				
10^o Cuts	0.98	0.98	0.89	0.89
5^o Cuts	0.98	0.98	0.89	0.89

Table 5-3 Summary of the of the correlations from the handset at 920MHz and 1800MHz

Finally, the polarisation correlation is listed following the spatial correlation and like angular diversity, the coupling effects give a better definition when they are taken into account. In both cases the correlations are high, which would be expected since the antennas are both co-polarised. Therefore it is concluded in these cases that there is not any useful contribution to the diversity from the polarisation.

It can be concluded from the correlation results that there is a high correlation at 920MHz due to low spacing and little contrast between the antenna patterns. At 1800MHz, there is angular de-correlation due to there being difference in azimuth field patterns and significant spacing above half a wavelength.

5.3 Mean effective gain measurements on the handset

As well as correlation, the Mean Effective Gain (MEG) of the antennas must also be evaluated in order to determine whether they have any system gain. Table 5-4 shows the MEG evaluated for the two antennas at the two frequencies in 5^o and 10^o steps to verify sufficient resolution in the measurements. As can be seen there is a comparable MEG at 920MHz of about 1dB difference, which is reasonable. However, at 1800MHz there is greater than 3dB difference, which is not good for diversity. The case is presented here that the PIFA antenna has greater directionality to facilitate reduced angular correlation although it does this at the expense of reduced MEG. Therefore there is not a good antenna diversity system at either of the frequencies in the case when the handset terminal is vertical since neither have low correlation and the same MEG together. Measurements were also carried out to evaluate the MEG of the meander antenna and the PIFA antenna when not in the presence of each other. In all cases, the results were comparable within 0.5dB. Since the profile of the two antennas are relatively low to each other, they do not actively distort each others radiation patterns and reduce their respective MEGs, which is an advantage to diversity.

Antenna	920MHz (dB)	1800MHz (dB)
PIFA at 10^o Cuts	-3.54	-4.58
PIFA at 5^o Cuts	-3.49	-4.54
Meander at 10^o Cuts	-4.59	0.77
Meander at 5^o Cuts	-4.54	0.71

Table 5-4 Mean Effective Gain evaluation of the antennas at the measurement frequencies used

5.4 Diversity performance of a vertical handset

Having established the correlation and MEG results, it can be concluded what exact system gain will be achieved from the vertical handset at both frequencies. Due to negligible difference between the selection combiner diversity gain and system gain are effectively the same. Therefore in Table 5-5, the degradation in diversity gain due to correlation is shown (assuming equation

(2.10) is valid). Further to this *k* is shown at the two frequencies and finally the resulting system gain is shown. As discussed in previous sections, there is degradation from high correlation at 920MHz, where as for 1800MHz there is degradation in diversity gain due to unequal mean branch power. Therefore the resulting system gain in both cases is about the same, around 4dB less than the maximum possible system gain of 10dB.

Frequency/MHz	**Degradation in diversity gain due to correlation/dB**	***k*/dB**	**System Gain/dB**
920	-2.42	-1.04	-6.54
1800	-0.34	-3.82	-5.84

Table 5-5 Comparison of system gain performance for the two GSM frequencies of the vertical handset

5.5 Effects of angle of arrival

All the results so far have been calculated on the basis that the mean AOA in elevation, $\overline{\theta}$, is 20^o and that also the standard deviation, σ, is 20^o. It is possible that the standard deviation could vary between 20^o and 80^o as discussed in chapter 2 although the mean does not vary significantly. Further to this, only the angular correlation would be affected by change in AOA in this case study so Table 5-6 shows the variation of angular correlation with σ.

σ/^{o}	ρ_{12} at 920MHz	$\lvert\rho_{12}\rvert$ at 920MHz	ρ_{12} at 1800MHz	$\lvert\rho_{12}\rvert$ at 1800MHz
20	-0.69 - j0.40	0.80	-0.44 – j0.40	0.59
40	-0.68 - j0.41	0.79	-0.49 – j0.38	0.62
80	-0.67 - j0.38	0.77	-0.50 – j0.40	0.64

Table 5-6 Variation of angular correlation with σ_A in an urban fading environment

Varying σ has negligible effect on the angular correlation as shown, which is consistent with the effects of angle of arrival presented in chapter 3. The same test was carried out for MEG and again there was negligible variation in the results all less than 1dB.

5.6 Effects of cross polar ratio

In the above results, 6dB cross-polar ratio (*XPR*) has also been assumed. The *XPR* could vary between 0 and 10dB in different fading environments as discussed in section 2.5 so Table 5-7 shows a comparison of angular correlation with varying *XPR*. Correlation changes beyond 0.1 in magnitude in this case so it would be necessary for the designer to vary the *XPR* when evaluating diversity to give an average performance. Table 5-8 also shows that the MEG varies anything up to 3dB as the *XPR* is changed, which will also affect the diversity.

***XPR*/dB**	ρ_{12} **at 920MHz**	$\lvert\rho_{12}\rvert$ **at 920MHz**	ρ_{12} **at 1800MHz**	$\lvert\rho_{12}\rvert$ **at 1800MHz**
0	-0.57 - j0.36	0.67	-0.40 - j0.40	0.57
3	-0.65 - j0.39	0.76	-0.46 - j0.40	0.61
6	-0.69 - j0.40	0.80	-0.44 - j0.40	0.59
10	-0.72 - j0.41	0.83	-0.53 - j0.39	0.66

Table 5-7 Variation of angular correlation with *XPR* in an urban fading environment

***XPR*/dB**	PIFA at 920MHz/dB	Meander at 920MHz/dB	PIFA at 1800MHz/dB	Meander at 1800MHz/dB
0	-5.26	-6.01	-5.81	-0.64
3	-4.22	-5.16	-5.08	0.19
6	-3.54	-4.59	-4.58	0.77
10	-3.04	-4.16	-4.20	1.19

Table 5-8 Variation of MEG with *XPR* in an urban fading environment

5.7 Effects of the human head

Evaluating diversity performance of the antenna when vertically orientated is not measuring the performance for a proper user application. It is more appropriate to undertake the investigation when the antenna is in talk position next to a phantom head. Carrying out such a test has many complications, however, when measuring the elevation patterns, the whole phantom and handset has to be rotated around the PIFA antenna's phase centre. Building a jig for such a purpose is a

long and laborious task that could not be implemented so the experiment was carried out using a simpler, although less reliable method.

For every elevation cut measured, the phantom was rotated on the platform while laid horizontally as shown in Figure 5-4 adjusting the height and position for every elevation cut that was measured. For every cut, the height was adjusted and the platform position was moved and aligned as appropriate. Therefore the phase centre had to be moved back into the correct position for every elevation cut that was taken, which yields some inaccuracy. The measurement was carried out at 920MHz only since the wavelength is higher and so this would help to reduce the possible phase error from re-positioning the antenna for every measurement.

Figure 5-4 Photograph showing the phantom set up on a platform in the anechoic chamber

The antenna was measured using the phantom with the handset against the head 60^{o} from the vertical so the handset was in line with the ear and mouth. Also the handset was measured without the phantom in this orientation so that the effects on spatial, angular and polarisation correlation due to the head alone could be evaluated. The S parameters and Z parameters changed with the presence of a phantom head by a small margin so they are presented below in Table 5-9 and Table 5-10 respectively. The coupling and self-impedances of the antennas do change mainly due to 3dB difference in coupling between the antennas.

	s_{11}/dB	s_{12}/s_{21}/dB	s_{22}/dB
Without Phantom	-20.09	-8.48	-12.16
With Phantom	-12.01	-11.53	-16.32

Table 5-9 Comparison of S-parameters with and without the presence of a phantom head

	z_{11}/Ω	$z_{12}/z_{21}/\Omega$	z_{22}/Ω
Without Phantom	38.16 - j28.94	-12.63 + j18.02	31.08 - j9.60
With Phantom	31.00 + j0.24	9.43 - j2.61	30.08 - j1.84

Table 5-10 Comparison of Z-parameters with and without the presence of a phantom head

5.7.1 Effects on correlation

Correlation with and without the phantom head present is compared in Table 5-11 and in all cases only 10^{o} elevation cuts were taken since it was impractical to take 5^{o} cuts. All correlations have been presented with the coupling effects included.

Type of Correlation	ρ_{12} **without phantom**	$\lvert\rho_{12}\rvert$ **without phantom**	ρ_{12} **with phantom**	$\lvert\rho_{12}\rvert$ **with phantom**
Overall	-0.33 - j0.70	0.72	-0.05 - j0.07	0.09
Angular	-0.67 - j0.13	0.68	0.02 - j0.03	0.04
Spatial	0.83 + j0.19	0.85	0.68 + j0.09	0.68
Polarisation	0.96	0.96	0.87	0.87

Table 5-11 Table showing the effects on correlation of the presence of a phantom head

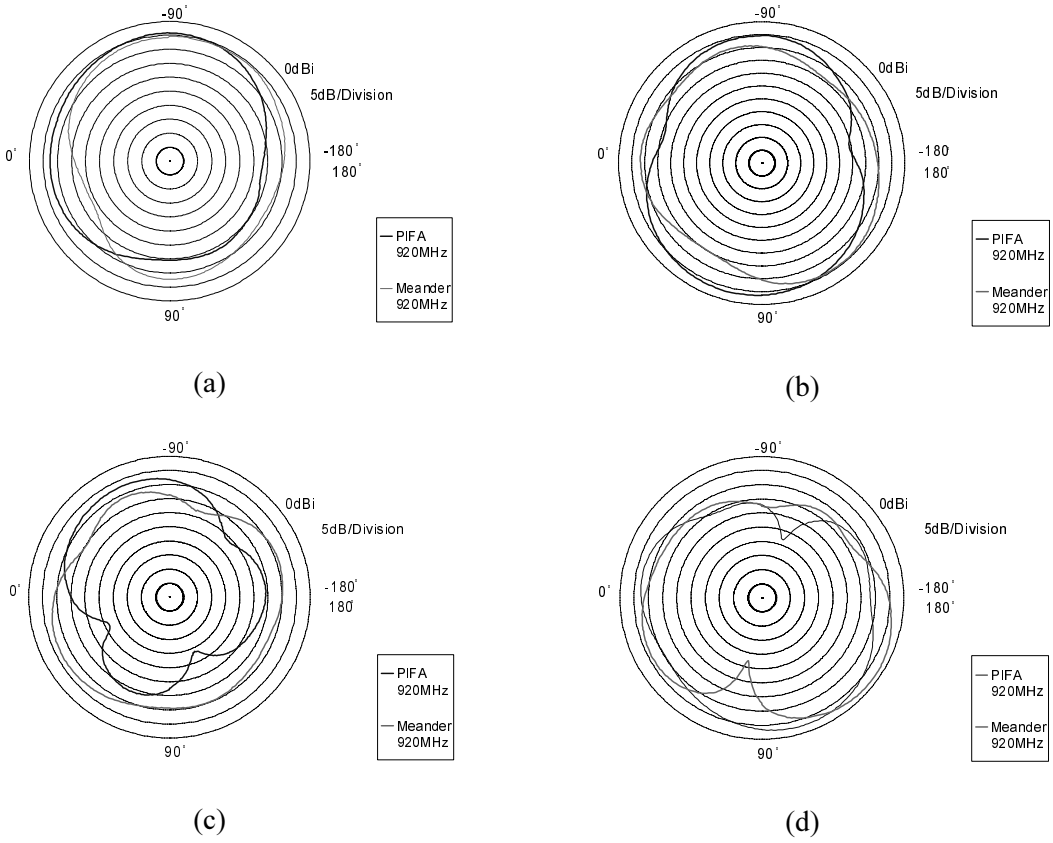

Figure 5-5 Comparison of the meander and the PIFA (a) E_θ without phantom (b) E_ϕ without phantom (c) E_θ with phantom (b) E_ϕ with phantom

Results in Table 5-11 indicate that there is a large reduction in the angular correlation with a small drop in polarisation correlation and spatial correlation. The azimuth patterns for the E_θ and E_ϕ polarisations are shown in Figure 5-5 with and without the presence of a phantom. As can be seen, in both polarisations, the presence of the head causes a greater difference between the two field patterns in both polarisations. Some degree of de-polarisation appears also to be caused by the head resulting in some polarisation de-correlation.

5.7.2 Effects on mean effective gain

Finally the mean effective gain is evaluated with and without the phantom and presented in Table 5-12. As expected, the presence of a head reduces the MEG considerably by about 5dB. However, the MEG values have less than 1dB difference in this configuration, which is helpful to diversity. It can be concluded from this that there is significantly better diversity performance in talk position with low correlation and equivalent MEG although this does come at the expense of loss in efficiency.

	MEG of PIFA /dB	MEG of Meander /dB
Without Phantom	-5.83	-5.54
With Phantom	-10.20	-10.81

Table 5-12 Comparison of MEG for the PIFA and meander with and without the presence of a phantom

5.7.3 Effects on diversity performance

As discussed in section 5.7.3, the system gain is the same as the diversity gain for this case also. To compare how the presence of phantom affects the diversity performance, results can be presented in Table 5-13 as in Table 5-5. In this case the reference is a single branch so therefore the system gains are comparable since the degradation due to correlation and branch power ratios are low. It must be noted here that if the reference antenna without the phantom was used for the system gain results with the phantom, system gain would reduce by a further 5dB. This has not been chosen in this case, however, since it is not a realistic reference for standard use. These results show that the diversity system is improved by the human head due to the decrease in correlation adding an extra 1dB but the head will be a disadvantage to the MEG of the antennas with or without diversity. However, the diversity antenna still improves performance so it is therefore beneficial.

	Degradation in diversity gain due to correlation/dB	***k*/dB**	**System Gain/dB**
Without Phantom	-1.59	-0.29	8.12
With Phantom	-0.02	-0.61	9.37

Table 5-13 Comparison of system gain performance with and without the presence of a human head

5.8 Diversity evaluation of IQHAs

An Intelligent Quadrifilar Helix Antenna (IQHA) is an example of a four-branch diversity system built upon four separate helix antennas made into one antenna. It is an appropriate choice for mobile to satellite communications as it provides the low directivity and circular polarisation requirements that are needed in such a scenario. The antenna is an intelligent antenna based on the

fact that it can work as an adaptive antenna to apply appropriate beam steering to communicate with satellites or terrestrial base stations coming from varying directions [Agius99].

From both measurements and simulations it has been found that an IQHA system gain has the potential to be as high as 23dB in a Rayleigh fading environment when using the Equal Gain Combining (EGC) method referenced to a single element of the antenna or otherwise 19dB system gain referenced to a standard quadrature fed IQHA [Leach00] also summarised in Table 5-14. As can be seen from the results, the system gain for Maximum Ratio Combining (MRC) is only 19dB when referenced to a single element; 4dB less than for EGC, which contradicts the fact that MRC has a higher output diversity gain [Jak94]. This is, however, different in the case of the IQHA because combining is applied at Radio Frequency (RF) rather than after demodulation, which is normal practice. If the signals are combined at RF then there is only one Gaussian noise source at the demodulator, where as if they are combined after demodulation then there are four Gaussian noise sources. Such combining without noise sources present causes an increased signal at the receiver, which in turn creates a new resultant antenna pattern on the IQHA from the co-phasing elements. The new antenna pattern will improve the MEG as a result so that this will add to the diversity already achieved. Therefore this section will investigate what improvement there is due to diversity and the improvement in MEG there is.

A further item that has not yet been investigated is why the IQHA provides sufficient de-correlation between the elements to assist diversity. Therefore the spatial, angular and polarisation diversity characteristics will be analysed to show why the IQHA has diversity.

	Standard Quadrature feed	Selection Combining	MRC	EGC
System Gain /dB	4	15	19	23

Table 5-14 Table showing the system gain results from simulations in a Rayleigh fading environment using different combining methods

5.9 IQHA specifications

Two IQHA antennas were measured with 10^{o} elevation cuts since it has already been proved from the handset measurements that this is a sufficiently accurate resolution. The first antenna was a standard sized IQHA centred at 2GHz in Figure 5-6 (a). The dimensions of this were 88mm in length and 14mm in diameter. The IQHA tracks were printed onto flexible printed circuit board 95mm in length with track width 2mm spaced 7mm apart. By appropriate geometry the IQHA

was formed by rolling the PCB into a cylinder [Aguis99]. Each port was fed with quarter wavelength semi rigid cables and a connector.

The second antenna was a reduced sized meandered IQHA [Chew02] in Figure 5-6 (b). The dimensions here were reduced to 45mm in length also with 14mm diameter. This was done by meandering the IQHA branches by 5 turns with track spacing of 4mm. This time, however, the total track length was 144mm.

Comparison of the measurements therefore will show how reduction in size will affect the diversity potential. The S parameters and Z parameters are not relevant in this application in terms of how they will affect diversity as will be seen so they are not presented here. All measurements carried out in this section are for a vertical IQHA.

(a)

(b)

Figure 5-6 Pictures showing the IQHA antennas measured for diversity analysis (a) the standard sized IQHA and (b) the reduced size meander line IQHA

5.10 Correlation measurements of IQHAs

The first stage of analysing an IQHA involves investigating the correlation between the four elements, including the spatial, angular and polarisation contributions. Since the feed points are all close together, the distance between the phase centres of the individual elements is negligible ($< 0.01\lambda$) so spatial correlation can be assumed to be unity based on principles laid out in chapter 4. Therefore only the angular and polarisation contributions need to be analysed. The angular diversity can be evaluated by correlating the individual elements measured, which are presented in Table 5-15 for both the standard sized IQHA and the meandered IQHA. The correlation

between the first and second element, ρ_{12}, and the first and third element, ρ_{13}, is shown. It is not necessary to present all the other correlations since in this instance, $\rho_{12} = \rho_{14} = \rho_{21} = \rho_{23} = \rho_{32} = \rho_{34}$ and $\rho_{24} = \rho_{42} = \rho_{13} = \rho_{31}$ provided there is a symmetrical structure where all the subscript numbers are respective to the relevant element feed point numbers shown in Figure 5-7. Impedance effects are not relevant in this case since $z_{11} = z_{22} = z_{33} = z_{44}$ and will therefore not change the correlation as shown by equation (3.66). Therefore Z parameters have no effect on diversity if there is no spatial diversity since polarisation diversity does not use them. The correlation results also assume there is uniform angle of arrival in azimuth and Gaussian angle of arrival in elevation as set out in chapter 2.

	ρ_{12}	$\lvert\rho_{12}\rvert$	ρ_{13}	$\lvert\rho_{13}\rvert$
Standard IQHA	-0.17 + j0.38	0.41	-0.51 + j0.00	0.51
Meandered IQHA	-0.29 + j0.49	0.57	-0.31 - j0.00	0.31

Table 5-15 Table showing the correlation between the elements for the standard IQHA and the meandered IQHA

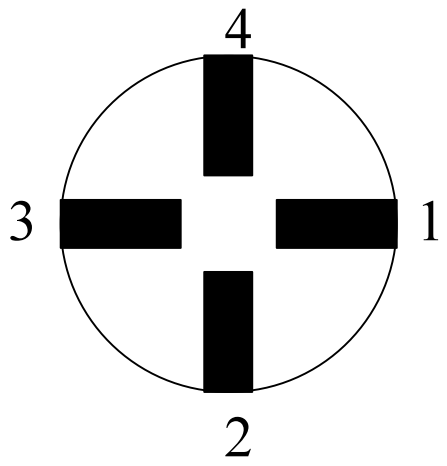

Figure 5-7 Diagram of the element numbers of an IQHA feed point

In the case of the standard IQHA the correlation is higher than the adjacent elements, where as in the case of a meandered IQHA the opposite of this is the case. However, the correlations are still low and degrade the diversity gain by only 2dB with a selection combiner [Sch66] assuming envelope correlation is derived from equation (2.10). Therefore the antennas provide useful angular de-correlation in an urban fading environment with such AOA characteristics. No measurements or simulations, however, have been carried out to give comparable results.

The polarisation correlation results are presented in Table 5-16 where it can be seen that in all cases, the correlation is high. There is some reduction in correlation for opposite elements in the case of the meandered IQHA although it is not a significant decrease. This would be expected since the meander lines will generate more cross polarisation. It can be concluded from these results that the IQHA is principally an angular diversity system with suitably de-correlated elements in an urban fading environment.

	ρ_{12}	$\lvert\rho_{12}\rvert$	ρ_{13}	$\lvert\rho_{13}\rvert$
Standard IQHA	0.92	0.92	0.94	0.94
Meandered IQHA	0.93	0.93	0.88	0.88

Table 5-16 Table showing the polarisation correlation results between elements for a standard IQHA and a meandered IQHA

5.11 Mean effective gain analysis of the IQHAs

The second phase of evaluating the diversity of IQHAs is the MEG both for single elements and combined elements to identify where system gain involves increase in efficiency and/or MEG. Therefore it can be determined where diversity is taking place. Evaluation of a single element can be carried out in the normal way and all elements will have the same MEG with uniform AOA distribution in azimuth. The field pattern of a standard quadrature fed IQHA [Leach00] can be evaluated by applying phase weights to resolve the total *E*-fields, $E_{\theta T}$ and $E_{\phi T}$, as follows:

$$E_{\theta T}(\theta,\phi) = \frac{E_{\theta 1}(\theta,\phi) - jE_{\theta 2}(\theta,\phi) - E_{\theta 3}(\theta,\phi) + jE_{\theta 4}(\theta,\phi)}{2} \tag{5.1}$$

$$E_{\phi T}(\theta,\phi) = \frac{E_{\phi 1}(\theta,\phi) - jE_{\phi 2}(\theta,\phi) - E_{\phi 3}(\theta,\phi) + jE_{\phi 4}(\theta,\phi)}{2} \tag{5.2}$$

where the factor of 2 in equations (5.1) and (5.2) accounts for the power splitting that would take place if the IQHA was measured in quadrature using hybrid couplers. Combining the fields in this way does not provide any diversity gain [Leach00] so therefore in one respect the quadrature fed IQHA could be used as a reference.

The highest system gain comes from EGC elements where the four branches are co-phased. This creates an equivalent *E*-field pattern calculated in Appendix E. Since the co-phasors are variable with time, the *E*-field pattern cannot be measured so easily. From the derivation in Appendix E, the resultant *E*-fields at each angle, $E_{\theta T}(\theta,\phi)$ and $E_{\phi T}(\theta,\phi)$, are as follows:

$$E_{\theta T}(\theta,\phi)=\frac{|E_{\theta 1}(\theta,\phi)|+|E_{\theta 2}(\theta,\phi)|+|E_{\theta 3}(\theta,\phi)|+|E_{\theta 4}(\theta,\phi)|}{2} \tag{5.3}$$

$$E_{\phi T}(\theta,\phi)=\frac{|E_{\phi 1}(\theta,\phi)|+|E_{\phi 2}(\theta,\phi)|+|E_{\phi 3}(\theta,\phi)|+|E_{\phi 4}(\theta,\phi)|}{2} \tag{5.4}$$

from which the gain patterns and the MEG can be calculated from.

A comparison of the MEG for a single branch, standard quadrature fed and EGC combined elements is presented in Table 5-17 for both the standard sized IQHA and the meandered IQHA. In both cases the results relate consistently only the meandered IQHA has reduced efficiency and likewise reduced MEG on each branch. The quadrature fed elements increase the MEG by around 3.5dB compared to a single element, which is consistent with results for a Rayleigh fading environment [Leach00] giving little diversity gain. The EGC combined elements increase in MEG by 5.5dB compared to a single element. This is small compared to the increase in signal to noise ratio found to be up to 23dB as in Table 5-14 so therefore the increase is largely due to diversity. Therefore in both cases, the increase in MEG indicates an increase in signal to noise ratio, *L*, described in chapter 2. The diversity gain is in the region of 17dB due to low enough correlation between the branches comparable with the maximum diversity gain of a four-branch equal gain combiner. Therefore an EGC combined IQHA has high diversity potential and MEG to provide maximum output. This maximum output is due to a diversity gain of 17dB with the addition of 5.5dB increase in MEG, resulting in 22.5dB system gain. It must be noted, however that in other fading environments with less uniform angle of arrival this performance would be less as is the case from other measurements undertaken [Leach00].

	Single Branch MEG/dBi	Quadrature Feed MEG/dBi	EGC Combined MEG/dBi
Standard IQHA	-6.90	-3.36	-1.50
Meandered IQHA	-9.57	-5.99	-4.13

Table 5-17 Comparison of MEG between a single branch, quadrature fed branches and equal gain combined branches for a standard IQHA and meandered IQHA

In the case of selection combining, the maximum branch is chosen at any one time. For a uniform angle of arrival and Gaussian elevation angle of arrival case, the MEG if each branch is the same. Therefore, the resultant MEG will always be the same as a single branch whatever branch is selected. Unlike ECC, selection combining will therefore not have any increase in MEG. This verifies therefore that the result obtained for selection combining in Table 5-14 is comparable

with the diversity gain of a four branch selection combiner and therefore diversity gain is the same as system gain in this case.

For Maximum Ratio Combining (MRC), the complex weights are optimised such that the signal to noise ratios of each branch are added together [Jak94]. A proof is shown in Appendix F that the resultant MEG for an MRC is in fact also the same as a single branch. This is also strictly conditional on the angle of arrival scenario used for this analysis, however. Therefore the diversity gain and system gain are also the same in this case. The system gain result for MRC in Table 5-14 is also comparable with the diversity gain from a four-branch diversity system.

The analysis carried out here therefore indicates why EGC gives a better output system gain since it has an advantage of a significantly higher increase in MEG (i.e. high signal gain, L). A comparison of the $\phi = 0$ elevation patterns (which are consistent for all values of ϕ) in Figure 5-8 indicate that the increased omni-directionality for EGC is significantly better than a single branch and a standard quadrature feed, thus providing higher MEG. Similar results are found for the meandered IQHA only there is reduction in efficiency in this case so the gain values are not as high.

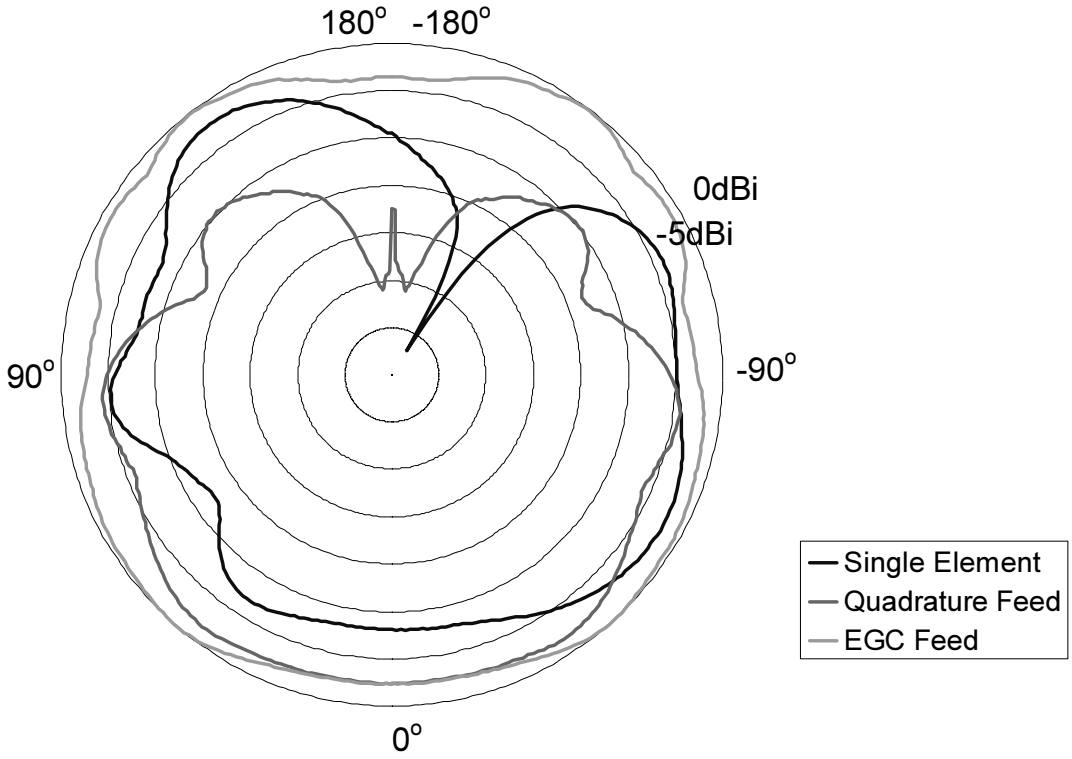

Figure 5-8 Polar plot showing the comparison of omni-directionality between differently fed elements

5.12 System Gain Analysis

Although the analysis of the IQHA does show clearly why EGC gives an improved output from other combining methods, and indeed where that is due to diversity, the system gain results have some discrepancy from the results in Table 5-14. This is due to the fact only a uniform angle of arrival in azimuth was applied for the results presented there, which would yield different correlation values. For the analysis undertaken, the elevation angle of arrival is also considered. Therefore the system gain results are summarised in Table 5-18 for a standard sized IQHA and Table 5-19 for a meandered IQHA so that they can be compared with Table 5-14.

Both the tables are presented in the same format. The degradation in diversity gain can be derived using the degradation factor in equation (2.12). For all types of combiner this is the same. In the case of selection combining, there is no gain in MEG since only 1 branch is selected at any one time, therefore the combined output MEG is the same as a single branch. For MRC this is also the case as explained in section 5.11. Only in the case of EGC is there an increase in MEG from the combined field pattern also explained in section 5.11.

Combination method	Degradation in diversity gain due to correlation/dB	Gain in MEG/dB	System gain referenced to single branch/dB
Selection Combining	-2.08	0	13.92
EGC	-2.08	5.4	21.32
MRC	-2.08	0	16.37

Table 5-18 Table summarising the system gain results obtained from the standard sized IQHA analysis

Combination method	Degradation in diversity gain due to correlation/dB	Gain in MEG/dB	System gain referenced to single branch/dB
Selection Combining	-2.12	0	13.88
EGC	-2.12	5.44	21.32
MRC	-2.12	0	16.33

Table 5-19 Table summarising the system gain results obtained from the meandered IQHA analysis

5.13 Conclusions

Results of diversity measurements carried out on a case study measurement of a mobile handset terminal comprising of a PIFA and a meander line monopole and two forms of IQHA have been presented. Two frequencies were measured for the handset, being 920MHz and 1800MHz and both these cases resulted in having similar diversity performance. However, their characteristics were different in that at 920MHz there was high correlation but similar mean branch power. The reverse was true for 1800MHz. Analysis was also carried out at 920MHz with a phantom head to investigate its effects. It was found here that the presence of the phantom did help to reduce the angular correlation and improve the diversity gain. However, the reference branch had a much lower MEG due to the presence of the head, although adding a diversity antenna on this basis would improve the output significantly.

For the IQHA measurements were carried out at 2GHz for a standard sized version and also one with the lines meandered to reduce the size. Results in both cases were comparable although the reference branch of the meandered antenna was lower in MEG by around 3dB. It was shown for both models that there is significant increase in system gain largely due to the four-branch angular diversity system it creates. The best results are achieved with EGC due to the increase in MEG being more significant than with other combining techniques. However, it must be noted that the results are strictly conditional upon the angle of arrival model used and would not be applicable in other cases. Further analysis would be required for such scenarios.

A publication, “Analysis of the Diversity Potential of an Intelligent Quadrifilar Helix Antenna”, will be presented at the *International Conference of Antennas and Propagation (ICAP)* in April 2003 containing the analysis work carried out on the IQHA in this chapter.

Chapter 6

6 Feasibility Study for Implementing a Simulated Mobile Fading Environment

Although diversity can be evaluated theoretically as shown in previous chapters there is a need to undertake real time measurements of the diversity as well for verification purposes. The theoretical predictions may provide useful guidelines to the designer in terms of optimisation although the actual diversity or system gain results are based on assumptions. Such assumptions are that the mathematical models used for angle of arrival (AOA) actually represent the real environment sufficiently. Measurement campaigns in real environments help to verify this although they are often time consuming and no two mobile terminals can be tested under the same test conditions in these case since the test method is not repeatable. Further to this it may be necessary to undertake a full conformance test of a mobile terminal in terms of testing the receiver and the antenna together. A multipath fading simulator would therefore be of benefit with the scope of manipulating the AOA to achieve initial evaluation of the mobile terminal diversity before testing in a real environment. Limits on the accuracy and versatility of the simulator will always be present and so they need to be taken note of. The aim of a fading simulator would therefore be to provide results that are repeatable, applicable to different AOA environments and economical in terms of time and cost compared to propagation measurements that would otherwise be necessary.

Methods of replicating a mobile fading environment have been developed in the past often in the context of field simulators [Arai01] and reverberation chambers [Rosen01][Hallb]. Although these methods have been shown to produce Rayleigh like fading in a mode stirred chamber with conducting walls, they are restricted to uniform angle of arrival all around the mobile. This does not reflect the AOA for an urban fading environment and it will not apply to specific angle of arrival models with non-uniform AOA such as outdoor to indoor propagation and ricean environments. Another idea for evaluating diversity has been proposed based on moving a mobile around a circle in a zone surrounded with sources that will yield different phases to generate fading [Kitch99]. This model is limited to an azimuth angle of arrival, however. In this chapter, a new concept proposal is presented based on Rayleigh sources that are positioned at appropriate

angles to reflect the desired angle of arrival model for the mobile. Simulations are also presented to verify the validity of the proposal and further work that will be necessary if such a concept was to be implemented

6.1 Outline of the concept

The concept of the fading simulator is outlined in Figure 6-1 below. In the centre is a mobile terminal, which will receive the resultant fading signals coming from the fading sources that surround it. Although the mobile is stationary, the fading being applied to incoming signals around the mobile terminal is representative of the motion that the mobile would normally experience. The incoming signals will not have only one but two independent polarisations and the magnitude will not be the same due to the cross-polar ratio, *XPR*, explained in chapter 2. Therefore, the fading sources are dual polarised as shown. The horizontal polarisation has an attenuator to vary the *XPR* that is used.

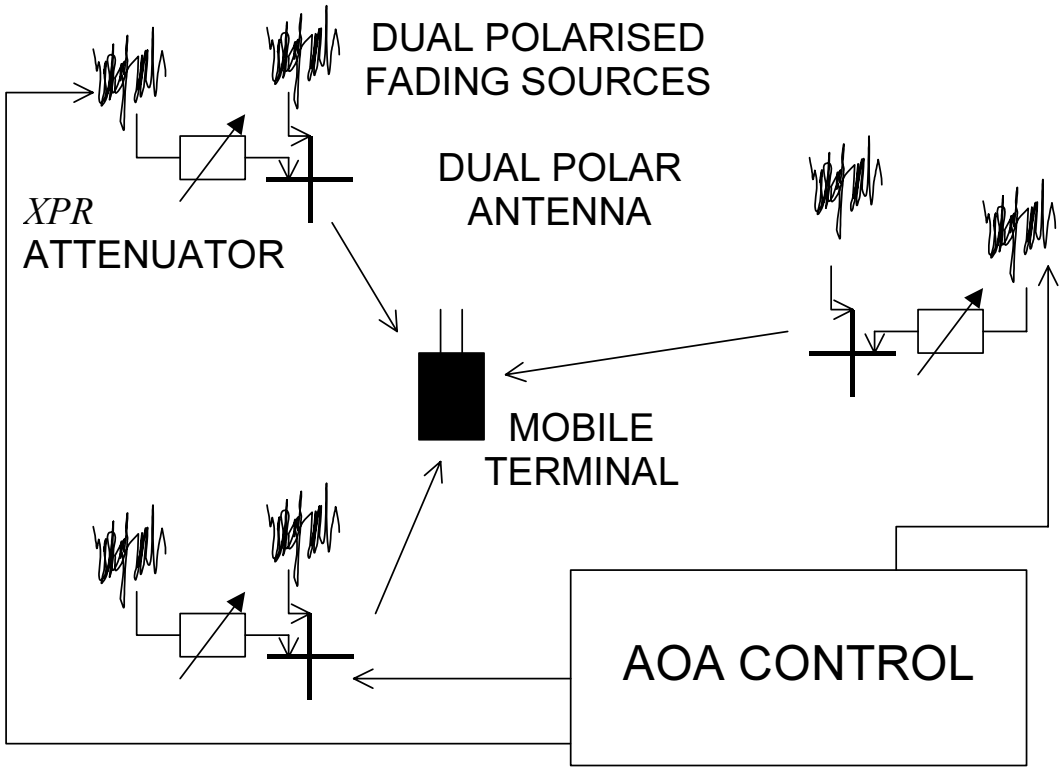

Figure 6-1 Diagram of the concept behind the proposed fading simulator

The dual polarised fading sources are consequently fed into dual polarised antennas. There are no particularly strict requirements on the antenna specifications other than that the field patterns of

the two polarisations should be the same. The actual field patterns the antennas have does not make any difference to the resultant fading signal at the mobile since only one incident RF signal reaches the mobile as shown by the arrows. The number of antennas around the mobile are dependent on the type of mobile terminals that are being tested and the AOA that is being simulated. Criteria for this will be discussed later. Essentially, with an appropriate number of antennas around the mobile terminal, it will be possible to control the magnitude or even "switch off" some of the sources to alter the different fading environments as necessary.

6.2 Fading Source Generation

For each polarisation of the antenna, there is a dynamic fading generator that is used to generate the appropriate fading source that represents motion at a given angle. A proposed method of doing this is shown in Figure 6-2 built on a method used by Arredondo [Arre73]. The signal will require an I channel and a Q channel so essentially two Gaussian independent noise sources are used for each polarisation. Therefore, four independent Gaussian noise sources are required for each antenna. The classical Doppler filter is applied so that an appropriate rate of change of fading signal can be simulated depending on the mobile speed.

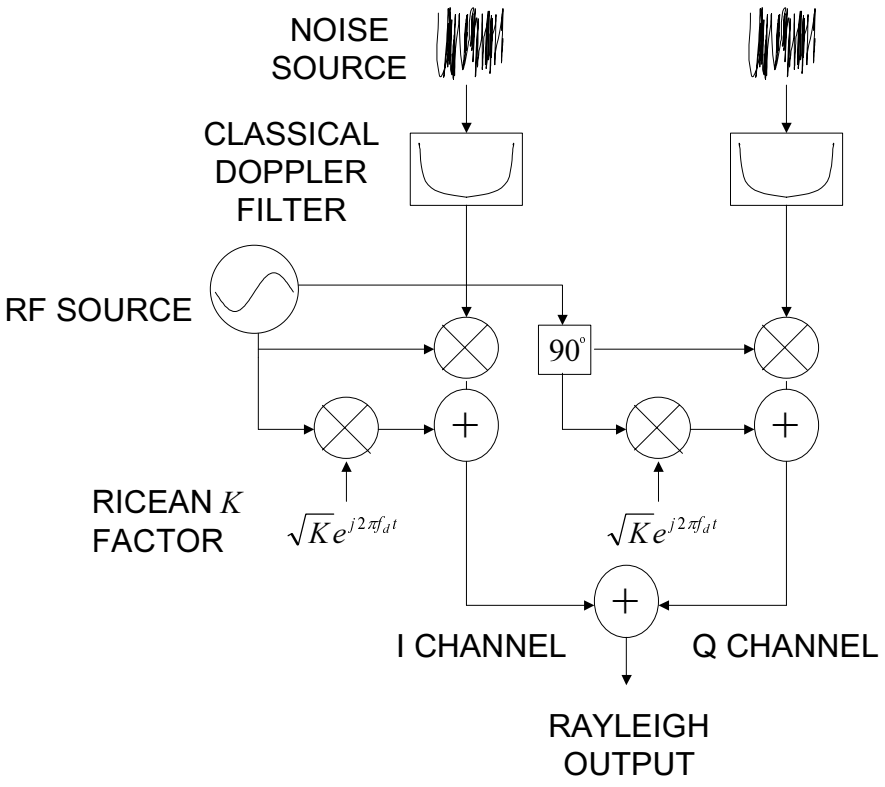

Figure 6-2 Dynamic fading generator with uniform phase distribution proposed by Arredondo

The one thing that has been added to this model not used by Arredondo is the Ricean *K* factor. For simulating a Ricean fading signal, rather than a Rayleigh signal, *K* can be made non-zero [Saund99]. The higher *K* is, the less fading there will be because the main signal will be more predominant. A further point to note is the frequency shifting factor $e^{j2\pi f_d t}$, which is essentially a phase shift, due to the Doppler shift frequency, f_d, in Hz at time *t* [Saund99]. If a Rayleigh signal is not required, *K* can be made zero. In the case of non-uniform angle of arrivals, *K* will not be zero and so an appropriate *K* factor will be required.

6.3 Criteria for number of source antennas

The correct number of source antennas selected is essential since there can be either too few antennas such that there is not suitable resolution of the AOA distribution while at the same time there may be too many that they do not benefit the system any further (which is uneconomical and unnecessary). It will be shown that as the 3dB beamwidth of antenna at the mobile is generally wide, then this limits the number of sources needed. To start with, it will be considered how many antennas need to be placed around the mobile in azimuth, not just necessarily for uniform AOA but any other model but for scenarios like outdoor to indoor and Ricean environments. Following this the elevation angle of arrival will be considered.

6.3.1 Criteria for azimuth angle of arrival

The beamwidth of the antenna under test has a great impact on the number of antennas chosen. This is illustrated in Figure 6-3(a) where two source antennas, A and B (not necessarily radiating the same power) can be considered the same as a single source antenna, C in Figure 6-3(b) giving a power level the same as the two antennas, A and B put together. Therefore when the beamwidth is wide, the antenna has no way of differentiating between two incoming signals that are within the width of the beam since the resultant power is the same. If the phase was different at the two points, it would be possible for signals A and B to be differentiated since the real and imaginary parts would add up together differently. In summary, when there is a wide beamwidth for both gain and phase, there will be a maximum number of source antennas required.

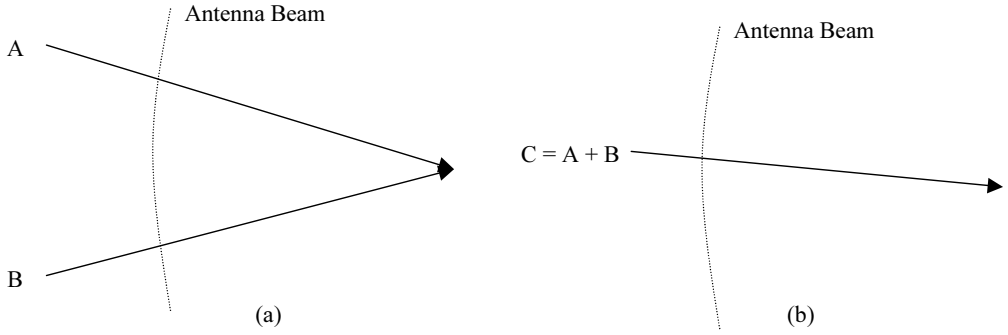

Figure 6-3 Diagram showing how wide antenna beamwidths on antennas cannot differentiate between two signals with close angular spacing

Therefore, depending on the beamwidth for both gain and phase, an appropriate number of source antennas needs to be chosen. Narrow beamwidths will require a large number of source antennas where as wide beamwidths of 360^{o} (or omni directional patterns) only require one source antenna. A criteron therefore needs to be set on the number of source antennas based on the beamwidth. Figure 6-4 illustrates a simple principle that would suggest an appropriate criteria. If the 3dB beamwidth, BW, of any antenna lobe in Figure 6-4 is narrow enough that the gain has at least 3dB difference at the two points then it is reasonable to assume that it can determine the difference between the two source antennas separated by angle ϑ. Therefore, if the beam was directed from one source antenna to the next it would identify the two incoming signals were present. Based on this principle, the following criteria would apply:

$$\vartheta > \frac{\mathrm{BW}}{2} \tag{6.1}$$

This could apply also to the phase although BW would be substituted for the beam over which the phase reduces by 30^{o}. Therefore BW needs to be used as the 3dB beamwidth and the 30^{o} beamwidth to determine the number of antennas from the following formulae:

$$N = \mathrm{div}\left(360, \frac{\mathrm{BW}}{2}\right) \tag{6.2}$$

This assumes that the antennas are equally spaced in the azimuth domain. The function “div” is an integer divide function, which will return the division of 360 and BW/2 rounded to the nearest whole number. If there is no 3dB beamwidth (i.e. the antenna is very omni-directional) then $N = 1$ would be required since it would not matter to the antenna under test where the source antenna was.

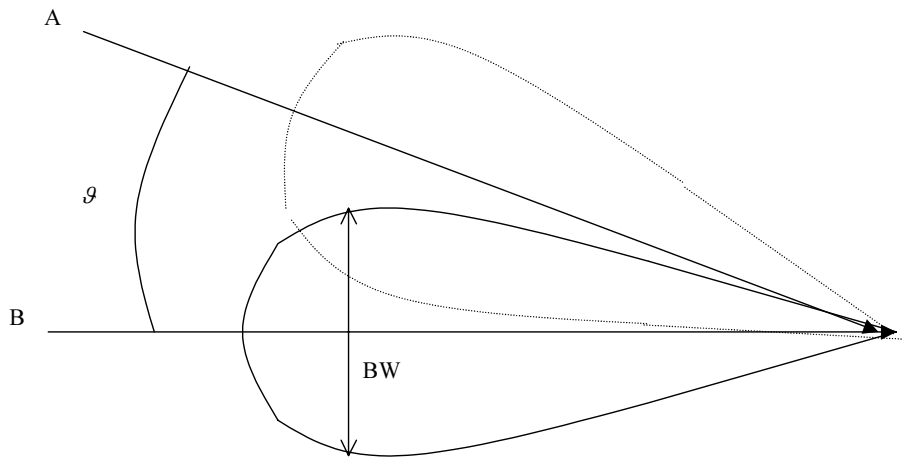

Figure 6-4 Diagram showing how a narrow beam will determine the difference between two source antennas

6.3.2 Criteria for elevation angle of arrival

This principle can be applied in elevation as well after making some adjustments. To begin with, the elevation pattern of the antenna in this instance would be considered as opposed to the azimuth pattern. Further to this, only a semi circle from 0^o to 180^o need be considered after the azimuth has already been considered. Therefore, in this situation, the equation becomes:

$$N = \text{div}\left(180, \frac{\text{BW}}{2}\right) + 1 \tag{6.3}$$

where BW this time is the 3dB beamwidth or the 30^o as before in elevation. An extra antenna is added so there is one at 180^0 as well as 0^0.

This would work in practice if the elevation angle of arrival was uniform although this is normally not the case so further additions need to be made. In the case of a Gaussian elevation AOA for example, the incoming signals are negligible between 0^o-30^o and also 100^o-180^o. Therefore redundancy comes about for these source antennas since they would not add any significant contributions. Therefore the number of source antennas for elevation are less. Setting the criteria within the limited angle of arrival window can consequently become complicated and experimentation is required as will be shown later.

6.3.3 Angle of arrival for urban fading environment

Applying the above principles to an urban fading environment with uniform azimuth angle of arrival and Gaussian elevation angle of arrival can be carried out easily enough once the typical beamwidth that mobile terminal antennas generally go down to is decided. In this situation the K factor in Figure 6-2 is zero so the complexity of the dynamic fading generator is reduced. Mobile terminals typically are generally omni-directional in azimuth and in elevation they would usually have wide beamwidths. It will be assumed here that 100^{o} would typically be as narrow as a mobile terminal antenna pattern would get in any instance. Therefore the proposal will be limited to antennas with beamwidths that go this narrow.

For 100^{o} beamwidth, the number of sources in azimuth would need to be 7. In elevation, if 20^{o} mean and 20^{0} standard deviation is chosen, the maximum number of antennas that could be needed within this range is 3 as will be shown later from experimentation. This would therefore amount to 21 source antennas and therefore 42 noise sources to account for both polarisations. Such a structure is not economical but improvements can be made further to overcome this.

6.3.3.1 Method to improve the economic limits

In azimuth, not all the sources need to be transmitted at the same time. If only one source was used in elevation, the seven azimuth sources could be accounted for with one source antenna using a turntable shown in Figure 6-5. A noise source can be radiated at the first location for a given time to obtain sufficient samples for analysis. Following this the turntable can be rotated 51.4^{o} where the next source with the same time duration can be transmitted again. This can be repeated to cover the remaining 5 points and then the 7 streams of data can be added together, which will give the same output at the mobile as if the 7 sources were radiated and added up at the same time.

This method will only work if the 7 sources are independent (i.e. completely uncorrelated). Therefore a minimum Doppler shift is required, which will cause the fading signals to vary rapidly enough such that when they get to the next source they will be uncorrelated in time. From simulating a mobile fading signal[§] with a velocity of $5kmh^{-1}$, it can be shown in Figure 6-6 that after 1 second, the autocorrelation is negligible. This has been carried out for 4 sets of random samples to verify the correlation is typical. It would take more than 1 second to reach the next source point so therefore when it does, the signal will be not correlated as required.

[§] Source code to simulate Classical Doppler spread supplied by Dr S Saunders, University of Surrey

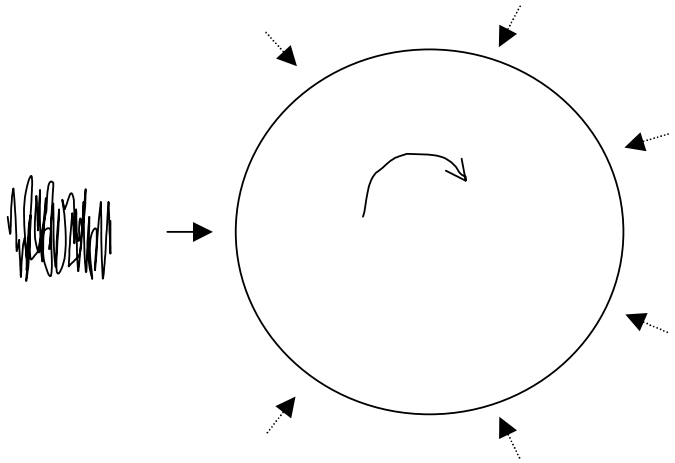

Figure 6-5 Illustration of how to rotate a mobile and take independent fading signals at 7 points

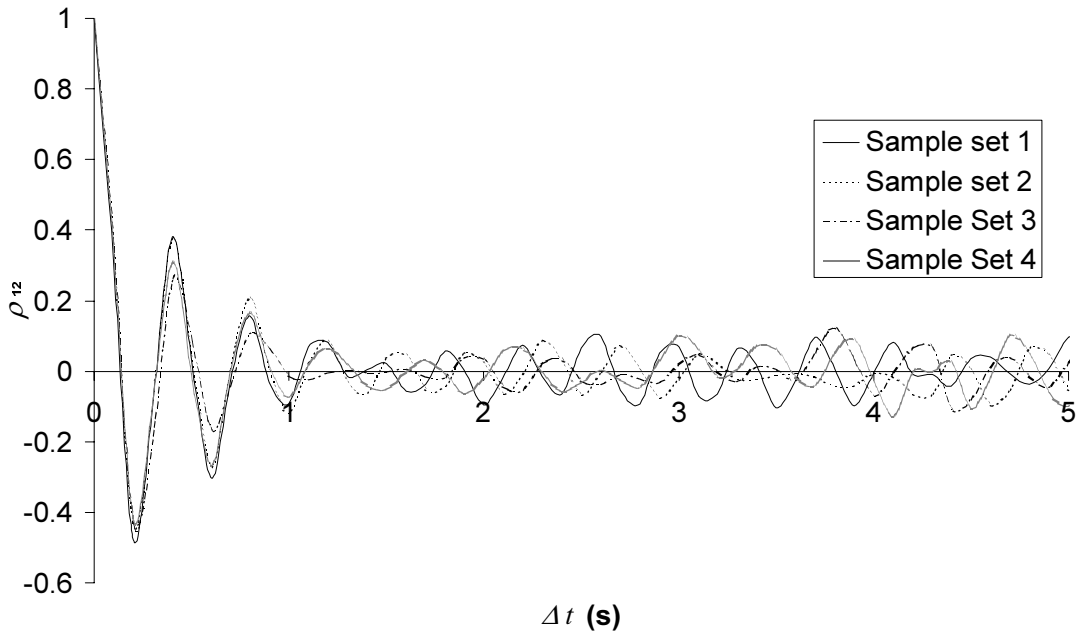

Figure 6-6 Diagram showing autocorrelation over time delay for noise samples

Using this method reduces the number of required source antennas significantly. Some conformance measurements, however, undertaking such tests may require all the source antennas to radiate simultaneously so its application may be limited.

6.4 Test Simulations for Uniform Azimuth Angle of Arrival

To investigate the validity of the proposal, some test simulations were carried out in both the horizontal and vertical plane to see if sufficiently accurate results could be achieved. The results also show comparisons with different numbers of sources to show how accuracy is affected.

6.4.1 Simulations for horizontal spatial correlation

By using 7 independent fading sources, they were applied to simulate horizontal spatial correlation to see if they would yield the correct results in comparison to the theory. All sources were elevated 20^o above the horizontal to see if the same correlation with a 20^o mean AOA in elevation could be replicated. After applying appropriate phases to each of the fading sources, the correlation could be calculated versus horizontal spacing between two points in space, *d*.

In Figure 6-7 sufficient consistency with the theoretical complex correlation is found for horizontal correlation when phase taps are applied appropriately to each fading source. The test was carried out for less than 7 sources as well so it can be seen how accuracy improves as the number of sources are increased.

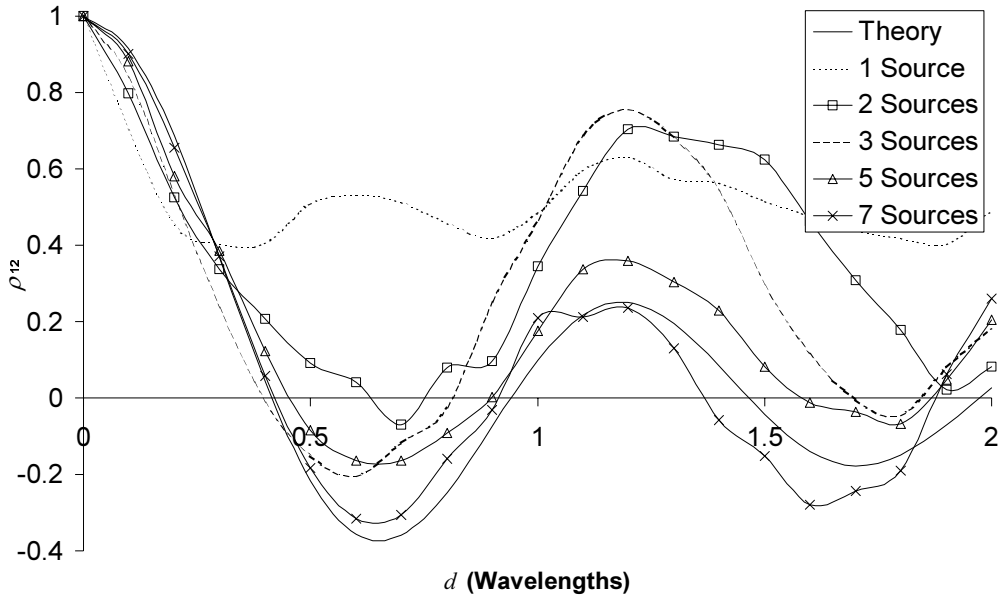

Figure 6-7 Graph showing comparisons of correlation versus horizontal distance with different numbers of fading sources

6.4.2 Simulations for polarisation correlation

Applying polarisation weightings to fading signals in the vertical and horizontal plane (with 6dB *XPR*), the polarisation diversity could be compared with theoretical also. Figure 6-8 shows there is suitable consistency when the horizontal polarisation is attenuated by 6dB to maintain the same cross-polar coupling as is assumed in the theory. Seven sources were also applied in this case as with the horizontal spatial correlation.

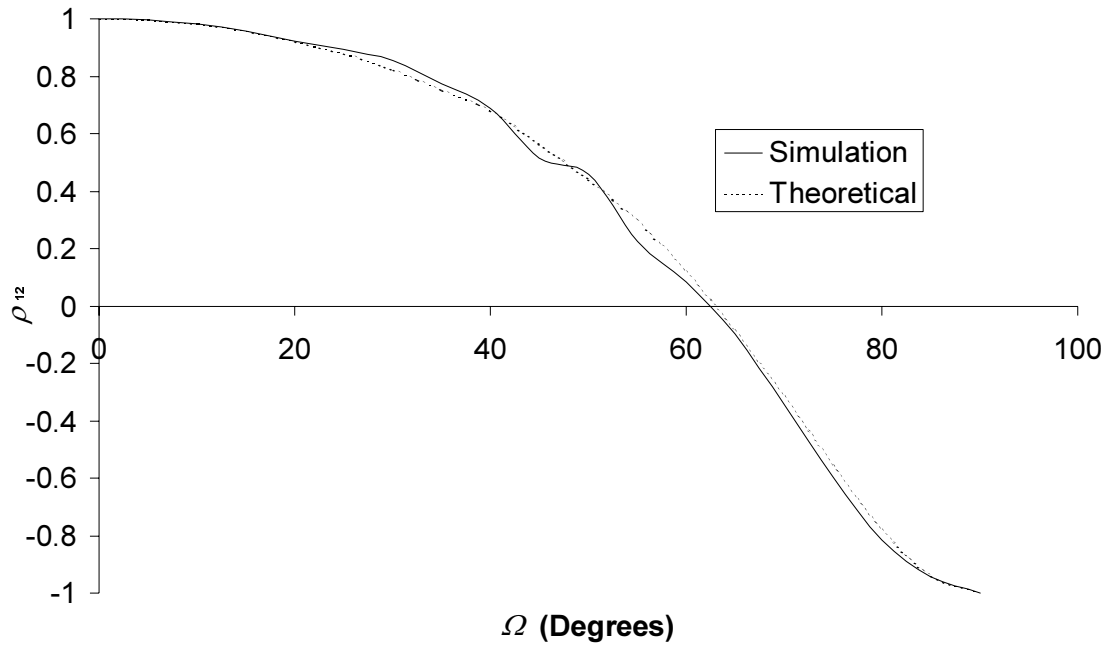

Figure 6-8 Graph showing polarisation correlation from simulations compared with theory

6.5 Further Work – Test Simulations for Non-Uniform Angle of Arrival

The results in the previous section were successful because they are not dependent on the elevation angle of arrival, which is non-uniform. Therefore, it is reasonably simple to use the 7 fading sources as arranged. Applying the setup to vertically spaced points and angular antenna patterns is a different case and more complex since the Gaussian elevation AOA is involved. Here, the Rayleigh Sources would not be suitable and a *K*-factor would be involved that is non-zero.

It is therefore at this point where extensive experimentation is required that is beyond the scope of this thesis. Appropriate *K* factors will need to be found for different angle of arrival environments with an appropriate number source antennas positioned and weighted as necessary to simulate an appropriate fading environment. There are different angle of arrival models that will be used in the future for Ricean distributions and outdoor to indoor propagation models that the simulator will need to be adaptable to.

6.6 Conclusions

A proposal for a simulator of a mobile fading environment that provides flexibility between different AOA and *XPR* environments has been presented. Its purpose would be to undertake

conformance or verification tests for prototype diversity antennas that would provide repeatable results with ease in contrast to real time propagation measurements.

Simulations were carried out to verify the validity for uniform angle of arrival in the case of horizontal and spatial diversity as well as polarisation diversity. Indications verify that the simulator gives suitable results compared to the theory, when there are 7 sources in azimuth. In other cases where the Gaussian elevation AOA has to be considered further work is necessary.

The feasibility of this facility depends on finding the appropriate *K* factors required to apply to the dynamic fading generators along with the appropriate positioning and weighting to apply to the source antennas. Following this it will allow the fading simulator to undertake multiple tests on a mobile terminal in a wide range of fading environments in a relatively short space of time.

Chapter 7

7 Conclusions and Further Work

A new method for modelling and evaluating diversity at the mobile has been presented. Considerations of angle of arrival and cross-polar coupling ratio in the mobile fading environment have been taken into account. Scenarios regarding the antennas have also been considered including the input impedances, mutual coupling and lower directivity field patterns. Further to this the efficiency of the antennas need to be taken into account when in the presence of each other, which has to be optimum as well as the actual diversity performance. The new method allows the designer to evaluate the spatial, angular and polarisation contributions, being the main aspects of antenna diversity. Knowledge of the diversity contributions and the antenna field patterns will allow the designer to interpret why the antennas have diversity and experiment with the results from different antenna designs or configurations to optimise the final design, both in terms of diversity and efficiency. Optimum performance will depend on low correlation, similar MEG between the two branches and comparable MEG with a chosen single branch reference suited to the application. Example applications have been presented of the evaluation method to show how diversity works in real case scenarios being that of a mobile handset and an Intelligent Quadrifilar Helix Antenna (IQHA). In many cases at the mobile terminal, angular diversity has a significant role, although there is still scope for both spatial and polarisation contributions.

7.1 Distillation

In the background theory in chapter 2, the concept of diversity receivers is outlined with definitions given for notations including diversity gain, complex and envelope correlation. Further to this, the effects of correlation and unequal mean branch power are outlined in a mobile fading environment. Importance of efficiency considerations at the mobile are also addressed. Given that evaluating an appropriate angle of arrival model is beyond the scope of this thesis, an appropriate model had to be chosen, which from the literature surveyed was assumed to be uniform in azimuth and Gaussian in elevation although it is evident that this is by no means likely to be a standard model in the future of mobile communications. This was only suited to urban mobile environments and other models will need to be researched in the future with standards set for

other mobile environments. Examples of typical diversity antennas were also summarised to determine the type of antennas that such an evaluation method would be used for.

Having established the appropriate background theory in chapter 2, chapter 3 presents mathematical analysis of the new models for spatial, angular and polarisation diversity having established the theory behind antenna impedance and mutual coupling. Polarisation diversity for the fading environment is presented based on two relative polarisations in space. From this it was shown that the best diversity receiver performance comes from around the $\pm 62.5^{o}$ configuration for low correlation and equal mean branch power although this does come at the expense of loss in MEG. Due to this the actual output from the receiver has a marginal improvement at $\pm 45^{o}$ configuration. Therefore a compromise is necessary. Characterisation of the polarisation diversity in a fading environment is also shown in terms of how the antennas would affect the measurement results. The model was also expanded to consider the third polarisation, which would be applicable when there is non-uniform AOA in azimuth.

A new model for spatial correlation was presented, based on the horizontal spacing, d, and the vertical spacing, h. It is possible that there will be both horizontal and vertical spatial correlation at the mobile when normally only vertical spacing is implemented at the base station. This model was further extended to consider the mutual coupling and impedance effects to evaluate the spatial diversity seen at the receiver. Further to this, the azimuth orientation was also accounted for the case of a non-uniform azimuth angle of arrival.

Angular diversity is presented by comparing the antennas when co-located with effects of input impedance considered. The impedance differences between the two antenna branches will cause a phase change to the angular correlation, although no change in magnitude. By example of closely spaced monopoles, it was shown how angular diversity can be achieved from closely spaced antennas although often at the expense of loss in efficiency and therefore MEG. In all cases, it was shown that change in standard deviation on the elevation angle of arrival (which can change dramatically in an urban environment) there is little effect on correlation although variation in cross polar ratio, between 0dB and 10dB does cause significant effect to the correlation and the resulting diversity. Therefore the performance would need to be averaged over this range.

Chapter 4 continues from chapter 3 to apply the new models to a method with which to analyse the diversity from antenna measurements or simulations. Spatial correlation is the simplest to evaluate based on the distance between the phase centres and the Z parameter matrix of the two antennas. Angular correlation can be evaluated in discrete form based on three dimensional elevation patterns taken in 10^{o} cuts. The same data can be used to evaluate the polarisation contributions by averaging the relative E_{θ} and E_{ϕ} polarisations from every angle.

Following the evaluation method, analysis was undertaken to show the interaction of spatial, angular and polarisation correlation to provide indicators as to how the designer should interpret the results. This could be achieved from the correlation results and the antenna field patterns both in azimuth and elevation. For horizontally spaced antennas only angular correlation from different azimuth patterns can change the overall correlation, difference in elevation has negligible effect although differing elevation patterns will normally have different azimuth patterns in any instance. The angular correlation will affect the spatial correlation differently based on the directivity of the antenna patterns and the angular orientation they have. De-correlation in azimuth will always reduce the correlation in the case of vertical correlation so there are no set conditions in this instance. Elevation patterns will have significant effect on vertical spatial correlation and with the non-uniform AOA it is concluded that for best performance, both in terms of correlation and MEG, the overlapping region between the antennas should be within the angle of arrival region. These principles only apply to cases where the angular correlation is comparable with the spatial correlation. Therefore, with angular correlation greater than 0.9, there is negligible angular contribution, although high angular contribution when less than 0.2. For spatial correlation, there is conrtibution when less than 0.1λ although high contribution when greater than 2λ. Polarisation contribution in chapter 4 was shown to be inherent within angular diversity with which the correlation could be used to identify any significant polarisation contribution within the two antennas.

An application of the method presented in chapter 4, was presented in chapter 5 with two case study examples. The first was a typical mobile handset with a PIFA and a meander line monopole antenna. The second was an analysis of the diversity potential of an IQHA. In both cases it could be shown from correlation results why there is diversity in the two situations and also where efficiency was gained, or lost in other cases. Therefore it could be seen whether any improvements were due to diversity or improved MEG.

Finally, chapter 6 proposed a model for simulating a mobile fading environment with variable angle of arrival to verify the diversity performance of a mobile terminal in different environments based on an array of Gaussian noise sources. Initial simulations indicated that the simulator works effectively for uniform AOA models and closely spaced antennas with wide beamwidths although this limits the versatility.

7.2 Further Work

From the conclusions drawn and the limitations of the work presented, the following main areas of further work can be carried out:

- In the future new AOA models will emerge for different environments for which measurements and simulations such as ray tracing analysis will need to be carried out. From these results some appropriate standards on AOA could be set for different mobile environments as a basis to evaluate correlation and MEG. Standards would need to include models such as indoor, outdoor to indoor and building to building propagation. In many of these cases, there will be a non-uniform AOA in azimuth. As discussed already, the models developed for spatial, angular and polarisation correlation can be adapted as necessary to any AOA model that does emerge in the future.
- In the case where there is a non-uniform AOA in azimuth, the relation between envelope correlation, ρ_e, and complex correlation, ρ_{12}, presented in chapter 2 does not hold and likewise the effects on diversity do not either. At present there is no knowledge as to how correlation will affect diversity in such a scenario. This therefore gives scope for further mathematical analysis and experimentation to devise appropriate look-up tables or formulae.
- As discussed, it is still unknown what a typical value is for cross-polar coupling ratio, *XPR*, is at the mobile and has been assumed to be 6dB like that of the base station in an urban environment. This may not be typical and could vary between different environments dramatically. Therefore there is scope to conduct measurement campaigns to investigate expected values of *XPR*.
- The relations and interaction of spatial and angular correlation presented in chapter 4 are dependent on the proposed AOA model for an urban environment and are likely to be considerably different in other AOA environments. Also they are limited to typical antenna patterns that may be used for a typical mobile terminal. There is therefore a case to investigate with further antenna models that may be appropriate for other mobile terminal applications and also with new AOA models as they emerge.
- It is evident in chapter 7 that there is still further work to be carried out on the simulated mobile fading environment to expand its scope to many AOA models and many kinds of antenna. Deeper analysis of the behaviour of angular distribution in a fading environment will help to indicate how it could be simulated more appropriately. A perfect simulation will never be possible although the scope should be suitable enough to generate results comparable with real results.

Bibliography

[Abm72] M. Abmorowitz, I. A. Stegun, "Handbook of Mathematical Functions", 1972, *Dover Publications inc.*, pp360.

[Abu94] H. Abu-Bakar, P. A. Matthews, "Direction of Arrival of Radio Signals Inside and Outside a Buildings", *Proceedings of the IEEE 44th Vehicular Technology Conference (VTC)*, part vol. 3, 1994, pp1754-1758.

[Ada86] F. Adachi, M.T. Feeney, A.G. Williamson, J.D. Parsons, "Crosscorrelation between the envelopes of 900MHz signals received at a mobile radio base station site", *IEE Proceedings Radar and Signal Processing*, vol. 133, no. 6, Part F, Oct 1986, pp506-512.

[Agius99] A-A Agius, "Antennas for Handheld Satellite Personal Communicators", *PhD Thesis, University of Surrey*, 1999.

[Alln89] J. E. Allnutt, "Satellite to Ground Radiowave Propagation", 1989, *IEE Peter Pergrinus Ltd*, pp11-13.

[Arai01] H. Arai, "Measurement of Mobile Antenna Systems", 2001, *Artech House*, pp162-177.

[Arre73] G. A. Arredondo, W. H. Chriss, E. H. Walker, "A Multipath Fading Simulator for Mobile Radio", *IEEE Transactions on Communications*, col. 21, no. 11, November 1973, pp1325-1328.

[Aul79] T. Aulin, "A Modified Model for the Fading Signal at a Mobile Radio Channel", *IEEE Transactions on Vehicular Technology*, vol. 28, no. 3 August 1979, pp182-203.

[Bal97] C. A. Balanis, "Antenna Theory Analysis and Design", Second Edition, 1997, *Wiley*.

[Balab68] N. Balabian, T. A. Bickart, "Electrical Network Theory", 1968, *Wiley*.

[Barb97] J. P. Barbot, P. Larzabal, A. J. Levy, "Wideband indoor propagation channel direction of arrival measurements", *IEEE Signal Processing Workshop on Signal Processing Advances in Wireless Communications*, 1997, pp193-196.

[Beach00] M.A. Beach, D.P. McNamara, P.N. Fletcher and P. Karlsson, "MIMO – A Solution for Advanced Wireless Access", *IEE 11th International Conference on Antennas and Propagation (ICAP)*, vol. 1, no. 480, pp231-235.

[Beck97] C. Beckman, U. Wahlberg, "Antenna Systems for Polarization Diversity", *Microwave Journal*, May 1997, pp330-334.

[Braun99] C. Braun, G. Engblom, C. Beckman, "Evaluation of Antenna Diversity Performance for Mobile Handsets Using 3-D Measurement Data", *IEEE Transactions on Antennas and Propagation*, vol. 47, no. 11, November 1999, pp1736-1738.

[Chew02] K. C. D. Chew, S. R. Saunders, "Improvements Relating to Multifilar Helix Antenna", *UK Patent Filing*, Application No. 0204014.5, February 2002.

[Cho96] K. Cho, T. Hori, K. Kagoshima, "Effectiveness of Four-Branch Height and Polarization Diversity Configuration for Street Microcell", *IEEE Transactions on Antennas and Propagation*, vol. 46, no.6, June 1998, pp776-781.

[Clarke66] R. H. Clarke, "A Statistical Theory of Mobile Radio Reception", *Bell System Technical Journal*, 1966, pp957-1000.

[Correia01] L. M. Correia, "Wireless Flexible Personalised Communications", 2001, *Wiley*.

[Coulb98] J. S. Colburn, Y. Rahmat-Samii, M. A. Jensen, G. J. Pottie, "Evaluation of Personal Communications Dual-Antenna Handset Diversity Performance", *IEEE Transactions on Vehicular Technology*, vol. 47, no. 3, August 1998, pp737-746.

[Cox86] D. C. Cox, R. R. Murray, H. W. Arnold, A. W. Norris, M. F. Wazowicz, "Cross-Polarzation Coupling Measurements for 800MHz Radio Transmission in and Around Houses and Large Buildings", *IEEE Transactions on Antennas and Propagation*, vol. 34, no. 1, January 1986, pp83-87.

[Deane91] G. G. Johnstone, J. H. B. Deane, "Relations between two-port parameters", *International Journal of Electronics*, vol. 71, no. 1, July 1991, pp107-116.

[Deit01] C. B. Dietrich, K. Dietze, J. Randall Nealy, W. L. Stutzman, "Spatial, Polarization and Pattern Diversity for Wireless Handheld Terminals", *IEEE Transactions on Antennas and Propagation*, vol. 49, no. 9, September 2001, pp1271-1281.

[Doug98] M. G. Douglas, M. Okoniewski, M. A. Stuchly, "A Planar Diversity Antenna for Handheld PCS Devices", *IEEE Transactions on Vehicular Technology*, vol. 47, no. 3, August 1998, pp747-754.

[Egg93] P. C. F. Eggers, J. Toftgard, A. M. Opera, "Antenna Systems for Base Station Diversity in Urban Small and Micro Cells", *IEEE Journal on Selected Areas in Communications*, vol. 11, no. 7, Septermber 1994, pp1046-1057.

[Erät97] P. Erätuuli. E. Bonek, "Diversity Arrangements for Internal Handset Antennas", *IEEE Conference on Personal Indoor Mobile Radio Communications (PIMRC)*, 1997, vol. 2, pp589-592.

[Ertel99] R. B. Ertel, J. H. Reed, "Angle and Time of Arrival Statistics for Circular and Elliptical Scattering Models", *IEEE Journal on Selected Areas in Communication*, vol. 17, no. 11, November 1999, pp1829-1840.

[Fang00] Shyh-Tirng Fang, "A Novel Polarization Diversity Antenna for WLAN Applications", *IEEE Antennas and Propagation Society International Symposium*, vol. 1, 2000, pp282-285.

[Fass00] S. Fassetta, A. Sibille, "Switched angular diversity BSSA array antenna for WLAN", *Electronics Letters*, vol. 36, no. 8, April 2000, pp702-703.

[Fuhl99] J. Fuhl, J-P Rossi, E. Bonek, "High Resolution 3-D Direction-of-Arrival Determination for Urban Mobile Radio", *IEEE Transactions on Antennas and Propagation*, col. 45, no. 4, April 1999, pp672-682.

[Green00] B. M. Green, M. A. Jensen, "Diversity Performance of Personal Communications Handset Antennas Near Operator Tissue", *IEEE Transactions on Antennas and Propagation*, vol. 48, no. 7, July 2000, pp1017-1024.

[Hallb01] P. Hallbjörner, K. Madsén, "Terminal Antenna Diversity Characterisation using Mode Stirred Chamber", *IEE Electronics Letters*, vol. 37, no. 5, March 2001, pp273-274.

[Hos94] S. Hosono, N. Goto, H. Arai, "A Flat Diversity Antenna by Disk Loaded Monopole and Three Notches", *IEEE Transactions on Vehicular Technology*, vol. 43, no. 2, May 1994, pp353-357.

[Huan00] C. P. Huang, A. Z. Elsherbeni, C. E. Smith, "Analysis and Design of Tapered Meander Line Antennas for Mobile Communications", *Applied Computational Electromagnetics Journal*, vol. 15, no. 3, November 2000, pp159-166.

[Ikeg80] F. Ikegami, S. Yoshida, "Analysis of Multipath Propagation Structure in Urban Mobile Radio Environments", *IEEE Transactions on Antennas and Propagation*, vol. 28, no. 4, July 1980, pp531-537.

[Jak94] W. C. Jakes, "Microwave Mobile Communications", *IEEE Press*, 1994.

[James00] J. R. James, K. Fujimoto, "Mobile Antenna Systems Handbook", Second Edition, 2000, *Artech House*.

[Jen94] M. A. Jensen, Y. Rahmat-Samii, "Performance Analysis of Antennas for Hand-Held Transceivers Using FDTD", *IEEE Transactions on Antennas and Propagation*, vol. 42, no. 8, August 1994, pp1106-1113.

[Kalli01] K. Kalliola, H. Laitinen, K. Sulonen, L. Vuokko, P. Vainikainen, "Directional Radio Channel Measurements at Mobile Station in Differenct Radio Environments at 2.15GHz", *Proceedings of the 4th European Personal Mobile Communications Conference, Vienna, Austria*, Feb 20-22 2001, no. 113.

[Katz01] M. Katz, E. Tiirola, J. Ylitalo, "Combining Space-Time Block Coding with Diversity Antenna Selection for Improved Downlink Performance", *IEEE 54th Vehicular Technology Conference (VTC)*, 2001 Fall.

[Kitch99] D. Kitchener, I. P. Llewellyn, D. K. Power, "A Novel Method for Evaluating the Diversity Performance of Cellular Terminal Antennas", *IEE National Conference on Antennas and Propagation*, no. 461, 1999, pp299-302.

[Knud01] M. B. Knudsen, "Antenna Systems for Handsets", *PhD Thesis*, Center for PersonKommunication, Aalbourg University, Denmark, September 2001.

[Ko01] S. C. K. Ko, R. D. Murch, "Compact Integrated Diversity Antenna for Wireless Communications", *IEEE Transactions on Antennas and Propagation*, vol. 49, no. 6, June 2001, pp954-960.

[Koz84] S. Kozono, T. Tsuruhara, M. Sakamoto, "Base Station Polarization Diversity Reception for Mobile Radio", *IEEE Transactions on Vehicular Technology*, vol. 33, no. 4, November 1984, pp301-306.

[Kuch00] A. Kuchar, J-P. Rossi, E. Bonek, "Directional Macro-Cell Channel Characterization from Urban Measurements", *IEEE Transactions on Antennas and Propagation*, vol. 48, no. 2, February 2000, pp137-146.

[Kuga96] N. Kuga, H. Arai, "A Planar Pattern Diversity Antenna", *IEICE International Symposium on Antennas and Propagation*, vol. 2 1996, pp365-368.

[Kuga98] N. Kuga, H. Arai, N. Goto, "A Notch-Wire Composite Antenna for Polarization Diversity Reception", *IEEE Transactions on Antennas and Propagation*, vol. 46, no. 6, June 1998, pp902-905.

[Leach00] S. M. Leach, "Optimum Control of Hand-Portable Antennas for Satellite and Terrestrial Mobile Communications", *PhD Thesis, University of Surrey*, September 2000.

[Leath96] P. S. H. Leather, "Antenna Diversity for Hand-Portable Radio at 450MHz:", *PhD Thesis University of Liverpool*, 1996.

[Lee72] W. C. Y. Lee, Y. S. Yeh, "Polarization Diversity System for Mobile Radio", *IEEE Transactions on Communications*, vol. 20, no. 5, October 1972, pp912-923.

[Lee73] W. C. Y. Lee, R. H. Brandt, "The Elevation Angle of Mobile Radio Signal Arrival", *IEEE Transactions on Communications*, vol. 21, no. 11, November 1973, pp1194-1197.

[Lee97] W. C. Y. Lee, "Mobile Communications Engineering", *McGraw Hill*, Second Edition, 1997.

[Lee01] E. Lee, P. S. Hall, P. Gardener, "Antennas for Future Mobile Communication Terminals", *IEE International Conference on Antennas and Propagation*, no. 480, vol. 1 2001, pp348-351.

[Lemp98] J. J. A. Lemiainen, K. I. Nikoskinen, "Signal Correlations and Diversity Gain of Two-Beam Microcell Antenna", *IEEE Transactions on Vehicular Technology*, vol. 47, no. 3, August 1998, pp755-765.

[Lieb97] M. Liebendörfer, U. Dersch, "Wireless LAN Diversity Antenna System for PCMCIA Card Integration", *IEEE Vehicular Technology Conference (VTC)*, vol. 3, 1997, pp2022-2026.

[Luk01] L. Lukama, K. Konstantinou, D. J. Edwards, "Polarization Diversity Performance for UMTS", *IEE 11th International Conference on Antennas and Propagation*, 2001, no. 480, vol. 1, pp193-197.

[Matt93] P. A. Matthews, A. H. Abu-Bakar, "Direction of Arrival of Radio Signals Within Buildings", *IEE International Conference of Antennas and Propagation (ICAP)*, 1993, no. 370, part 1, pp142-145.

[Mitch96] J. Michael Johnson, Y. Rahmat-Samii, "Wideband Tab Monopole Antenna Array for Wireless Adaptive and Mobile Information Systems Application", *IEEE Antennas and Propagation Society International Symposium*, vol. 1, 1996, pp718-721.

[Mur01] S. C. K. Ko, R. D. Murch, "A Diversity Antenna for External Mounting on Wireless Handsets", *IEEE Transactions on Antennas and Propagation*, vol. 49, no. 5, May 2001, pp840-842.

[Nørk01] O. Nørklit, P. D. Teal, R. G. Vaughan, "Measurement and Evaluation of Multi-Antenna Handsets in Indoor Mobile Communication", *IEEE Transactions on Antennas and Propagation*, vol. 49, no. 3, March 2001, pp429-437.

[Ogawa97] K. Ogawa, T. Uwano, "Analysis of a Diversity Antenna Comprising a Whip Antenna and a Planar Inverted-F-Antenna for Portable Telephones", *Electronics and Communications in Japan*, vol. 80, pt. 1, no. 8, 1997, pp39-49.

[Pars02] J. D. Parsons, "The Mobile Radio Propagation Channel", *Wiley*, 2nd Edition, 2002.

[Paul92] A. Paul, V. Brown, A. R. Noerpel, "Pattern Diversity Antennas for Mobile Communication", *URSI International Symposium on Electromagnetic Theory*, 1992, pp108-110.

[Ped96] G.F. Pedersen, J. Bach Andersen, "Handset Antennas for Mobile Communications: Integration, Diversity and Performance", *Review of Radio Science*, *Oxford*, 1996, pp119-139.

[Ped97] G. F. Pedersen, S. Widell, T. ∅stervall, "Handheld Antenna Diversity Evaluation in a DCS-1800 Small Cell", *IEEE Conference on Personal Indoor Mobile Radio Communications (PIMRC)*, vol. 2, 1997, pp584-588.

[Perini98] P. L. Penri, C. L. Holloway, "Angle and Space Diversity Comparisons in Different Mobile Radio Environments", *IEEE Transactions on Antennas and Propagation*, vol. 46, no. 6, June 1998.

[PieSte60] J.N Pierce, S. Stein, "Multiple Diversity with Nonindependent Fading", *Proceedings IRE*, vol. 48, January 1960, pp89-104.

[Rosen01] K. Rosengren, P-S Kildal, "Study of Distributions of Modes and Plane Waves in Reverberation Chambers for Characterization of Antennas in a Multipath Environment", *Microwave and Optical Technology Letters*, vol. 30, no. 6, September 2001, pp386-391.

[Saund99] S. R. Saunders, "Antennas and Propagation for Wireless Communication Systems", *Wiley*, 1999.

[Sch66] M. Schwartz, W. R. Bennet and S. Stein, "Communication Systems and Techniques", *McGraw Hill*, 1966.

[Schlub00] R. Schlub, D. V. Thiel, J. W. Lu, S. G. O'Keefe, "Dual-band six-element switched parasitic array for smart antenna cellular communications systems", *Electronics Letters*, vol. 36, no. 16, August 2000, pp1342-1343.

[SCM02] "Spatial Channel Model Text Description", SCM-077, *Spatial Channel Model Ad Hoc Group*, *3GPP*, November 20th 2002.

[Scott99] N. L. Scott, M. O. Leonard-Taylor, R. G. Vaughan, "Diversity Gain from a Single-Port Adaptive Antenna Using Switched Parasitic Elements Illustrated with a Wire and

Monopole Prototype", *IEEE Transactions on Antennas and Propagation*, vol. 47, no. 6, June 1999, pp1066-1070.

[Sib97] A. Sibille, C. Roblin, G. Poncelet, "Circular switched monopole arrays for beam steering wireless communications", *Electronics Letters*, vol. 33, no. 7, March 1997, pp551-552.

[Skjæ97] G. F. Pedersen, S. Skjærris, "Influence on Antenna Diversity for a Handheld Phone by the Presence of a Person", *IEEE Vehicular Technology Conference (VTC)*, vol. 3, 1997, pp1768-1772.

[Sulo02] K. Sulonen, P. Vainikainen, K. Kalliola, "The effect of angular power distribution in different environments and the angular resolution of radiation pattern measurement on antenna performance", *COST273 Technical Document (European Co-operation in the field of Scientific and Technical Research)*, TD(02)028, January 17th 2002.

[Taga90] T. Taga, "Analysis of Mean Effective Gain of Mobile Antennas in Land Mobile Radio Environments", *IEEE Transactions on Vehicular Technology*, vol. 39, no. 2, May 1990, pp117-131.

[Taka96] J. Takada, Y. Takeuchi, "An Effect of a Head on an Antenna Pattern Diversity for a Portable Handset", *IEICE International Symposium on Antennas and Propagation (ISAP)*, vol. 2, 1996, pp377-380.

[Tholl93] D. Tholl, M. Fattouche, "Angle of Arrival Analysis of the Indoor Radio Propagation Channel", *IEEE International Conference on Universal Personal Communications*, 1993, vol. 1, pp79-83.

[Turk94] A. M. D. Turkmani, A. A. Arowojolu, P. A. Jefford, C. J. Kellett, "An Experimental Evaluation of the Performance of Two-Branch Space and Polarization Diversity Schemes at 1800MHz", *IEEE Transactions on Vehicular Technology*, vol. 44, no. 2, May 1995, pp318-326.

[Vaug86] R. G. Vaughan, "Signals in Mobile Communications: A Review", *IEEE Transactions on Vehicular Technology*, vol. 35, no. 4, November 1986, pp133-145.

[Vaug87] R. G. Vaughan, J. Bach Andersen, "Antenna Diversity in Mobile Communications", *IEEE Transactions on Vehicular Technology*, vol. 36, no. 4, November 1987, pp149-172.

[Vaug90] R. G. Vaughan, "Polarization Diversity in Mobile Communications", *IEEE Transactions on Vehicular Technology*, vol. 39, no. 3, August 1990, pp177-186.

[Vaug98] R. G. Vaughan, "Pattern Translation and Rotation in Uncorrelated Source Distributions for Multiple Beam Antenna Design", *IEEE Transactions on Antennas and Propagation*, vol. 46, no. 7, July 1998, pp982-990.

[Vaug99] R. G. Vaughan, "Switched Parasitic Elements for Antenna Diversity", *IEEE Transactions on Antennas and Propagation*, vol. 47, no. 2, February 1999, pp399-405.

[Want77] K. Wantanbe, H. Mishima, Y. Ebine, "Measurements of Elevation Angle of Land Mobile Radio Signal Arrival", *Transactions of the IECE of Japan*, vol. E60, no. 11, Nov 1977, pp663-664.

[Zwick98] T. Zwick, C. Fischer, W. Wiesbeck, "A Statistical Channel Model for Indoor Environments Including Angle of Arrival", *IEEE 48th Vehicular Technology Conference (VTC)*, vol. 1, part 1, 1998, pp615-619.

Appendix A Results from elevation angle of arrival in urban environments

Reference	Frequency	Antennas or Method Used	Elevation Angle Results	Comments
[Taga90]	900 MHz	Parabolic reflector, 22^o half power beamwidth	Vertical average 20^o, horizontal average $30\text{-}50^o$. $20\text{-}90^o$ standard deviation in both cases.	Results obtained by having the parabolic reflector measure at angles -10^o, 0^o, 20^o and 45^o
[Kalli01]	2.154GHz	Sphere of 32 dual polar patch antennas with 60^o beamwidth.	Response found between -10^o and 40^o	Results dependent on BS height.
[Ertel99]	N/A	Elliptical and circular models applied.	Laplacian distribution between -40^o and 40^o.	Assumes the surrounding environment at the base station is similar to that of the mobile.
[Fuhl99]	890MHz	Single monopole using ESPRIT algorithm.	Between 0^o to 30^o.	Not easy to distinguish whether any angles occur at $< 0^o$.
[Want77]	873MHz	Monopole and beam tilt antenna with elevations of 0^o, 30^o and 60^o.	High response at 0^o and 30^o.	Limited in the scope although shows consistency with other measurements.
[Abu94]	870MHz	Planar array antenna with beamforming.	Between 0^o and 30^o.	Minor differences between the MUSIC algorithm and measured values were shown.

[Ikeg80]	205MHz	Rotating 12 element yagi-uda antenna measuring at 0^o and 30^o and 50^o.	More significant at 0^o and 30^o.	
[Vaug86]	N/A	Analysis of existing results at the time.	Assumes that the elevation angle is between 0^o and 30^o.	
[Jakes94]	N/A	Analysis of existing results at the time.	Concludes the arrival angles are between 11^o and 39^o.	
[Lee73]	836MHz	16^o half power beamwidth 3 element collinear dipole compared with 39^o whip antenna.	Mainly concentrated in the 16^o region.	
[Aul79]	N/A	Modelling of Rayleigh Fading Channel used by Clarke using modifications to accommodate elevation angle of arrival.	Uniform Azimuth and either a rectangular or sinusoidal elevation distribution between the horizontal and a small angle above the horizontal.	Model is restricted to vertical polarisation only and the elevation pattern is based on rough assumptions that have since been improved upon.

Appendix B Results of indoor mobile angle of arrival measurements

Model	**Frequency**	**Antennas or Method Used**	**Results**	**Comments**
[Zwick98]	N/A	Ray Tracing and Statistical Modelling	Uniform elevation in NLOS case outside the transmit room. More Gaussian with a LOS case.	These trials give limited information, more detail was given on the azimuth AOA and also the TOA.
[Matt93]	870MHz	Monopole antenna moved over a 10x10 horizontal grid	Mainly 0^o elevation when in the same room or next door. Variation between 25^o and 40^o elevation seen on different floors.	Limited results are given due to limitations of measuring equipment. Measurements also became inconsistent with expectations.
[Tholl93]	900MHz 1300MHz	9 element array using the MUSIC algorithm	Uniform distribution in azimuth	
[Barb97]	2.2GHz	20 element circular array antenna	Uniform distribution in azimuth in NLOS cases	

Appendix C Derivation of correlation for vertical and horizontal spacing

Taking a closer look at Figure 3-9, the path length difference, Δl, is defined by taking three separate right angle triangles that link with the required dimensions as shown in Figure C-1.

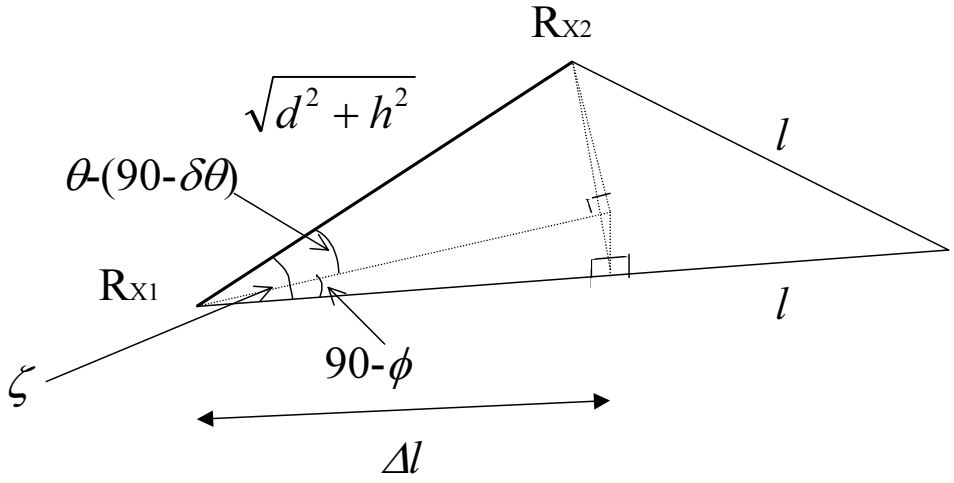

Figure C-1 Diagram showing the phase delay in the case of two dimensional spatial correlation

Simple trigonometry can be used to derive Δ by inspection of the three right angle triangles in Figure C-1. Therefore:

$$\Delta l = \sqrt{d^2+h^2}\cos\left(\theta-\left(90-\delta\theta\right)\right)\cos\left(90-\phi\right) \tag{C.1}$$

where:

$$\delta\theta = \tan^{-1}\left(\frac{h}{d}\right) \tag{C.2}$$

This can be simplified to:

$$\Delta l = \sqrt{d^2+h^2}\sin\left(\theta+\delta\theta\right)\sin\phi \tag{C.3}$$

Hence, $\cos\zeta$ can be derived as:

$$\cos\zeta = \frac{\Delta l}{\sqrt{d^2 + h^2}} = \sin(\theta + \delta\theta)\sin\phi \tag{C.4}$$

It is important to note that when ϕ is negative, the set of right angle triangles reverse and effectively the whole structure turns upside down. This affects the elevation angle so that in this circumstance:

$$\cos\zeta = \sin(\theta - \delta\theta)\sin\phi \tag{C.5}$$

Therefore to cover all angles, the equation needs to be modified as follows:

$$\cos\zeta = \sin(\theta + \delta\theta\,\mathrm{sgn}\,\phi)\sin\phi \tag{C.6}$$

where $\mathrm{sgn}\,\phi$ returns –1 for ϕ less than zero and +1 otherwise.

The final important condition to note is that the equation is valid as long as the three triangles exist. In the case when $\delta\theta = 90^{o}$ this is not the case so the exception to the rule for this case is that in this case $\cos\zeta$ is the same as $\cos\theta$ which applies to purely vertical spatial correlation.

Appendix D Spatial correlation for non-uniform azimuth angle of arrival

For the case of a non-uniform angle of arrival, a further angle, $\delta\phi$, needs to be added to the model used in appendix C to determine the three dimensional relative locations of the two points in space. Figure C-1 is therefore modified as follows:

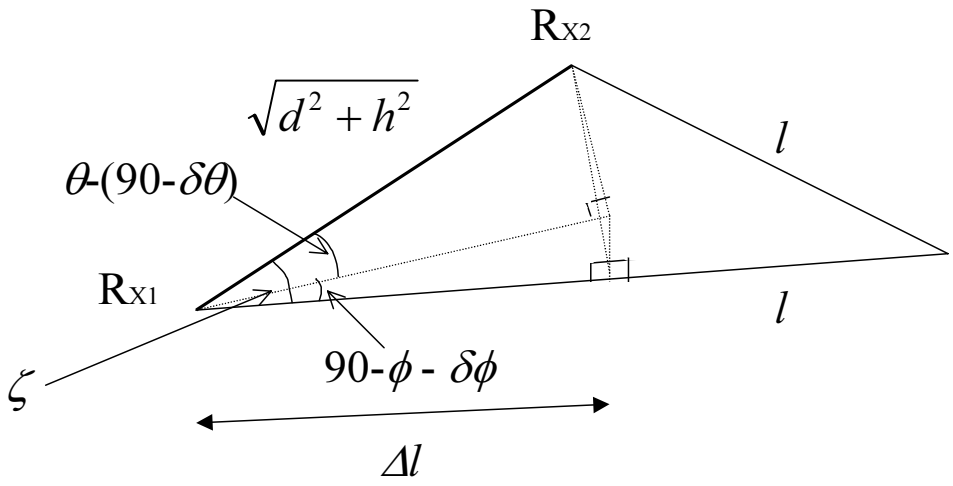

Figure D-1 Diagram showing the phase delay in the case of three dimensional spatial correlation for non uniform azimuth angle of arrival

Therefore, the phase delay, Δl, in this case resolves to be:

$$\Delta l = \sqrt{d^2+h^2}\,\sin(\theta+\delta\theta)\sin(\phi+\delta\phi) \tag{D.1}$$

Therefore the general term for $\cos\zeta$ becomes:

$$\cos\zeta = \sin(\theta+\delta\theta\,\mathrm{sgn}(\phi+\delta\phi))\sin(\phi+\delta\phi) \tag{D.2}$$

These terms can therefore be substituted in to the closed form integral to derive the spatial correlation.

Appendix E Derivation of *E*-field pattern for an equal gain combined IQHA

For the case of four branches of an IQHA there are four output voltages, v_1, v_2, v_3 and v_4. In the case of the first branch, the voltage is a sum of the incoming E-fields at the given random angles. Therefore:

$$v_1 = \sum_{i=1}^{N} \sqrt{\left|E_{\theta 1}(\theta_i,\phi_i)\right|^2 + \left|E_{\phi 1}(\theta_i,\phi_i)\right|^2}\, e^{j\gamma_i} \tag{E.1}$$

where γ_i is a given phase for each angle at sample *i.* The *E*-field, $E_{\theta 1}$ and $E_{\theta 2}$, values are applied at each sample angle. Therefore, for a number of samples, N, the magnitude of v_1 is:

$$\left|v_1\right| = \sum_{i=1}^{N} \sqrt{\left|E_{\theta 1}(\theta_i,\phi_i)\right|^2 + \left|E_{\phi 1}(\theta_i,\phi_i)\right|^2} \tag{E.2}$$

The total voltage, v_T, output for an EGC when all four branches are co-phased is therefore as follows:

$$\begin{aligned} v_T &= \frac{\left|v_1\right| + \left|v_2\right| + \left|v_3\right| + \left|v_4\right|}{\sqrt{4}} \\ &= \frac{\sum_{i=1}^{N} \sqrt{\left|E_{\theta 1}(\theta_i,\phi_i)\right|^2 + \left|E_{\phi 1}(\theta_i,\phi_i)\right|^2} + \sum_{i=1}^{N} \sqrt{\left|E_{\theta 2}(\theta_i,\phi_i)\right|^2 + \left|E_{\phi 2}(\theta_i,\phi_i)\right|^2}}{2} \\ &\quad + \frac{\sum_{i=1}^{N} \sqrt{\left|E_{\theta 3}(\theta_i,\phi_i)\right|^2 + \left|E_{\phi 3}(\theta_i,\phi_i)\right|^2} + \sum_{i=1}^{N} \sqrt{\left|E_{\theta 4}(\theta_i,\phi_i)\right|^2 + \left|E_{\phi 4}(\theta_i,\phi_i)\right|^2}}{2} \end{aligned} \tag{E.3}$$

Therefore, to resolve the E_θ polarisation only at each angle, $E_{\theta T}$, the E_θ components are effectively zero. Therefore:

$$E_{\theta T}(\theta_i,\phi_i) \approx \frac{\left|E_{\theta 1}(\theta_i,\phi_i)\right| + \left|E_{\theta 2}(\theta_i,\phi_i)\right| + \left|E_{\theta 3}(\theta_i,\phi_i)\right| + \left|E_{\theta 4}(\theta_i,\phi_i)\right|}{2} \tag{E.4}$$

Likewise for the E_θ components:

$$E_{\phi T}(\theta_i,\phi_i) \approx \frac{\left|E_{\phi 1}(\theta_i,\phi_i)\right| + \left|E_{\phi 2}(\theta_i,\phi_i)\right| + \left|E_{\phi 3}(\theta_i,\phi_i)\right| + \left|E_{\phi 4}(\theta_i,\phi_i)\right|}{2} \tag{E.5}$$

Appendix F Derivation of mean effective gain for a maximum ratio combined IQHA

The principles applied for EGC in Appendix E are similar for MRC. In this case, the combined voltage output, v_T, for an MRC is defined as follows [Leach00]:

$$v_T = \frac{\sqrt{|v_1|^2 + |v_2|^2 + |v_3|^2 + |v_4|^2}}{\sqrt{4}} = \frac{\sqrt{\left(\sum_{i=1}^{N}\sqrt{|E_{\theta 1}(\theta_i,\phi_i)|^2 + |E_{\phi 1}(\theta_i,\phi_i)|^2}\right)^2 + \left(\sum_{i=1}^{N}\sqrt{|E_{\theta 2}(\theta_i,\phi_i)|^2 + |E_{\phi 2}(\theta_i,\phi_i)|^2}\right)^2 + \left(\sum_{i=1}^{N}\sqrt{|E_{\theta 3}(\theta_i,\phi_i)|^2 + |E_{\phi 3}(\theta_i,\phi_i)|^2}\right)^2 + \left(\sum_{i=1}^{N}\sqrt{|E_{\theta 4}(\theta_i,\phi_i)|^2 + |E_{\phi 4}(\theta_i,\phi_i)|^2}\right)^2}}{2} \quad \text{(F.1)}$$

To resolve the total power, P_T, this is derived by:

$$P_T = \frac{|v_T|^2}{2} = \frac{\left(\sum_{i=1}^{N}\sqrt{|E_{\theta 1}(\theta_i,\phi_i)|^2 + |E_{\phi 1}(\theta_i,\phi_i)|^2}\right)^2 + \left(\sum_{i=1}^{N}\sqrt{|E_{\theta 2}(\theta_i,\phi_i)|^2 + |E_{\phi 2}(\theta_i,\phi_i)|^2}\right)^2 + \left(\sum_{i=1}^{N}\sqrt{|E_{\theta 3}(\theta_i,\phi_i)|^2 + |E_{\phi 3}(\theta_i,\phi_i)|^2}\right)^2 + \left(\sum_{i=1}^{N}\sqrt{|E_{\theta 4}(\theta_i,\phi_i)|^2 + |E_{\phi 4}(\theta_i,\phi_i)|^2}\right)^2}{4} \quad \text{(F.2)}$$

If the angle of arrival is uniform in azimuth and Gaussian in elevation as discussed in chapter 2, the rule holds that:

$$\left(\sum_{i=1}^{N}\sqrt{|E_{\theta 1}(\theta_i,\phi_i)|^2 + |E_{\phi 1}(\theta_i,\phi_i)|^2}\right)^2 \equiv \left(\sum_{i=1}^{N}\sqrt{|E_{\theta 2}(\theta_i,\phi_i)|^2 + |E_{\phi 2}(\theta_i,\phi_i)|^2}\right)^2 \equiv \left(\sum_{i=1}^{N}\sqrt{|E_{\theta 3}(\theta_i,\phi_i)|^2 + |E_{\phi 3}(\theta_i,\phi_i)|^2}\right)^2 \equiv \left(\sum_{i=1}^{N}\sqrt{|E_{\theta 4}(\theta_i,\phi_i)|^2 + |E_{\phi 4}(\theta_i,\phi_i)|^2}\right)^2 \quad \text{(F.3)}$$

Therefore, the total power when the four outputs are added is the same as that of a single branch. Likewise, thus resulting in the same MEG when the four branches are combined with an MRC. This is conditional, however, on the angle of arrival used.